Visually guided flight in birds using the budgerigar (*Melopsittacus undulatus*) as a model system

by

Parthasarathy Bhagavatula

Supervisors: Prof. M.V.Srinivasan

Dr. Charles Claudianos

Prof. Michael Ibbotson

A thesis submitted for the degree of Doctor of Philosophy of

The Australian National University

January 2011

To,

Google, Budgie, Icarus, Casper, Spice, Four, One, Two and Drongo, most wonderful budgerigars.

Contents

Page No

Declaration

This is to certify that:

The thesis comprises only my original work towards the PhD except where indicated,

Due acknowledgement has been given in the text to all other material used.

1) Chapter 2 The Camera calibration experiment was carried out by myself and Mohit Garg, with initial advice and assistance from Dr. Marie Dacke.

2) Chapter 3 The experimental arena was designed by me. The ceiling camera mount was designed and fabricated by Dean Soccol. The data acquisition computer was set up by Richard Lamont and maintained initially by Mark Snowball. All experiments were performed by me. The data was analysed by me using custom written Matlab script written by myself, Prof. M.V Srinivasan and Mohit Garg.

3) Chapter 4 The experimental arena (flight tunnel) was designed by myself and Tom Steginga. All electrical fittings were installed by a QBI approved electrician. The data acquisition computer was set up by me and Mohit Garg. All experiments were performed by me. The calibration pattern was printed by QBI graphics team. The data was analyzed by me using custom written Matlab scripts written by myself, Prof. M.V. Srinivasan, Mohit Garg, Vinh Thai Ngugen, and Richard Lamont.

4) Chapter 5 The textured patterns used in the obstacle avoidance experiments were printed on cloth by the QBI graphics team. All experiments were

performed by me. The data was analyzed by me, using custom written Matlab script written by myself, Vinh Thai Nguyen and Johnathan Hunt.

5) Chapter 6 All experiments were performed by me. The data was analyzed using custom written Matlab script written by myself, Prof. M.V. Srinivasan, Vinh Thai Nguyen and Johnathan Hunt.

6) All chapters in this thesis were written by me with substantial input from Prof. M.V.Srinivasan. The thesis draft was proof read by Dr. Josh Van Kleef, Dr. Peter Kozulin and Owen Carr.

Parthasarathy Bhagavatula

20.4.2011

Acknowledgements

Thesis advisors @ ANU and UQ

I would like to express my sincere thanks and deep gratitude towards my thesis advisors Prof. M.V.Srinivasan, Dr. Charles Claudianos and Dr. Michael Ibbotson for providing me with the valuable opportunity to carry out this project under their guidance. Their invaluable help, suggestions and encouragement have been a constant source of inspiration throughout the tenure of this project.

Funding agency

I would like to thank the ARC Centre of Excellence in Vision Science for providing me the timely funding to make this PhD successful.

People and friends @ ANU

I would like to thank Cathie Stewart Moore, Michelle Powderly, Sue and the administrative staff at the ANU. I would like to thank Owen Carr for all the timely help he provided on my many Canberra visits.

People and friends @ UQ

I would also like to thank all the administrative staff at the Queensland Brain Institute for their timely help. A special note of thanks to Jake Carroll for religiously backing up all my research data on to tape drives.

A special note of thanks to Prof. Rudiger Wehner at University of Zurich for the enlightening discussions on animal navigation

I would like to thank my mother, father and my sister for all the patience shown by them during my five and a half year absence.

List of Publications

During the course of this project the following journal articles, posters and public presentations have been made which are based on the work presented in this thesis. They have been listed here for reference.

1) Bhagavatula P, Claudianos C, Ibbotson M, Srinivasan M, (2009) Edge Detection in Landing Budgerigars (*Melopsittacus undulatus*). PLoS ONE 4(10): e7301. doi:10.1371/journal.pone.0007301.

2) Bhagavatula P, Claudianos C, Ibbotson M, Srinivasan M, (2010) Lateralization of obstacle avoidance in freely flying budgerigars (*Melopsittacus undulates*). International Congress of Neuroethology. Salamanca, Spain.

3) Bhagavatula P, Claudianos C, Ibbotson M, Srinivasan M, (2010) Head , body and wing kinematics of budgerigars (*Melopsittacus undulatus*) executing complex flight maneuvers. International Congress of Neuroethology. Salamanca. Spain.

4) Srinivasan M, Bhagavatula P, Claudianos C, Ibbotson M (2009) From photoreceptors to behaviour in birds and bees. ANS 2009 Satellite Meeting, ARC Centre of Excellence in Vision Science.

List of Figures

fluctuations that are induced in the photoreceptors by the moving stripes, one finds that the responses for all of the striped drums peak at the same temporal frequency, as shown in e. Thus, the strength of the optomotor response appears to be governed by the temporal frequency of the intensity fluctuations that are produced by the moving pattern, and not by its angular velocity.

Figure 1.5 Schematic illustration of a directionally selective elementary motion detector (Srinivasan et al., 1999). A and B represent two photoreceptor cells in neighbouring ommatidia. The arrow shows an object moving from left to right in front of the two photoreceptors A and B. The moving object induces a signal in B at a later time than in A. The signal from each photoreceptor passes through the temporal filter R and then through a second set of temporal filters L and H. Ultimately, the signal coming through R and L from photoreceptor A is multiplied with the signal coming through R and H from the neighbouring photoreceptor B. As a result of this scheme of correlating signals from neighbouring photoreceptors, the elementary movement detector generates a strong response when the object moves from left to right, but not when it moves in the opposite direction.

Chapter 2 General methods

Figure 2.1 Schematic diagram of the tunnel showing the position of the lights and the screens. The red arrow shows the direction of bird flight for the experiments in Chapter 4, and the blue arrow the direction of bird flight for the experiments in Chapter 5 and Chapter 6.

Figure 3.2 Results of colour discrimination control experiment. Four birds, trained on the Dreadnought Grey disc as described in the 'Methods' section, subsequently chose the Dreadnought Grey disc (over the Kingfisher Blue disc) 50 times in 60 test trials.

Figure 3.3 Spectral plots. (A) Absorbance spectra of the visual pigments of the Budgerigar. (B) Illumination spectrum of the room in which the experiments were carried out. (C) Reflectance spectra of the various discs used in the experiments.

Figure 3.4 Three dimensional representations of various discs in colour space. The colours of the blue background and of the various grey discs, shown as vectors representing the relative excitations of the red, green and blue photoreceptor channels. The UV excitation is not depicted, as it is very low. The blue vector represents the blue background. The green vectors represent the various grey discs, except for one grey disc (Dreadnought Grey), which is shown in red. The vectors for all of the grey discs have almost identical directions, indicating that the hues of the grey discs (as perceived by the birds) are all very similar.

Figure 3.5 Summary of bird landings. The left hand panels show examples of the positions and orientations of landings of one bird when the disc was Snow White (A), Jet Black (B), Kingfisher Blue (C) (control) and Dreadnought Grey (D). The dot denotes the head position and the line the body orientation. The background was a constant Kingfisher blue in all cases. The right hand panels show the radial distributions of normalized landing densities for these discs in

regions A, B and C (see Figure 3.1B). They represent a total of 390 landings from 3-6 birds.

Figure 3.6 The left hand panels show examples of the distributions of landings of one bird when the disc was Mouse Grey (A), Azure Blue Grey (B), and Sombre Grey (C). The dot denotes the head position and the line the body orientation. The background was a constant Kingfisher Blue in all cases. The right hand panels show the radial distributions of landing densities for these discs. They represent a total of 397 landings from 3-6 birds.

Figure 3.7 Relative photoreceptor excitations for the various colour discs. Upper panel: The vertical dotted line facilitates reading of the excitations induced by the Dreadnought Grey disc in the red, green, blue and UV photoreceptors, and comparison with the excitations induced in the red and green receptors by the Kingfisher Blue background (horizontal red and green dotted lines, respectively). Lower panel: Values of α obtained for the various grey cards. α is the ratio of the density of the landings in the boundary region (region B in Figure 3.1B) to the average overall landing density (measured over regions A, B and C in Figure 3.1B). The data represent a total of 787 landings from 3-6 birds. The number in each bar denotes the number of landings analyzed. (***) indicates that the value of α is highly significantly different from 1.0 ($p < 0.00005$), (*) indicates a marginally significant difference ($0.01 < p < 0.05$), and the absence of this symbol indicates that α is not significantly different from 1.0 ($p > 0.3$). A pictorial representation of the various grey discs, as viewed against the blue background, is shown in Figure 3.7 lower panel.

Figure 3.8 Relationship between the luminance signals for the various coloured discs. Variation of the luminance signal (UV+B+G+R) and the (R+G) signal for the various coloured discs, calculated as described in 'Methods'. The vertical dotted line facilitates reading of the (UV+B+G+R) signal and the (R+G) signal induced by the Dreadnought Grey disc, and comparison with the corresponding signals induced by the Kingfisher Blue background (horizontal blue and red dotted lines, respectively).

Chapter 4 The use of optic flow in flying budgerigars.

Figure 4.1 Schematic illustrations of the 7 experimental configurations used in the study. The abbreviations are: LHRV – left horizontal and right vertical, LVRH- left vertical and right horizontal, LVRV- left vertical and right vertical; LVRB- left vertical and right blank, LBRV- left blank right vertical, LBRB- left blank and right blank and LHRH- left horizontal and right horizontal.

Figure 4.2 Plan views of 5 randomly chosen trajectories of budgerigars flying in a tunnel in which both walls were lined with (a) vertical stripes, (b) the left wall with vertical stripes and the right wall with horizontal stripes, and (c) vice versa. In each case flight is from the top of the image toward the bottom. (Left and right are defined from the bird's viewpoint: hence LVRH is in the middle panel). The dashed vertical line denotes the midline of the tunnel. The histograms show the distributions of trajectory positions for the total number of flights analyzed (N), the small arrowheads indicate the mean trajectory position, and the horizontal bars show the standard error of the mean. Data were analyzed from 5 birds, producing a total of 45-50 flights for each condition.

Figure 4.3 Plan views of 10 randomly selected trajectories of budgerigars flying in a tunnel in which (a) the left wall was blank and the right wall was lined with vertical stripes, and (b) vice versa. In each case flight is from the top of the image toward the bottom. The dashed vertical line denotes the midline of the tunnel. The histograms show the distributions of trajectory positions for the total number of flights analyzed (N), the small arrowheads indicate the mean trajectory position, and the horizontal bars show the standard deviation. Data were analyzed from 5 birds, producing a total of 51 flights for each condition.

Figure 4.4 Plan views of 5 randomly selected trajectories of budgerigars flying in a tunnel in which both walls were (a) blank, (b) lined with horizontal stripes. In each case flight is from the top of the image toward the bottom. In each case flight is from the top of the image toward the bottom. The dashed vertical line denotes the midline of the tunnel. The histograms show the distributions of trajectory positions for the total number of flights analyzed (N), the small arrowheads indicate the mean trajectory position, and the horizontal bars show the standard deviation. Data were analyzed from 5 birds, producing a total of 45-50 flights for each condition.

Figure 4.5 A and B Side views (views in the y-z plane) of all of the flights for each of the experimental conditions. The circle 'o' represents the position of the head and the '-' denotes the body orientation of the bird. Each colour represents the flight trajectory of a different bird. The y-axis shows the height above the ground, and the z-axis shows the position of the bird along the length of the tunnel. The flight trajectories are shorter at a higher height and longer at a lower height because the top camera has a cone shaped field of view of 95 degrees.

Figure 4.6 Profiles of speed versus position (left hand panels) and mean flight speeds (dotted lines in left hand panel show the mean of mean flight speed when both walls were blank (red), or carried vertical stripes (green) or horizontal stripes (blue). Green, blue and red bars (right hand panels) show mean flight speeds when the patterns on the walls were blank (red bar - LBRB), or lined with vertical stripes (green bar - LVRV) or horizontal stripes (blue bar - LHRH). The error bars in the right hand graph show the standard deviation (left set of bars) and the standard error (right set of bars). Data are shown for three different birds: Caspar, One and Two.

Figure 4.7 Data as in Figure 4.6, but computed for axial flight speed versus time, rather than total flight speed versus time. Green, blue and red bars (right hand panels) show mean axial flight speeds when the patterns on the walls were blank (red bar - LBRB), or lined with vertical stripes (green bar - LVRV) or horizontal stripes (blue bar - LHRH). The error bars in the right hand graph show the standard deviation (left set of bars) and the standard error (right set of bars). Data are shown for three different birds: Caspar, One and Two.

Figure 4.8 Results of Multcompare statistical analysis of mean speed and mean axial speed across the three different experimental conditions LBRB, LVRV and LHRH for three birds: Casper (A), One (B) and Two (C). The results of the statistical analysis (testing for statistical difference at the $p < 0.05$ level) are summarized below each panel.

Figure 4.9 Box plot representation of mean speed and mean axial speed for the three different birds, for each of the three different conditions. In each panel of the figure, the horizontal red lines represent the median values of flight speed.

The bottom and top edges of the blue boxes correspond to the 25th and 75th percentiles of the data sets. The notches in the blue boxes represent 95% confidence intervals for the median values: If the notches in two data sets do not overlap, this means that their median values are significantly different at the $p < 0.05$ level. The whiskers represent the data points that are farthest above and below the median value, and within 1.5 times the inter-quartile range (25% to 75%), i.e. within 1.5 times the height of the box. The red asterisks denote samples that lie outside the whiskers.

Figure 5.1A Configuration for control experiments, in which the tunnel carried no obstacles or apertures. The budgerigar was released in front of camera 2 and its flight path covered the entire length of the tunnel. The bird exited the tunnel from the door near the blue screen at the far end.

Figure 5.1B and C Illustration of the configuration for the single-aperture experiments with the flanking panels carrying a checkerboard texture (B) or no texture (C).

Figure 5.1 D and E Further experimental configurations in which the aperture is flanked by one textured panel and one untextured panel.

Figure 5.1F Experimental configuration for the double aperture experiments. The central panel can be moved to change the size of the apertures on either side corresponding to the Table 5.1.

Figure 5.2 Percentage of collisions while negotiating the narrow gap between the obstacles with different types of patterns.

Figure 5.3 (A-D) Flight trajectories of a right-biased bird (One: shown in green) negotiating a tunnel with an aperture of variable width, positioned at 3000 mm. The aperture is absent in (A) (control condition). Its width is 75% of the tunnel width in (B), 50% in (C), and 25% in (D). (E-H): Corresponding data for a left-biased bird (Casper: shown in blue).

Figure 5.4 Trajectories of a right-biased bird (One; shown in green), and a left-biased bird (Casper; shown in blue) while negotiating the narrowest aperture of width 17 cm. The flanking walls are textured in A and E, and blank in B and F. In C and G, the aperture is flanked by a blank wall on the left and a textured wall on the right. The opposite is true for D and H. As explained in the text, the bias of each bird can be overridden by a visually asymmetrical aperture.

Figure 5.5 Panels A and B show trajectories of a left biased bird while making a choice between two apertures of different sizes. In panel A the right aperture is 40 mm wide while the left aperture is 60 mm wide. In panel B the right aperture is 10 mm wide and the left aperture is 90 mm wide. Panels C, D and E show trajectories of a right biased bird while making a choice between two apertures of different sizes. In Panel C the right aperture is fully blocked while the left aperture is 100 mm wide and the right biased bird has no option but to take the left aperture. In panel D the right aperture is 10 mm while the left aperture is 90 mm wide. Here the bird tries to fly through the right aperture but is unable to do so and then changes its flight path to go through the left aperture. In panel E the left aperture is blocked and the bird flies through the right opening.

Figure 5.6 A Results of two-aperture experiment for bird One, showing percentage choice frequencies for the right-hand aperture as a function of the

position of the central panel. 0 mm denotes the central position, when both apertures are of equal width. Positive values of position denote displacements of the central panel to the right (left-hand aperture wider than right-hand aperture) and negative values of position denote displacements of the central panel to the left (right-hand aperture wider than left-hand aperture). The dashed horizontal line represents the random-choice level of 50%. The symbols next to each data point indicate a statistically significant difference of the choice frequency from the random-choice level of 50%, calculated as described in "Methods". [$p<0.05$: (*); $p < 0.02$: (**); $p<0.00001$: (***)].

Figure 5.6 B Results of two-aperture experiment for bird Casper, showing percentage choice frequencies for the right-hand aperture as a function of the position of the central panel. 0 mm denotes the central position, when both apertures are of equal width. Positive values of position denote displacements of the central panel to the right (left-hand aperture wider than right-hand aperture) and negative values of position denote displacements of the central panel to the left (right-hand aperture wider than left-hand aperture). The dashed horizontal line represents the random-choice level of 50%. The symbols next to each data point indicate a statistically significant difference of the choice frequency from the random-choice level of 50%, calculated as described in 'Methods'. [$p < 0.05$: (*); $p < 0.02$: (**) and $p < 0.00001$: (***)].

Figure 5.6 C. Results of two-aperture experiment for bird Two, showing percentage choice frequencies for the right-hand aperture as a function of the position of the central panel. 0 mm denotes the central position, when both apertures are of equal width. Positive values of position denote displacements of the central panel to the right (left-hand aperture wider than right-hand

aperture) and negative values of position denote displacements of the central panel to the left (right-hand aperture wider than left-hand aperture). The dashed horizontal line represents the random-choice level of 50%. The symbols next to each data point indicate a statistically significant difference of the choice frequency from the random-choice level of 50%, calculated as described in 'Methods'. [$p < 0.05$: (*); $p < 0.02$: (**) and $p < 0.00001$: (***)].

Figure 5.6 D. Results of two-aperture experiment for bird Drongo, showing percentage choice frequencies for the right-hand aperture as a function of the position of the central panel. 0 mm denotes the central position, when both apertures are of equal width. Positive values of position denote displacements of the central panel to the right (left-hand aperture wider than right-hand aperture) and negative values of position denote displacements of the central panel to the left (right-hand aperture wider than left-hand aperture). The dashed horizontal line represents the random-choice level of 50%. The symbols next to each data point indicate a statistically significant difference of the choice frequency from the random-choice level of 50%, calculated as described in 'Methods'. [$p < 0.05$: (*); $p < 0.02$: (**) and $p < 0.00001$: (***)].

Figure 5.6 E. Results of two-aperture experiment for bird Saras, showing percentage choice frequencies for the right-hand aperture as a function of the position of the central panel. 0 mm denotes the central position, when both apertures are of equal width. Positive values of position denote displacements of the central panel to the right (left-hand aperture wider than right-hand aperture) and negative values of position denote displacements of the central panel to the left (right-hand aperture wider than left-hand aperture). The dashed horizontal line represents the random-choice level of 50%. The symbols next to

flanked by blank panels in (6.4 A and B), panels carrying a checkerboard texture in (C and D), and through a tunnel that had no aperture in (6.4 E and F). In each pair of panels, the left-hand panel shows data from a left-biased bird (a bird that approaches the aperture from the left) and the right-hand panel shows data from a right-biased bird (a bird that approaches the aperture from the right). In 6.4 A-D the red vertical dashed line shows the position of the aperture. In 6.4 E-F this line shows where the aperture would have been located, had it been present.

Figure 6.5 Examples showing the roll of the head (red) and body (blue) as a function the axial position of the head along the tunnel, for birds flying through a tunnel with an aperture flanked by blank panels (6.5 A and B), panels carrying a checkerboard texture (6.5 C and D), and through a tunnel that has no aperture (6.5 E and F). In each pair of panels, the left-hand panel shows data from a left-biased bird (a bird that approaches the aperture from the left) and the right-hand panel shows data from a right-biased bird (a bird that approaches the aperture from the right). In 6.5 A-D the red vertical dashed line shows the position of the aperture. In 6.5 E-F this line shows where the aperture would have been located, had it been present.

Figure 6.6 Examples showing the trajectories of the head (red dots) and left and right wings (green and black lines, respectively) as viewed from above, as a function of the axial position of the head along the tunnel. The birds flew through a tunnel with an aperture flanked by blank panels in (6.6 A and B), panels carrying a checkerboard texture in (6.6 C and D), and through a tunnel that had no aperture in (6.6 E and F). In each pair of panels, the left-hand panel shows data from a left-biased bird (a bird that approaches the aperture from the

left) and the right-hand panel shows data from a right-biased bird (a bird that approaches the aperture from the right). (The full video shows that it approaches from the right hand side even though its not very evident on the graph.) In 6.6 A-D the red vertical dashed line shows the position of the aperture. In 6.6 E-F this line shows where the aperture would have been located, had it been present.

Figure 6.7 Examples showing the trajectories of the head (red dots) and left and right wings (green and black lines, respectively) as viewed from the side, as a function of the axial position of the head along the tunnel. The birds flew through a tunnel with an aperture flanked by blank panels in (6.7 A and B) panels carrying a checkerboard texture in (6.7 C and D) and through a tunnel that had no aperture in (6.7 E and F). In each pair of panels, the left-hand panel shows data from a left-biased bird (a bird that approaches the aperture from the left) and the right-hand panel shows data from a right-biased bird (a bird that approaches the aperture from the right). In 6.7 A-D the red vertical dashed line shows the position of the aperture. In 6.7 E-F this line shows where the aperture would have been located, had it been present.

Figure 6.8 Plots of axial position of wing tips relative to the head, as a function of the axial position of the bird in the tunnel. The green and black curves correspond to the left and right wing tips, respectively. The aperture is flanked by blank panels in 6.8 A and B and by checkerboard panels in 6.8 C and D. In 6.8 E and F the tunnel carries no aperture (control condition). In each pair of panels, the left-hand panel shows data from a left-biased bird (a bird that approaches the aperture from the left) and the right-hand panel shows data from a right-biased bird (a bird that approaches the aperture from the right). In

6.8 A-D the red vertical dashed line shows the position of the aperture. In 6.8 E-F this line shows where the aperture would have been located, had it been present.

Figure 6.9 Plots of head, body and wing tip heights as a function of head axial position when the aperture is flanked by blank panels (6.9 A and B), or checkerboard panels (6.9 C and D). In 6.9 E and F the tunnel carries no aperture (control condition). The green and black curves correspond to the left and right wing tips, respectively. In each pair of panels, the left-hand panel shows data from a left-biased bird (a bird that approaches the aperture from the left) and the right-hand panel shows data from a right-biased bird (a bird that approaches the aperture from the right). In 6.9 A-D the red vertical dashed line shows the position of the aperture. In 6.9 E-F this line shows where the aperture would have been located, had it been present.

Appendix 1

Figure A1.1 Schematic diagram of the tunnel with a swinging perch. The budgerigars take off upon slow rotation of the perch to land on the swinging perch.

Figures A1.2, A1.3 and A1.4 Illustration of three different configurations of a landmark stripe on the floor.

Figure A1.5 'Chicane' arrangement of obstacles used for the multiple obstacle avoidance experiment.

Figure A2.1 Illustration of total transit times as predicted by a model of a flock of budgerigars negotiating two simultaneously presented apertures of width d mm (left-hand aperture) and (D-d) mm (right-hand aperture), where D, the sum of the widths of the two apertures, is 100 mm. The curves show the variation of the total transit time with d for strategies A (blue), B (green), C (black), D (dashed black) and E (red), as described in the text. For clarity, the curve for strategy D is shown displaced slightly upwards.

Figure A2.2 Probability functions for the choice of the right-hand aperture (red curve) and the left-hand aperture (blue curve) as a function of the width d of the left-hand aperture, for the optimum strategy (E) described in the text.

Figure A2.3. Choice probability functions for individual birds with a range of different bias parameters (B) varying from 0 mm to 100 mm in steps of 10 mm The choice probability for each bird is modelled by a step function (dashed blue curve). The continuous red curve shows the resulting average choice probability function for the entire flock.

Figure A2.4. Choice probability functions for individual birds with a range of different bias parameters (B) varying from 0 mm to 100 mm in steps of 10 mm. The choice probability for each bird is modelled by a logistic function (dashed blue curve). The continuous red curve shows the resulting average choice probability function for the entire flock.

Figure A3.1. Illustration of the geometry of the diamond marker, and the effects of a change in roll attitude. The long axis of the marker is 3-4, and is pitched upward by an angle φ (brown figure). The blue figure shows the new view of the marker when it has rolled right-side-down, about the 3-4 axis, by an angle θ.

Figure A3.2. Two overhead views of the diamond marker. In **a** the roll is right-side-downward, and in **b** the roll is left-side-downward. In both cases, the pitch is assumed to be upward, i.e. corner 3 is higher than corner 4.

List of Tables

List of Videos

Chapter 2

Video 2.1 shows the motion capture view of the bird in flight in the x-y plane (this is a view from the end of the tunnel, behind the bird). The plot shows the position of the head ('+'), the body ('*') the left wing tip ('o') and the right wing tip ('o'). The solid black lines depict the boundaries of the obstacle.

Video 2.2 shows the motion capture view of the bird in the x-z plane (this is a view from the ceiling of the tunnel, above the bird). The plot shows the position of the head ('+'), the body ('*') the left wing tip ('o') and the right wing tip ('o'). The solid red lines depict the tunnel boundaries and the solid black lines the boundaries of the obstacle.

All videos for chapter 2 are in .avi format.

Chapter 3

Video 3.1 The video shows a budgerigar landing on the edge of a Jet Black disc placed on a uniform Kingfisher Blue background.

Video 3.2 The video shows a budgerigar participating in a disc choice experiment and is able to distinguish between a Kingfisher Blue card and a Dreadnought Grey card, both placed on a uniform Kingfisher Blue background. The budgerigar finally lands on a Dreadnought Grey card.

Video 3.1 is in .mov and .wmv file format.

Video 3.2 is in .avi file format.

Video 4.1 shows the flight of a budgerigar when both walls carry vertical stripes (LVRV-Left vertical and right vertical stripes).

Video 4.2 shows the flight of a budgerigar when the right wall carries vertical stripes and the left wall carries horizontal stripes (LHRV-Left horizontal and right vertical).

Video 4.3 shows the flight of a budgerigar when the left wall carries vertical stripes and the right wall carries horizontal stripes (LVRH-Left vertical and right horizontal).

Video 4.4 shows the flight of a budgerigar when the right wall is devoid of any stripes and the left wall carries vertical stripes (LVRB-left vertical and right blank).

Video 4.5 shows the flight of a budgerigar when the left wall is devoid of any stripes and the right wall carries vertical stripes (LBRV-Left blank and right vertical).

Video 4.6 shows the flight of a budgerigar when both the left and right wall are blank.

Video 4.7 shows the flight of a budgerigar when both the left and right wall carry horizontal stripes.

All videos in the main folder were filmed at 250 frames per second. The videos in the truncated videos folder have been down sampled to 25 frames per second.

All videos are in .avi file format.

Chapter 5

Video 5.1 Control flight without any obstacles.

Video 5.2 An experimental flight in which the aperture is 50 % of the total width of the tunnel. No deviations in the flight trajectory are observed.

Video 5.3 An experimental flight in which the aperture is 25% of the total width of the tunnel. No deviations in the flight trajectory are observed.

Video 5.4 An experimental flight in which the aperture is 12.5% of the total width of the tunnel. The panels flanking the aperture are decorated with a checkerboard pattern. It can be seen that the bird is right biased.

Video 5.5 An experimental flight in which the aperture is 12.5% of the total width of the tunnel. The panels flanking the aperture are decorated with a checkerboard pattern. It can be seen that the bird is left biased.

Video 5.6 An experimental flight in which the aperture is 12.5% of the total width of the tunnel. The panels flanking the aperture are blank, without any patterns. It can be seen that the bird is right biased.

Video 5.7 An experimental flight in which the aperture is 12.5% of the total width of the tunnel. The panels flanking the aperture are blank, without any patterns. It can be seen that the bird is left biased.

Video 5.8 An experimental flight in which the aperture is 12.5% of the total width of the tunnel. The aperture is flanked by a checkerboard panel on the right–hand side and a blank panel on the left-hand side. The bird has a right-bias, as established from other flights through a symmetrically decorated aperture. Despite its right-bias, the bird enters the aperture from the left-hand side, flying closer to the blank panel and further away from the checkerboard panel. Evidently, the bird's inherent right-bias is overridden by a tendency to avoid the textured panel, which provides strong optic flow cues.

Video 5.9 An experimental flight in which the aperture is 12.5% of the total width of the tunnel. The aperture is flanked by a checkerboard panel on the left–hand side and a blank panel on the right-hand side. The bird has a right-bias, as established from other flights through a symmetrically decorated aperture. The bird enters the aperture from the right-hand side, flying very close to the blank panel, causing the right-hand wing to collide with it.

Video 5.10 An experimental flight in which the aperture is 12.5% of the total width of the tunnel. The aperture is flanked by a checkerboard panel on the right –hand side and a blank panel on the left-hand side. The bird has a left-bias, as established from other flights through a symmetrically decorated aperture. It enters the aperture from the left-hand side, flying closer to the blank panel and further away from the checkerboard panel.

Video 5.11 An experimental flight in which the aperture is 12.5% of the total width of the tunnel. The aperture is flanked by a checkerboard panel on the left

–hand side and a blank panel on the right-hand side. The bird has a left-bias, as established from other flights through a symmetrically decorated aperture. Despite its left-bias, the bird enters the aperture from the right-hand side, flying closer to the blank panel and further away from the checkerboard panel. Evidently, the bird's inherent left-bias is overridden by a tendency to avoid the textured panel, which provides strong optic flow cues.

Chapter 6

Video 6.1A Control flight without any obstacles. No significant head or body roll is registered by the head and body tracking dots.

Video 6.1B An experimental flight in which the aperture is flanked by checkerboard panels on both sides. The head tracking dot does not show any significant roll but the body tracking dot does. The wings fold upwards while passing through the aperture, and do not collide with the flanking panels

Video 6.1C An experimental flight in which the aperture is flanked by blank panels on both sides. The head tracking dot does not show any significant roll but the body tracking dot does. The bird collides with the blank wall on the left side while negotiating the aperture.

Video 6.2A A control flight of the budgerigar without any obstacles in its flight path. The video shows the motion capture view of the bird in flight in the x-y plane (this is a view from the end of the tunnel, behind the bird). The plot shows the position of the head ('+'), the body ('*') the left wing tip ('o') and the right wing tip ('o'). Bird is right biased. The dotted lines show the position of the obstacle in experimental conditions but absent in the control experiments.

Video 6.2B An experimental flight of the budgerigar in which the aperture is flanked by blank panels on both sides (not seen in video). The video shows the

motion capture view of the bird in flight in the x-y plane (this is a view from the end of the tunnel, behind the bird). The plot shows the position of the head ('+'), the body ('*') the left wing tip ('o') and the right wing tip ('o'). The solid black lines depict the boundaries of the obstacle. Note the higher degree of banking when the budgerigar is negotiating blank obstacles. The bird is right biased as seen in the video.

Video 6.2C An experimental flight of the budgerigar in which the aperture is flanked by checkerboard panels on both sides (not seen in video). The video shows the motion capture view of the bird in flight in the x-y plane (this is a view from the end of the tunnel, behind the bird). The plot shows the position of the head ('+'), the body ('*') the left wing tip ('o') and the right wing tip ('o'). The solid black lines depict the boundaries of the obstacle.

Note: There are no truncated videos for chapter 6. All videos for chapter 6 are in .avi format.

Note: There are no truncated videos for chapter 6.

Chapter 7

Video 7.1 shows a number of wild birds visiting a feeder. Each bird lands consistently on the edge of the platform. The video was filmed by Prof. M.V.Parthasarathy, Cornell University, Ithaca, NY, USA.

Appendix

Video AV1 A budgerigar landing on a moving perch.

Video AV2 A budgerigar following a landmark on the floor close to the left wall.

Video AV3 A budgerigar following a landmark on the floor close to the right wall.

Video AV4 A budgerigar following a landmark diagonally present on the floor.

Video AV5 A budgerigar negotiating two obstacles during its flight through the tunnel.

Abstract

A glance at a bird flying rapidly and safely through dense foliage would convince anyone that these creatures are masters of aerial flight. In order to achieve such mastery birds need to be able to process visual information accurately, and in real time, to generate effective motor outputs. In this thesis I use the budgerigar, *Melopsittacus undulatus*, as a model system to explore some of the principles that underlie visual guidance of bird flight. The budgerigar is a particularly agile flier with a well developed visual system. In this thesis, behavioural experiments are performed with these birds designed to investigate the strategies they use to guide landing and fly along passages, through narrow gaps and past obstacles.

Life as a bird requires an ability to land smoothly, safely and precisely on tree branches, regardless of whether the branch is stationary or moving in the breeze, and at a wide range of ambient light levels. The experimental results in this thesis demonstrate, for the first time, that visual features such as edges play an important role in directing the landings of birds. I find that budgerigars show a strong preference to land at visually contrasting edges. Experiments, in which the colours on either side of a visual boundary are manipulated, reveal that the edge-detecting mechanism that guides landings is 'colour-blind', and is most likely driven by the red double-cone photoreceptor channel. The colour-blindness of the landing behaviour is intriguing, because budgerigars are known to possess excellent tetrachromatic colour vision. This finding has close parallels with the behaviour of honeybees that also tend to land at contrasting edges, and

display colour-blindness in their landing behaviour. This is despite the fact that bees, like birds, are endowed with good colour vision.

In their natural habitat, birds fly rapidly and safely through narrow spaces between trees and branches of trees. This ability is investigated by training budgerigars to fly along tunnels in which the walls are decorated with various visual patterns. Analysis of high-speed stereo recordings of the birds' flights under these various conditions has provided evidence that (a) flight speed is controlled by regulating the magnitude of the optic flow (the speed of image motion) that is experienced by the two eyes; and (b) birds fly close to the midline of the tunnel, avoiding collisions with either wall, by balancing the magnitudes of the optic flow that are experienced by the two eyes. Here, again, birds seem to show striking parallels with honeybees, that are known to negotiate tunnels safely by balancing the optic flow cues in the lateral visual fields.

Birds commonly fly through cluttered environments that contain widely varying species of trees, as well as man-made structures like buildings, power lines and windmills. Little is known about how birds are able to negotiate these obstacles and navigate paths through them. Here I examine the fine structure of bird flight during these complex manoeuvres by recording their flights in an obstacle-laden chamber and tracking the trajectories of the head, body, and wing tips, as well as the orientations of the head and the body. The results indicate that:

(a) Birds close their wings temporarily when passing through a narrow gap.

(b) When negotiating a gap or flying past an obstacle the head displays relatively little roll or pitch – it maintains a relatively constant, horizontal

attitude. However, the attitudes of the body and the strokes of the wings can vary widely during the manoeuvre, and seem to be tailored to the nature of the gap or the obstacle.

(c) Birds display individual biases when flying past obstacles, some consistently flying to the left of the obstacle and others to the right. This bias is evident when birds are required to choose to fly through one of two equal-sized apertures, but when one aperture is larger they tend to prefer it, regardless of the direction of their bias. The results here suggest that this lateralization of behaviour manifests itself primarily at the individual level, although further work, with a greater sample size, would be required to determine whether there is also a weak bias at the population level.

So far, much of the literature on bird flight has focused on long-range migration, with little attention being devoted to the challenges of short-range navigation. My studies reveal, for the first time, some of the elegant visuomotor strategies that birds employ to control their flight on a moment-to-moment basis. In orchestrating some of these manoeuvres birds seem to use strategies that are very similar to those used by bees, suggesting that some of the principles that underlie visual guidance may be shared by all flying animals. On the other hand, the intricate details of the birds' behaviour when flying through complex environments reveals a level of sophistication and adaptation that we have only begun to uncover, and which is likely to be the subject of many future studies.

Key Words: Edge detection, Optic flow, Obstacle avoidance.

Chapter 1
General Introduction

1.1 Bird migration

Among all the species in the animal world, migration is most common in birds (Berthold et al., 2003). The earliest species of birds that could fly were thought to be nomadic and would move about randomly in search of food. However, overtime, birds evolved a more systematic and periodic pattern of movement from one place to another, in order to cope with changing seasons and changes in the availability of food. This regular pattern of movement is known as migration (Berthold et al., 2003).

It is thought that migration evolved in order to meet foraging requirements. Birds migrate to areas where there is an abundant supply of food during breeding as well as non-breeding seasons. The earliest bird species were short-range migrants. Short-range migration depends on real time navigational inputs like vision, hearing and olfaction. But over the course of time, as long-range navigation evolved in birds, the requirement for more precise navigational information also increased. Birds evolved the ability to perceive and exploit navigational cues that are provided by the sun compass, the star compass, the earth's magnetic field and prominent visual and olfactory landmarks.

The process of migration has evolutionary advantages, which maintain the selection pressure for migration to occur (Salewski and Bruderer, 2007). Birds living in higher latitudes undertake migration southwards to lower latitudes in winter, to avoid adverse weather conditions as seen in the case of Siberian

cranes (*Grus leucogeranus*), which migrates from Siberia over the Himalayas to the breeding grounds of northern India (Higuchi et al., 2003). Likewise, birds that live in lower latitudes in the winter will migrate to higher latitudes in summer to take advantage of the longer daylight periods and more abundant food supply to raise their young ones.

Bird migration has been extensively investigated in a wide variety of species. The instinct to migrate appears to be an innate behaviour in birds (Berthold et al., 2003). In spite of its advantages, migration carries a high risk of injury and death due to accidents and predation. Migratory birds can be broadly categorized into long distance migrants, short distance migrants and non-migrant resident birds. In some species of birds such as *Corapipo altera,* only a few individuals in a given population migrate while the others remain as resident birds. Such birds are called partial migrants (Boyle, 2008).

Migratory birds are found on all continents and occupy diverse ecological niches. A classic example is the Arctic tern (*Sterna paradisaea*), which migrates from pole to pole -- an epitome of long distance migration (Carsten Egevanga, 2010). A systematic analysis of bird flight would reasonably include;

1.2 Navigation and orientation in birds

It is useful to consider avian capacities in relation to long and short distance migration.

1.2.1 Long distance migration

Long distance migration requires the aid of multiple navigational cues such as landmarks, the earth's magnetic field, the sun compass, the star compass, the direction of prevailing winds and the locations of thermal and obstructional up-drafts (Wiltschko and Wiltschko, 2003; Woodcock, 1940). These navigational cues are perceived by various sense organs in the birds.

During long distance migration, birds navigate over diverse topographical features. Homing pigeons (*Columba livia*) are able to use roads for orientation and guidance (Biro et al., 2007; Lau et al., 2006). These birds can also perceive the earth's magnetic field in order to set their flight direction in relation to 'magnetic signposts' based on local variations of magnetic intensity (Mouritsen and Ritz, 2005).

Some birds such as the European starling (*Sturnus vulgaris*) use the sun as a compass for their orientation (Schmidt-Koenig, 1990). Arctic seabirds are able to navigate their way along great circle routes (orthodromes) when they fly over high latitudes (Alerstam et al., 2001; Wehner, 2001). They accomplish this by using their sun compass for navigation while keeping their internal clocks set to the time zone at the point of departure.

Other birds such as the Indigo buntings (*Passerina cyanea*) use the star compass for navigation. This was demonstrated by conducting experiments in a planetarium where the positions and orientations of star constellations could be changed under controlled conditions (Emlen, 1967).

Larger birds like eagles and hawks undertake migration over large land masses, where they exploit thermal air currents to gain or maintain altitude (Scorer, 1954). Migrating birds like pelicans (*Pelecanus onocrotalus*) fly in a V formation to reduce atmospheric drag in flight and hence conserve energy (H Weimerskirch, 2001).

Migratory birds also fly at different altitudes in the migratory route based on the prevailing weather conditions, which can change with seasons (Ritchie, 1995). These birds often make scheduled stops for rest and rejuvenation along their migratory route (Leu and Thompson, 2002). Birds like the Albatross (*Diomedea exulans*) use olfactory cues when navigating large oceans in search

of fish. They have a large olfactory bulb and are able to track fish odours in experimental trials at sea. These experiments in the natural environment provide direct evidence of the role played by the olfactory system in foraging behaviour (Nevitt et al., 2008). The importance of olfaction in pigeon migration has also been investigated. It has been shown in some experiments that olfactory cues are essential for the development of the navigational map (Gagliardo et al., 2009).

1.2.2 Short distance migration

Short distance migration is a feature of all bird species. Most short distance migration involves localized movement from one place to another in search of food (foraging), or for roosting, nesting or predator avoidance. In order to carry out short distance migration, birds use different navigational strategies. The navigational information is perceived from the local surrounding environment and consists of visual, olfactory and auditory inputs. Birds have to avoid different kinds of natural obstacles like trees, branches of trees and rock faces, manmade obstacles like buildings, power lines and wind farms (Daniel and Willard, 1978; M.A.Farfan, 2009).

Short-range bird migration has not been investigated in detail. The most common model system used to investigate short distance navigational strategies in birds is the pigeon (*Columba livia*). Studies in pigeons have demonstrated the importance of the visual system in walking, landing and takeoff behaviour (Davies and Green, 1988; Davies and Green, 1990; Green et al., 1992; Green et al., 1994).

Cave swiftlets use echolocation to avoid obstacles while flying through dark caves where they roost and build nests (Griffin and Thompson, 1982). They fly under conditions of total darkness by bouncing sound 'clicks' off the

walls of the cave. This is a classic example of a bird using auditory cues to aid navigation.

There is evidence that pigeons use olfactory cues for navigation (Schmidt-Koenig, 1987). When homing pigeons are released at a considerable distance from home with frosted lenses covering their eyes, they are able to return to within 1-2 km of home with relative ease. On the basis of these observations, Koeing concluded that homing pigeons follow olfactory cues in order to navigate. However this hypothesis has proved controversial and goes into direct conflict with the magnetic homing hypothesis. Experiments involving bilateral sectioning of the ophthalmic branch of the trigeminal nerve, attachment of a magnet to the upper cere area and local anaesthesia of the region around the beak have shown that pigeons make use of the earth's geomagnetic field to navigate. It was also shown that the magnetic sensitivity works due to the presence of magnetite based magnetoreception in the upper beak of the pigeon. In order to investigate the olfactory and magnetic senses, independent methods of blocking or sectioning the olfactory nerve and the ophthalmic branch of the trigeminal nerve have to be adopted (Cordula V. Mora, 2004).

However, among the three senses, namely, vision, olfaction and audition, the vision is likely to play a critical role in short range migration, and in executing moment-to-moment manoeuvres.

1.3 Visually guided flight in birds

Vision is critical for a variety of tasks undertaken by birds – such as pecking on seeds, landing precisely near the nest entrance, landing on the branch of a tree and flying safely between tree branches. Visually guided flight has been investigated in a few species such as pigeons, gannets, falcons, and owls. Birds

like falcons and eagles, which fly at higher altitudes, depend on visual inputs for navigation, as well as for detection and capture of prey (Jones et al., 2007).

Visual information about objects and especially about their boundaries is essential for recognizing objects and distinguishing them from their backgrounds. Almost every object in the real world has a boundary. Boundary information is essential for perception of objects in all creatures, including birds. Chapter 3 describes a study that investigates how birds use the visual contours of objects to guide their landings.

Birds also need to have accurate information about the distances of various objects in their immediate environment, so that they can fly safely past or between them without experiencing collisions. Two previously studied mechanisms of range perception in birds are (a) cues based on ocular accommodation and (b) cues based on stereo information.

Ocular accommodation involves a change in the focal length of the lens, which causes the image on the retina to remain in focus. The extent to which the lens must accommodate to maintain an object in focus on the retina provides a measure of the object's range. Indeed, barn owls (*Tyto alba*) use accommodation information for distance estimation, as do chameleons and toads (Collett, 1977; Ingle, 1968). The accommodation information is used for depth perception during seed pecking, as has been demonstrated by behavioural experiments in which the focal length of the lens was artificially manipulated by placing lenses of different focal length in front of the eye. However, in birds, accommodation does not seem to provide useful distance cues at large ranges (Wagner and Schaeffel, 1991).

Another cue that birds use to gauge depth is stereo. The main function of stereo is to compute depth by measuring the disparity between the images of an object in the two retinae. The disparity occurs due to the horizontal separation of the two eyes. This causes the object being viewed by the two eyes to be seen along different lines of sight, a phenomenon known as parallax. The brain then computes the depth information by comparing the relative positions of the images of the object in the two retinae (Pettigrew and Konishi, 1976). Birds like barn owls (*Tyto alba*) use stereo vision to gauge the distances to objects in the frontal visual field, a strategy which is similar to that employed by predatory birds like falcon (Fox et al., 1977). The computational strategies used for stereo vision in birds like owls are similar to those used by mammals, in that they both rely on extracting disparity information to perceive depth. Stereoscopic depth information can also help break camouflage, as in the case of a textured object viewed against a similarly-textured background, (Fox et al., 1977; Willigen et al., 1998).

In principle, the distances to objects in the environment can also be gleaned from optic-flow cues. When an observer moves in a straight line, the images of various objects in the environment move on their retina. The speed of motion of the image of each object depends upon (a) the observer's speed (b) the distance of the object from the observer and (c) the angular direction of the object relative to the observer's heading direction (Srinivasan, 1993). The relative motion between the images of two objects in the scene is known as 'motion parallax'. Motion parallax can be used as a cue to determine the relative ranges of various objects in the scene. For example, if two objects are in the

same viewing direction, the nearer object will appear to move faster than the one farther away.

Thus, motion parallax allows the observer to determine the distances to various objects purely from monocular information. In case of birds such as owls, motion parallax information is used to calibrate the stereoscopic information during development (van der Willigen et al., 2002). The owls move their heads from side to side in order to derive motion parallax information from monocular vision. They also make use of the stereo information that is provided by the two eyes, for depth perception. The combined use of the two systems for depth perception in birds is known as 'Primary-depth-cue-equivalence' (van der Willigen et al., 2002). The computational strategies for depth perception operate in a similar way in birds and mammals, even though they have evolved independently (van der Willigen et al., 2002).

1.4 Structure and organization of avian eyes

The avian visual system consists of a pair of simple eyes, also known as camera eyes. Figure 1.1 shows the basic structure of a bird eye. The positioning and structure of the eyes vary from one bird species to another.

The general structure of an avian eye is similar to that of any vertebrate eye. The avian eye however does not have a spherical shape, but is much more flat, enabling a greater area of the retina to be in focus (Jones et al., 2007). The walls of the eyeball are composed of three layers namely, the cornea / sclera, the choroid and the retina.

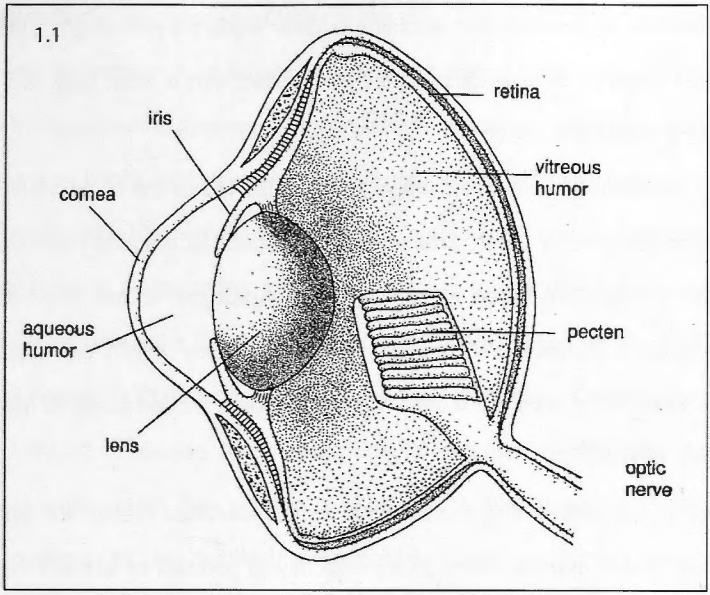

Figure 1.1 General structure of an avian eye (Waldvogel, 1990).

The cornea is the transparent outer most layer in the front of the eye. This layer continues peripherally as the sclera -- a tough, collagenous layer that provides structural integrity to the eye. Avian eyes also possess a sclerotic ring -- a collection of small bones around the eye ball -- (Curtis and Miller, 1938) whose function is to provide additional support to the eyeball, since the eye is not spherical in shape.

The choroid is a pigmented layer, situated between the sclera and the retina. It contains the arteries and veins that convey the blood supply to and from the retina. The pigment present in the choroid is essentially composed of melanin, which prevents internal reflection of light (Jones et al., 2007). The lens is transparent and flexible, and is composed primarily of lens proteins. The lens divides the eye into two chambers – the anterior chamber in front of the lens and the posterior chamber behind it. The anterior chamber between the cornea

and the lens is smaller, and contains a clear watery liquid matrix called the aqueous humour. The posterior chamber is filled with a clear jelly like matrix called the vitreous humour.

The lens has a convex shape and is attached to the ciliary muscles by means of the zonular fibres. This enables the shape of the lens to be changed in order to focus the image on to the retina. In addition to this, the cornea in some birds is connected to the 'Cramptom's muscles' which can change its shape, thus giving birds more accommodation power as compared to mammals (Dennis, 1997).

In front of the lens is the iris, attached to the so-called dilator and sphincter muscles. These muscles work antagonistically to contract or expand the pupil, thus regulating the amount of light arriving at the retina. Thus, the iris functions like a variable aperture in a camera.

The nature of the ocular media, comprising the cornea, aqueous humour, lens and vitreous humour varies between different bird species (Lind and Kelber, 2009).

The retinae of birds do not possess blood vessels (they are termed 'anangiotic'). However, a structure called the pecten oculi provides nourishment and oxygen to the retina through the presence of rich blood vasculature in it. The pecten is a non-sensory structure, which is highly pigmented and rich in blood supply. The primary role of the pecten is to provide nourishment and oxygen by diffusion through the vitreous medium, as well as to maintain acid-base balance (Jones et al., 2007). The size of the pecten varies between bird species. In addition to the pecten, blood supply to the avian retina is through a vascular layer behind the choroid called the choriocapillaris (Fred and Kenneth, 1984).

The retina is the photosensitive layer in the eye. The photoreceptive cells in the retina are the cones and the rods, whose number and distribution on the retina varies from species to species. The cones cells are responsible for vision under conditions of bright light, and for colour vision. There are two classes of cones in the retina of birds namely, single cones and double cones. There are four spectral types of single cones, which are sensitive to red, green, blue and near-ultraviolet or ultraviolet (UV) light, respectively (Bowmaker et al., 1997). The spectral sensitivity of these cone types, and their number and distribution on the retina vary from species to species. The importance of ultraviolet sensitive cones in avian vision has been investigated to a limited extent where it has been to shown to play a role in discriminating blackberries that carry a wax coating, which reflects strongly in the ultraviolet. This enables the birds to distinguish such berries from a background of green foliage, which does not reflect ultraviolet light (Burkhardt, 1982). It has also been shown in laboratory experiments with zebra finches that UV vision helps discriminate between various types of seed (Church et al., 2001). Zebra finches and budgerigars also use ultraviolet - induced fluorescence for mate choice. The female birds show a preference for males that show the strongest ultraviolet - induced fluorescence from the plumage (Arnold et al., 2002; Bennett et al., 1996; Pearn et al., 2001).

The inner segments of cone cells contain oil droplets with a high concentration of carotenoid pigments that block short wavelengths and transmit long wavelengths (Bowmaker et al., 1997). These oil droplets help to enhance colour discrimination by reducing the spectral overlap between spectrally adjacent cones (Vorobyev, 2003). In some birds, nearly half the population of the cone cells is composed of so-called 'double' cones. Each double cone consists of two cone cells, which are in physical as well as electrical contact

with each other (Hart, 2001). The primary cone cell has an oil droplet in its inner segment, while the accessory segment does not have an oil droplet (Nishimura et al., 1980). The double cones are sensitive to long wavelengths (Goldsmith and Butler, 2005; Goldsmith and Butler, 2003). The exact function of double cones is still not known but previous studies suggest that they could be responsible for motion perception and brightness discrimination (Hart, 2001; v. Campenhausen and Kirschfeld, 1998). They are not involved in colour vision in birds (Goldsmith and Butler, 2005). My studies (Chapter 3) suggest that the double cones could be responsible for the detection of object boundaries (Bhagavatula et al., 2009).

The rods are responsible for vision under low light levels. There is only one class of rods in the retina of birds, and they do not contain oil droplets (Kram et al.). Birds such as owls have a large number of rods in their retina, as they are nocturnal. The fovea, or *area centralis*, is the region of the retina that has the highest density of cone cells and is free of rod cells. Birds like raptors (eagles, hawks and falcons) are bifoveate, with a central and temporal fovea. The central fovea is responsible for lateral vision and fixation to distant objects, whereas the temporal fovea is responsible for frontal and binocular vision. These birds have a very high visual acuity in both the frontal and lateral fields of view and can view objects separated by 180 degrees, without having to turn their heads. However, owls, Andean condors and American black vultures are an exception in that they have a single fovea (Jones et al., 2007). In the case of owls, the eyes are positioned at the front of the head and hence have a high degree of binocular overlap. Their retinae possess only a single, temporal fovea, suggesting that the eyes are dedicated primarily to high-acuity vision in the frontal visual field. These features are consistent with the need for high-

acuity, frontal stereo vision for interception and capture of prey (Jones et al., 2007). Pigeons have laterally positioned eyes with a single fovea. They have a lateral visual field of view of about 300 degrees with minimum binocular overlap. This organization is typical of birds that are prey, as it enables reliable detection of a potential threat from almost any direction. There is also a blind spot in the retina where photoreceptors are absent. This corresponds to the retinal region in which the optic nerve leaves the eye.

The avian visual system has been investigated in detail from an anatomical and physiological perspective. There is diversity among bird species with respect to the shape of the head, bill, position and structure of the eyes, and with respect to how the visual information is processed by the brain (Jones et al., 2007; Martin, 2007).

However, a large number of questions related to visually guided flight in different species of birds remain unexplored. Critical questions, such as the precision of landing on the moving branch of a tree, flying through narrow gaps and avoiding obstacles while flying between branches of trees remain largely unaddressed. Evidently, birds have evolved an effective set of visual algorithms that process information in real time and generate effective motor outputs which enable birds to solve these problems. It remains an open question as to what these algorithms are.

1.5 Visual control of flight in landing birds

Prof. David Lee at the University of Edinburgh originally proposed the so-called 'tau theory' to describe the landing behaviour of birds mathematically. 'Tau' (τ) is defined as the time to contact or to pass a landmark during flight at a constant approach velocity. When gannets (*Sula bassana*) dive into the ocean to catch

fish, they close their wings at a specific time point (τ) before touching the water surface (Lee and Reddish, 1981). Interestingly, the plummeting birds hold τ relatively constant at 820 milliseconds, irrespective of the speed at which they approach the water. This is a useful strategy, because, from the point of view of achieving effective motor control it is more important to ensure that the wings close at a specific *time* before touching the surface, rather than at a particular distance from the surface. A constant-distance strategy will produce premature wing closure at slow diving speeds, and delayed wing closure at high diving speeds.

Visual control of flight during landing has also been studied in pigeons and hawks (Davies and Green, 1990). Films of the landing trajectories of hawks and pigeons revealed that, while hawks extend their feet at a time τ = 160 ms prior to landing, pigeons do not use time-to-contact in the same way. Rather, pigeons control their braking while landing by holding the rate of change of τ ($\dot{\tau}$) constant.

How do birds make a decision about where to land? (Moinard et al., 2004) investigated the landing behaviour of domestic chickens. They observed that chickens tend to fixate the target at a location on the retina that is not a region of high visual acuity. Their data suggests that chickens do not inspect potential landing sites with high visual acuity. This finding is very significant, as the region of high visual acuity is located around the *area centralis* -- an area of the retina that is rich in single cone cells and devoid of double cones and rods. All areas that lie outside this region are rich in double cones, which are thought to be responsible for motion detection (Hart, 2001). Thus, it is possible that chickens tend to fixate the landing site using an area of the retina that is rich in double

cones. My thesis investigates the idea that double cones play an important role in motion perception and contrast detection.

Chapter 3 of this thesis describes an investigation of the landing behaviour of budgerigars, and evaluates the roles played by the different spectral classes of photoreceptors in this task.

1.6 Optic flow

The term 'Optic flow' was coined by Gibson in the year 1950 (Gibson, 1950) Optic flow is defined as the apparent motion of the environment that we perceive while we travel through the environment. When we ride a bicycle or travel in a bus, objects that are closer to us appear to move faster than objects that are farther away. The magnitude of the optic flow that is induced by an object also depends on the angle between the object and the observer's direction of motion. This magnitude is zero when the object is directly in the line of motion, and is largest when the object is positioned laterally, i.e. 90 degrees from the direction of the observer's motion. Although the optic flow is almost zero for objects directly in front of the moving observer, the edges of the object, which are not in directly in front, will induce optic flow and the object will appear to enlarge in size as the Observer moves towards it. Optic flow has gained considerable interest in visual neuroscience as it provides the viewer with rich information about the three dimensional nature of the surroundings. The use of optic flow information for navigation has been reported primarily in flying insects, such as bees and flies (Kern et al., 2006; Kirchner and Srinivasan, 1989; Schilstra and Hateren, 1999; Srinivasan et al., 1996; Srinivasan et al., 1991; Srinivasan and Zhang, 2000).

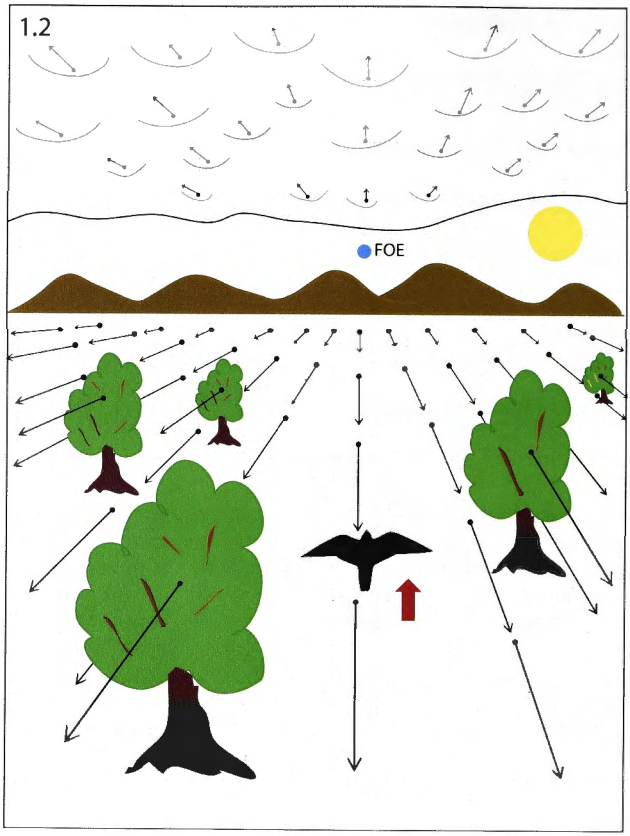

Figure 1.2 The pattern of optic flow pattern that would be experienced by a bird while flying over the country side. The red arrow shows the direction of flight. The black arrows show the flow fields experienced by the bird during flight by various objects like trees, ground features and the clouds in the sky. The Blue dot shows the 'Focus of Expansion' (FOE), which lies directly ahead in the visual field of the bird and does not produce any optic flow. The yellow circle shows the position of the sun which is located at infinite distance from the bird and hence does not produce any optic flow.

Figure 1.2 illustrates the pattern of optic flow that would be perceived by a bird while flying in a straight line over the countryside. Objects like trees, which are closer to the bird, would induce a large magnitude of optic flow as compared to the ground, which is relatively farther away. Mountains at a distance, or the clouds in the sky would induce comparatively weak optic flow, as they are located very far away. The sun, which is millions of miles away, appears virtually stationary and does not induce any optic flow. Thus, when an observer moves in a straight line, the magnitude of the optic flow that is generated by an object in the environment depends upon (a) its distance from the observer (b) its bearing in relation to the observer's heading direction and (c) the speed of motion of the observer.

1.6.1 Optic flow in birds

Birds navigating through a cluttered environment require real time information about the position of the ground and the surrounding obstacles in the form of trees and branches. However, in order to fly in a collision free manner in such a diverse and constantly changing environment, birds also have to process visual information accurately, and in real time, to generate motor outputs. Some studies of visually guided flight have been undertaken in pigeons and to a lesser extent in chickens, gannets, hawks and humming birds. However, most of these studies have focussed primarily on landing behaviour.

Zebra finches (*Taeniopygia guttata*) use saccadic gaze shifts in order to segregate translational optic flow from rotational optic flow. However these birds have been observed to keep their head stable between each saccade, presumably in order to gather lateral optic flow information for the purpose of estimating the range to objects (Eckmeier et al., 2008).

Optic flow can be categorized into two types, namely, 'rotational' and 'translational' optic flow

1.6.2 Rotational optic flow

In flying insects and birds, rotational optic flow provides information about unwanted yaw, pitch and roll movements of the body. For any rotational movement about the three body axes -- or any other axis -- the image of the environment on the retina moves in the opposite direction (Figure 1.3).

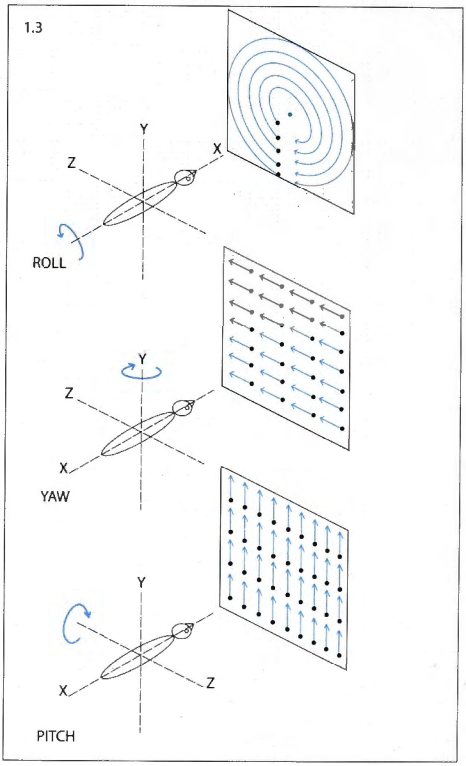

Figure 1.3 Illustration of how yaw, pitch and roll can be sensed by the rotational optic flow information that is experienced by the visual system, and used to make compensatory adjustments during flight.

Flying insects sense the patterns of optic flow that are induced by these rotations, and their wings generate torques to counteract deviations from the desired flight direction and attitude (Borst and Egelhaaf, 1993; Egelhaaf and Borst, 1993; Götz, 1964; Götz, 1965; Hassenstein and Reichardt, 1956; Kern et al., 2006; Krapp and Hengstenberg, 1996; Reichardt, 1969; Srinivasan and Zhang, 2004). For example, if an insect, while flying through the environment, experiences a downdraft of wind that causes a downward pitch of the body and head, then the image on the retina will move upwards. The insect can then use this information in order to make a compensatory upward pitch adjustment to restore its original flight attitude. Hence, the rotational optic flow that is sensed by the visual system of an insect can be thought of as the input to a visually driven gyroscope that helps stabilize flight direction and attitude. In blow flies (*Calliphora vicina*), fast saccadic movements of the head and body were recorded by placing miniature sensor coils on the head and thorax (Schilstra and Hateren, 1999). These experiments showed for the first time that roll movements of the thorax are compensated by counter roll movements of the head, thus assuring that the head maintains a constant attitude with respect to the horizontal. Similarly, the yaw turns of the thorax are followed by compensatory yaw movements of the head, which starts with a delay and finishes earlier than the body yaw movement. Stabilization of the head about all of the three angular degrees of freedom (yaw, pitch and roll) is better than stabilization of the thorax. The function of these head movements is to (i) stabilize vision and reduce motion blur, and (ii) reduce the rotational optic flow component so that the residual translational optic flow can be used to extract information on the range to objects (Schilstra and Hateren, 1999).

Since it is difficult to estimate head movements using high-speed video data, Kern and colleagues developed an algorithm based on available data about the position of the body to estimate the position and attitude of the head. This algorithm accurately estimates the position of the head and also provides better insight into how blow flies are able to derive lateral optic flow information by stabilizing their head movements during flight (Kern et al., 2006; Reichardt, 1969).

1.6.3 Translational optic flow

Translational optic flow is generated in an observer's retina when they move in the environment along a straight line.

Translational optic flow can provide information about a bird's forward flight velocity, as well as information on the relative distances of various objects in the environment (Figure1.2). When an observer moves forward along a straight line, the translational optic flow vectors radiate outward from a point directly in front of the observer called the focus of expansion (FOE; see Figure 1.2). The optic flow will be zero at the FOE, but all points around the FOE will generate optic flow vectors whose magnitudes increase as the viewing direction moves away from the FOE. Of course, the magnitude of the optic flow in a particular viewing direction will also depend upon the distance of the object that is being viewed – it will be inversely proportional to the object's range.

Chapter 4 of this thesis examines the role of optic flow cues in guiding budgerigar flight.

1.6.4 Investigating the perception of rotational optic flow: The optomotor response

Our present understanding of motion detection in insects derives from the study of the so-called 'optomotor response'. This response manifests itself as a tendency to follow the angular movement of the surrounding objects during locomotion. This compensatory reaction, known as the 'optomotor response', helps the animal maintain straight and level flight. Any deviation from the intended straight-line course evokes a compensatory response from the insect which tends to return it to the original course (Götz, 1964; Götz, 1965; Hassenstein and Reichardt, 1956; Reichardt, 1969).

In the sixties, Werner Reichardt and colleagues (Reichardt, 1969) carried out a series of elegant behavioural experiments in which a tethered fly was suspended in an arena consisting of a drum which displayed black and white stripes. When the drum was rotated it was observed that the fly would rotate in the same direction about the vertical axis. The properties of the optomotor response are illustrated in Figure 1.4.

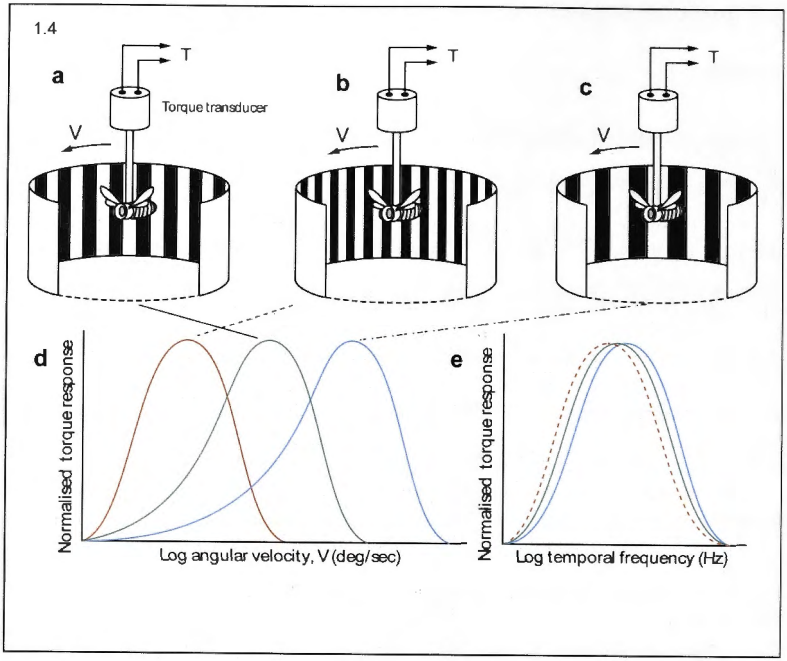

Figure 1.4 Experiments investigating the characteristics of the optomotor response of flying insects. The stimulus consists of a rotating drum carrying stripes of various spatial periods, as illustrated in a, b and c. The response is measured as the yaw torque produced by the tethered, flying insect as it views the turning drum. For each spatial period, the response varies as a bell-shaped function of the angular velocity of the drum, as shown in d. As the spatial period of the stripes is lowered (i.e. as the stripes are widened) the peak of the response occurs at a higher rotational velocity, as shown in d. However, if the responses are re-plotted as a function of the temporal frequency of the intensity fluctuations that are induced in the photoreceptors by the moving stripes, one finds that the responses for all of the striped drums peak at the same temporal frequency, as shown in e. Thus, the strength of the optomotor response

appears to be governed by the temporal frequency of the intensity fluctuations that are produced by the moving pattern, and not by its angular velocity.

When a tethered insect is placed in a rotating drum with striped patterns on the walls, the rotation of the drum will evoke a compensatory response from the insect, which will attempt to turn in the direction of the drum. The tether holding the insect is connected to a torque transducer, which measures the yaw torque that the insect produces during flight. This yaw torque is a measure of the insect's turning tendency, the so-called optomotor response.

If the angular period of the stripes lining the drum is kept constant and the angular velocity (rotational speed, in degrees/second) of the drum is varied, the strength of the optomotor response varies in a bell-shaped curve as shown in the green curve of Figure 1.4d. The response is weak at very low angular velocities (approaching a stationary drum) as well as at very high angular velocities, but is strong at an intermediate velocity. If the stripes are made finer, (angular period decreased, Figure 1.4b), one obtains a similar bell shaped curve, but with the peak shifted toward the left, to a lower angular velocity (red curve, Figure 1.4d). Making the stripes coarser (increasing the angular period, Figure 1.4c) has the opposite effect (blue curve, Figure 1.4d). An interesting insight appears, however, if these curves are re-plotted to show the variation of the response as a function of the temporal frequency of optical stimulation that the moving striped pattern elicits in the photoreceptors. This temporal frequency is given by the number of dark (or bright) stripes passing the receptive field of a given photoreceptor per second. All of the curves then peak at the same temporal frequency, and exhibit similar widths (Figure 1.4e). This implies that the movement-detecting system underlying the optomotor response is not

sensitive to the angular velocity of rotation of the drum *per se*: the angular velocity at which the response is strongest depends upon the angular period of the stripes. The optomotor response thus depends upon the temporal frequency of optical simulation that is induced by the stripes, and not by the angular velocity of the stripes. This property is true for a number of insect species [e.g. *Chlorophanus* beetle: (Hassenstein and Reichardt, 1956); housefly *Musca*: (Fermi and Richardt, 1963), (Wehrahn, 1986), (Eckert, 1973); fruitfly *Drosophila*: (Götz, 1964; Götz, 1965), as well as honeybees (Kunze, 1961)].

1.6.5 The Hassenstein-Reichardt model of movement perception

Hassenstein and Reichardt (Hassenstein and Reichardt, 1956) investigated the optomotor response of the beetle *Chlorophanus.* The beetle was attached by its thorax to a stationary tether inside a rotating striped drum. Its tendency to turn with the drum was expressed in the form of leg movements, which the investigators monitored by tracking the rotation of a Y maze globe that the insect held with its feet. The rate at which the beetle rotated this globe was taken to be a measure of the strength of the beetle's (intended) turning response. Quantitative analysis of the variation of the strength of the beetle's turning response with the speed and spatial texture of the striped pattern on the drum led to the development of a model of motion perception which has now come to be known as the *Reichardt correlation model* of motion perception (Reichardt, 1969).

According to this model, movement of the image on the retina is detected as follows. Consider two neighbouring retinal photoreceptors, A and B, viewing adjacent regions of a moving scene (Figure 1.5).

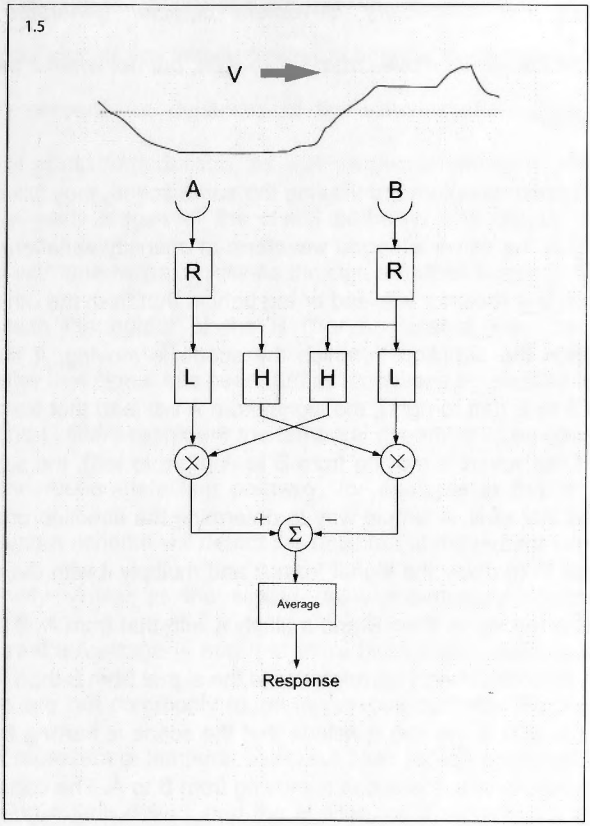

Figure 1.5 Schematic illustration of a directionally selective elementary motion detector (Srinivasan et al., 1999). A and B represent two photoreceptor cells in neighbouring ommatidia. The arrow shows an object moving from left to right in front of the two photoreceptors A and B. The moving object induces a signal in B at a later time than in A. The signal from each photoreceptor passes through the temporal filter R and then through a second set of temporal filters L and H. Ultimately, the signal coming through R and L from photoreceptor A is multiplied with the signal coming through R and H from the neighbouring photoreceptor B. As a result of this scheme of correlating signals from neighbouring

photoreceptors, the elementary movement detector generates a strong response when the object moves from left to right, but not when it moves in the opposite direction.

Since the two photoreceptors are viewing the same scene, they will register the same signal (i.e. the same temporal waveform of intensity variation). However, the signal from one receptor will lead or lag behind that from the other receptor, depending upon the direction in which the scene is moving. If the scene is moving from A to B (left to right), the signal from A will lead that from B. On the other hand, if the scene is moving from B to A (right to left), the signal from A will lag behind that of B. A simple way to determine the direction of movement, then, would be to (i) delay the signal from A and multiply it with the signal from B; and (ii) delay the signal from B and multiply it with that from A. If the delayed signal from A is more strongly correlated with the signal from B than the delayed signal from B is with A, we can conclude that the scene is moving from A to B; and if the opposite is true, the scene is moving from B to A. The correlations are performed by the 'Multiplication' boxes, and the 'Average' box, which computes the time average of the multiplied signals. The response of the circuit is positive (excitatory) if the scene moves to the right and negative (inhibitory) if the scene moves to the left. A neural circuit of this nature, that uses delay followed by multiplication, can provide a reliable indication of the direction of motion of the scene along one axis (left or right) within a small patch of the insect's visual field. Conceptually, it is known as an 'Elementary Movement Detector (EMD)' (Borst and Egelhaaf, 1993).

The EMDs that are actually believed to be present in the insect eye do not perform a simple delay-and-correlate. Rather, they incorporate different

temporal filters of the photoreceptor outputs, as shown in Figure 1.5. The photoreceptor signals are initially filtered in time by the temporal filters labelled R, which represent the dynamics of the visual system. This includes the dynamics of photo transduction, as well as the dynamics of other processes occurring at early stages of the visual pathway. The output of the R filter associated with one receptor passes through a further temporal filter, L, and is multiplied with the output of the R filter associated with the neighbouring receptor, after that signal has been further processed by another temporal filter, H. The L and H filters represent the temporal dynamics of processing at higher levels of the motion-detecting pathway, for example in the lamina and the medulla. Such a scheme will detect the direction of movement in a manner that is qualitatively similar to the simple delay-and-multiply scheme discussed above. Its real advantage is that it is more biologically realistic, because pure time delays are not commonly found in nervous systems. For example, the L filter could represent a temporal low-pass filter (which produces a phase lag, approximating a time delay), and the H filter could represent a temporal high-pass filter (which produces a phase lead, approximating a time advance). The model is excellent at predicting the variation of the strength of the steady-state optomotor response as a function of the speed, spatial structure and contrast of a motion stimulus consisting of a moving sinusoidal grating (Hassenstein and Reichardt, 1956; Reichardt, 1969).

The validity of the Reichardt model has been investigated in a number of insects (see references above) and other animals including birds (Wolf-Oberhollenzer and Kirschfeld, 1994) and wallabies (Ibbotson et al., 1998).

1.7 Obstacle avoidance in flying birds

Birds often fly through cluttered terrain composed of natural obstacles like trees, branches of trees, hills, valleys and so on. In addition, birds encounter manmade structures like buildings, power lines and windmills. Most of these obstacles are encountered during short-range navigation when flight altitudes are lower. Moving obstacles, such as windmill blades, pose a threat to birds (Desholm and Kahlert, 2005). Obstacle avoidance has been investigated in pigeons (*Columba livia*). A subpopulation of neurons in the nucleus rotundus in the pigeon brain produces a strong response when a pigeon approaches an object in its flight path. These neurons respond at a specific time point before collision occurs, and the response is independent of the velocity of approach or the size of the object, suggesting that these neurons may indeed be computing the time to contact, Tau. Their study, however, falls short of making a claim about the role of these neurons (Wang and Frost, 1992). In a separate study, tree swallows (*Tachycineta bicolor*), when confronted with two apertures through which they can potentially fly, will choose to fly through the large aperture (Mandel et al., 2008).

No systematic study has been carried out to investigate the importance of vision in facilitating obstacle avoidance during bird flight. Chapters 5 and 6 of this thesis address this problem in greater detail.

1.8 The budgerigar, a model system for the study of visually guided flight in birds

The budgerigar (*Melopsittacus undulatus*) is a native Australian bird found mostly in inland Australia. The wild type budgerigar has a predominantly green

body and a yellow head. Budgerigars are primarily desert birds, which live in large flocks in the wild. They are local migrants, moving from one place to another in search of seed and water. The local migratory pattern is determined by the seasons and the amount of rainfall in a particular region (Wyndham, 1982). In the wild the budgerigar is predominantly a seed eating species. Budgerigars fall under the category of least concern (LC) in the IUCN (International Union for the Conservation of Nature) Red Data Book (http://www.iucnredlist.org/apps/redlist /details/142523/0). They are easy to breed in captivity, and are popular as a pet.

All the budgerigars sold in pet shops are bred for the colour of their plumage. The breeding is not scientifically documented and is carried out in a largely ad hoc fashion. No importance is given to the genetic basis of colour vision during such breeding practices. Moreover, the genome of the budgerigar has not been sequenced and the loci of the various genes responsible for vision and feather colour have not been mapped to the chromosomes. Thus, results obtained from experiments carried out with budgerigars with different feather colours other than the wild type budgerigars are likely to be biased. Hence it is advisable to carry out experiments involving colour vision, and vision in general, using wild type budgerigars.

One the earliest studies of the visual system of the budgerigar were carried out in 1935 by Martin Plath on their colour discrimination ability (Plath, 1935). His observations revealed that budgerigars have the ability to discriminate between eight different colours, namely, yellow, orange, red, violet, ultraviolet, ice blue, sea green and leaf green (Plath, 1935).

Budgerigars have a well-developed visual system, which is composed of four different types of single cones containing photopigments that are sensitive respectively to red (λmax 581 nm), green (λmax 513 nm), blue (λmax 462 nm) and ultraviolet (λmax 365 nm) (Bowmaker et al., 1997; Goldsmith and Butler, 2003). Each cone carries an oil droplet in its inner segment, which acts as a long pass filter that transmits light of wavelengths greater than a particular cut off value (Vorobyev, 2003). In addition to the four classes of single cones, the retina of the budgerigar carries a further class of cones called the double cones. About 50% of the total photoreceptors in the retina are composed of double cones. Each double cone is composed of two cone cells, which are in electrical and physical contact with each other, the primary one with an oil droplet and the accessory one without an oil droplet (Hart, 2001).

The ability of the budgerigar to see fluorescence induced by ultraviolet light helps it in mate selection (Arnold et al., 2002; Pearn et al., 2001). Due to its excellent ability to perceive colours both in the visible and ultraviolet region of the spectrum, the budgerigar is an excellent model system for the study of colour vision and visually guided behaviour in birds (Arnold et al., 2002; Bhagavatula et al., 2009).

The flicker fusion frequency of the budgerigar is known to be in the vicinity of 115 Hz (Ginsburg and Nilsson, 1971). This enabled some of the experiments described in this thesis (the experiments in Chapter 3) to be carried out using standard fluorescent tubes operating at a standard line power frequency of 50 Hz, which produces flicker at 100 Hz (Ginsburg and Nilsson, 1971). However in all remaining experiments, high-frequency fluorescent lamps running at 40,000 Hz were used (see General Methods chapter (Chapter 2)).

The eyes of budgerigars are positioned laterally on either side of the head, thus making them suitable experimental animals for investigating the use of lateral vision in birds. Hence the choice of budgerigar to investigate the importance of lateral optic flow in free flying birds. The number of fovea in the retina of a budgerigar is not known, and there is some unpublished evidence that they may not have one at all (Mitkus, pers communication). Budgerigars can be trained to fly from a perch to a feeder, or to another perch. (Further technical details about the maintenance and training of the budgerigar are discussed in the 'General Methods' chapter (Chapter2) section 2.3 of this thesis). Budgerigars, being agile fliers, have also served as experimental subjects in studies of flight metabolism (Tucker, 1966).

1.9 Objective of this thesis

Considerable progress has been made at The Australian National University's Research School of Biological Sciences (presently the Research School of Biology) towards unravelling how flying insects use visual information to manoeuvre and navigate effectively in their natural world. Work over the past decade has shown how insects use their visual system to avoid collisions with obstacles, negotiate narrow gaps, control flight speed, estimate distance flown, and orchestrate smooth landings (Srinivasan and Zhang, 2004). It appears that insects rely heavily on cues derived from optic flow (the pattern of image motion that is experienced by the eyes during flight through the environment) to execute these manoeuvres.

On the other hand, relatively little is known about how vision guides moment-to-moment flight in birds. The broad aim of my thesis is to explore the visually guided flight behaviour in an iconic Australian bird, the budgerigar. Using a series of custom designed experimental arenas with different visual

patterns and designs, I have tried to address some of the questions highlighted below, under controlled laboratory conditions.

Specifically, the aims of this study are

To investigate the visual cues that budgerigars use to (a) find stationary targets and land at them, (b) negotiate narrow passages, (c) avoid collisions with obstacles close to their flight path and (d) control head and body orientations during flight.

The second chapter of this thesis describes the general aspects of the experimental methods used in this study, including the technique of stereo motion capture which was used for all the experiments (with the exception of Chapter 3), as well as the budgerigar maintenance and training procedures.

The third chapter investigates what visual cues budgerigars use to target their landings. It details the mechanism of edge detection used by the budgerigar to guide it precisely to the landing site.

The fourth chapter explores how budgerigars use optic flow cues to steer safely through narrow passages.

The fifth chapter begins to investigate how budgerigars avoid obstacles and select flight paths through cluttered environments. It also addresses the problem of laterality and side bias in free flying budgerigars.

The sixth chapter investigates the finer details of head and body movements that budgerigars produce while negotiating narrow spaces.

In addition to the results chapters, other minor observations and future directions are discussed in the Appendix 1.

A mathematical model describing how budgerigars choose between two apertures of different sizes is presented in Appendix 2.

The geometry of the markers that are used to track the orientations of the head and the body of budgerigars in flight is discussed in detail in Appendix 3.

Chapter 2
General Methods

2.1 Ethics Statement

All experiments were carried out in accordance with the Australian Laws on the protection and welfare of laboratory animals, and with the approval of the Animal Experimentation Ethics Committees of The Australian National University, Canberra, Australia, and the University of Queensland, Brisbane, Australia.

2.2 Subjects and housing

Adult male wild type budgerigars (n=3-8, approximately 1 year old) served as subjects for the experiments. The birds were obtained from different local breeders. Male budgerigars were identified by a characteristically green plumage and a distinctly blue colouration of the cere. The birds were housed in pairs in identical cages of length 47 cm, breadth 34.5 cm and height 82 cm, and were not under acoustic or visual isolation. A photograph of the budgerigar handler and experimenter – namely, myself - was permanently affixed on the inside back wall of each cage. This process of imprinting proved useful as it helped the budgerigars become accustomed to the handler (experimenter).

All of the birds were housed indoors in a room of length 400 cm, width 300 cm and height 240 cm in Canberra and length 474 cm, width 294 cm, height A 332 cm and height B 269.5 cm (Two different values of height indicate a sloping roof) in Brisbane. The lights were controlled by an automatic timer (WF, WF-60A, Hagemeyer, UK Ltd.), which provided a 12:12 L:D photoperiod in

Canberra and by an automatic timer (HPM, Excel Light Switch and Timer, Cat XL770T) in Brisbane.

Seed and water were provided *ad libitum*. The budgerigars were supplied with commercial budgerigar seed mix (*Trill* budgerigar seed mix, Wacol, Queensland, Australia). The feed contained a mixture of seeds, shell grit and essential vitamins and minerals. The birds were also fed occasionally with apples and greens.

Daily, the birds were moved to an adjoining screened patio (in Canberra) of length 763 cm, width 203 cm and height 231 cm and (in Brisbane) of length 540 cm, width 230 cm and height 180 cm, where they were released from their cages and allowed to fly between perches. This enclosure provided the opportunity for regular flight as well as exposure to natural daylight. It also contained a bird bath.

2.3 Training

The budgerigars were all trained to take off upon slow rotation of the perch. This method worked well, and was used in preference to other methods ((Tucker, 1968) e.g. Where a mild electrical shock was applied to the feet).

Inexperienced birds learned faster when they had an opportunity to observe the behaviour of an experienced bird in the experimental arena (Goldsmith and Butler, 2005). Hand feeding of young budgerigars helped in their habituation to the experimenter. Vocalization ('Good' and 'No') and pitch modulation by the experimenter, which could be interpreted by the budgerigars as appeasement or threat (Morton, 1977) also helped in the training.

The training of the budgerigars was carried out in the following stages.

Stage 1 involved training the bird to sit on a perch. This was done by pressing the perch gently against the bird's chest. After a few repetitions over a few days, the bird would automatically move on to a perch that was placed in front of it.

Stage 2 involved acclimatising the bird to being moved from one location to another whilst sitting on the perch. The experimenter presented a perch to the budgerigar, which had now been trained to climb on to it, as described above. Then the perch, along with the budgerigar, was gently moved out of the cage into the experimental arena. Care was taken to ensure that the perch was moved smoothly and steadily. Any sudden movements of the perch were avoided as it would scare the bird and delay the training procedure.

Stage 3 involved training the budgerigar to take off from the perch upon slow rotation of the perch. The procedure was simple and did not cause any distress to the birds. Furthermore, it allowed the experimenter to have complete control over the time point at which the budgerigar was induced to take off.

Stage 4 involved training the budgerigar to fly towards and land on another wooden perch, placed at the other end of the experimental arena. A perch was fixed at one end of the tunnel while the bird was released from the other end by slow rotation of the perch. After a few training trials, the budgerigar learned to fly towards the end of the tunnel and land on the fixed perch. This training step was essential as it taught the bird to fly along the entire length of the tunnel.

Stage 5 involved training the budgerigar to fly the entire length of the tunnel, turn 180 degrees and fly back to the experimenter. This step was employed to train the budgerigars for the experiments described in Chapter 4 (The use of optic flow by flying budgerigars).

Stage 6 involved training the budgerigar to fly the entire length of the tunnel and then exit at the end of the tunnel. In order to induce the budgerigar to exit at the

end of the tunnel a partner bird was kept in a cage outside the exit of the end of the tunnel. This training step was employed to train the budgerigar for the experiments described in Chapter 5 (Obstacle avoidance in flying budgerigars) and Chapter 6 (Head and body movements of budgerigars during complex flight manoeuvres).

The duration of training that was required varied with each individual bird. Typically, this duration was 7-10 days.

Training was deemed to be complete when the following conditions were met:

i) The birds took off consistently upon slow rotation of the perch.

ii) The birds completed training requirements in stages 4, 5 and 6.

iii) The birds did not give alarm calls during flight and showed no signs of discomfort. The procedures described above are the general training methods, used in all experiments performed in this thesis. Any modifications or deviations from these procedures are described in the individual chapters.

2.4 Tunnel design

The dimensions of the tunnel were as follows: length=728 cm, width=136 cm and height=244 cm as shown in Figure 2.1.

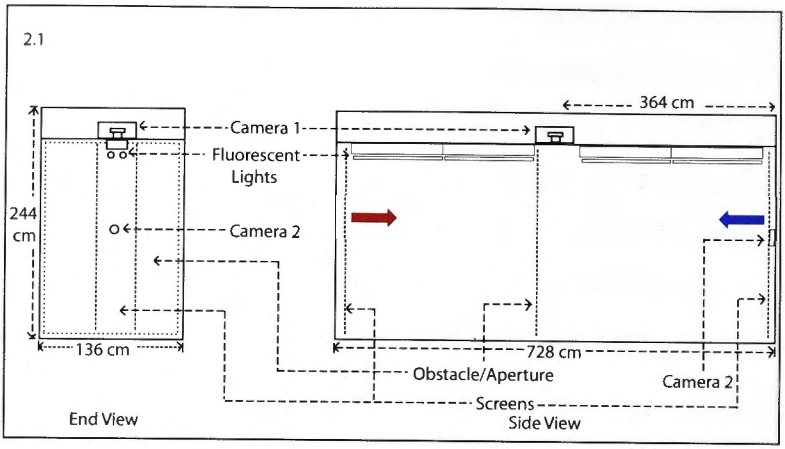

Figure 2.1 Schematic diagram of the tunnel showing the position of the lights and the screens. The red arrow shows the direction of bird flight for the experiments in Chapter 4, and the blue arrow the direction of bird flight for the experiments in Chapter 5 and Chapter 6.

The indoor tunnel was climate controlled (Temperature: 23-25°C, Relative Humidity: 35-40%). The walls and roof of the tunnel were painted with Dulux low sheen Acrylic (white 56289801) containing Wattyl Divinity Dye (Product number: IV68). The floor of the tunnel was painted with Dulux low sheen Acrylic (white 56289801) containing the following Wattyl Pewter Cup Dye (Product number: IV113) and provided no visual texture. This helped to provide a contrasting background against the birds when they were filmed from above. Illumination in the tunnel was provided using Osram fluorescent light tubes, (L 36W/880 Skywhite FLH1, EAN/Product: 4008321002976, Osram, Australia, Pennant Hills, NSW, Australia) operating at 40 kHz using a high frequency electronic ballast (PC T8 Pro 18-58W-240V 50/60/0 Hz, twin lamp Tridonic Atco Australia, Pty Ltd, Tullamarine, Victoria, Australia). There were four lamps in the middle of the tunnel ceiling and each lamp carried two tubes. Black paper (Elle card

135040 ERA1 Black 220 gsm) strips of width 11 cm were cut and pasted on the wall of the tunnel at regular intervals of 11 cm, to create horizontal or vertical gratings.

2.5 Filming and analysis of bird flight in three dimensions

To capture the birds' flight trajectories in three dimensions, I used two synchronized video cameras, placed at different locations in the experimental arena. The synchronized image sequences captured by the two cameras were used to determine the position of the bird (or of a specific part of its anatomy) in three dimensional space, in the form of three dimensional Cartesian co-ordinates.

2.5.1 Camera configuration and installation

Two high speed cameras (DRS lightning RDT, DRS Technologies Inc, USA) were connected to a custom configured Pentium 4 computer, through their respective PCI cards. The cameras were concealed in the ceiling and the rear of the tunnel, with their optical axes oriented 90 degrees to each other as shown in Figure 2.1 and 2.2. The two cameras were synchronized and controlled by special-purpose software (*Midas 2.0*, Xcitex, Inc, USA).

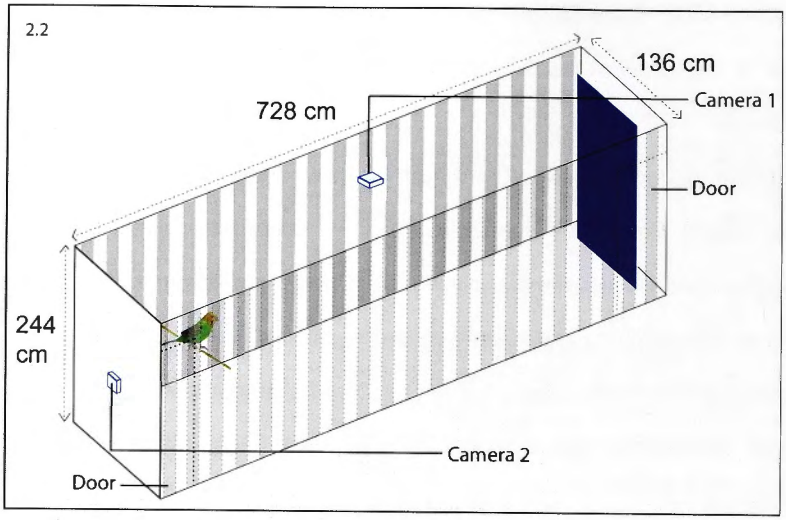

Figure 2.2 Arrangement of two high-speed cameras for filming the bird flight trajectories.

2.5.2 Camera calibration and reconstruction of 3-D trajectories

The stereo calibration of the high speed cameras was carried out using the J.Y. Bouguet camera calibration toolbox (http://www.vision.caltech.edu/bouguetj/calib_doc/). A calibration checkerboard composed of 15 cm x 15 cm black and white checks was prepared on a large sheet of paper (Elle card 135041 A1 White 220 gsm) and fixed to a plywood board as shown in Figure 2.3. With both cameras running, a video sequence pair was captured while the position and orientation of the checkerboard (placed on a stand) were varied smoothly over time, so as to cover all or most of the visual fields of the two cameras. In executing this movement, care was taken to ensure that the face of the checkerboard was always fully visible to both cameras.

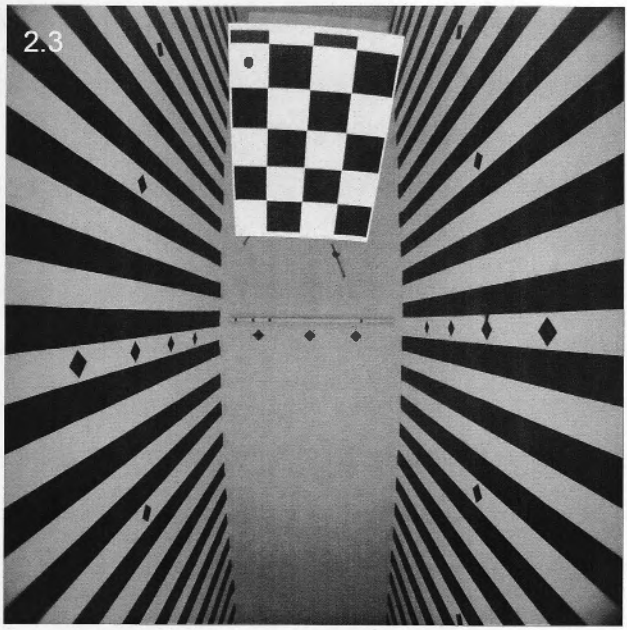

Figure 2.3 Checkerboard pattern (3x4 matrix) used for camera calibration (Each square in the checked pattern is 15 cm X 15 cm and is printed on Elle card 135041 A1 White 220 gsm). The tracking dots on the wall were used for the tunnel calibration as discussed later in Figure 2.4.

The video sequence pair was then fed into special-purpose camera calibration software written in Matlab (http://www.vision.caltech.edu/bouguetj/calib_doc/). The first section of this software (the camera calibration section) used this sequence to calibrate the dual camera setup. It returned information on the 3-D position of the nodal point of one camera relative to the other, the 3-D orientation of the optical axis of one camera with respect to the other, as well as the calibration parameters for each camera to account for various optical distortions such as pincushion and barrel distortion. In performing this calibration, the software only used those pairs of synchronised images in which the checkerboard was clearly and fully visible to both cameras. When the

number of well-conditioned frame pairs was insufficient to perform a reliable calibration, the software produced an error message requesting capture of a fresh checkerboard calibration sequence.

The second section of the software (3-D reconstruction software) was then used to determine the 3-D positions and trajectories of any object (or objects) moving within the experimental arena, as filmed by the video cameras. This procedure involved (a) feeding the synchronized video sequence of the object (or objects) that was captured into the software, (b) displaying each pair of synchronized frames in succession, (c) digitizing the pixel (x and y) co-ordinates of each object within each frame (either manually or semi-automatically), and (d) using the digitized co-ordinates to compute the 3-D trajectory (in x, y and z co-ordinates) of the object (or objects). The program created an output file comprising a sequence of 3-D coordinates defining the successive positions of the object (or objects) with respect to time. The output files created in this way were then analysed using Matlab scripts developed specifically for this purpose. These scripts enabled visualization and analysis of the birds' flight trajectory.

2.5.3 Digitization procedures

2.5.3.1 Digitization of tunnel layout and geometry

The 3-D reconstruction program was first used to reconstruct the geometry of the experimental tunnel in which the birds were flown and to investigate various aspects of their visually guided flight, as will be described in Chapters 4, 5 and 6. This was useful because the known geometry of the tunnel could be used to check the operation and accuracy of the camera calibration and 3-D reconstruction software.

Diamond shaped test markers of 3 cm X 3 cm were placed along the walls and floor of the tunnel as shown in Figure 2.4, at intervals of 350 mm along the transverse axis of the tunnel (on the floor, along the x-axis), 350 mm along the vertical axis (on the two side walls, along the y-axis) and 650 mm along the tunnel's axial dimension (on the floor and side walls, along the z-axis). The procedure described in section 2.5.2 above was used to calibrate the cameras, digitize the positions of these markers, and compute their positions. The results are shown in Figure 2.4.

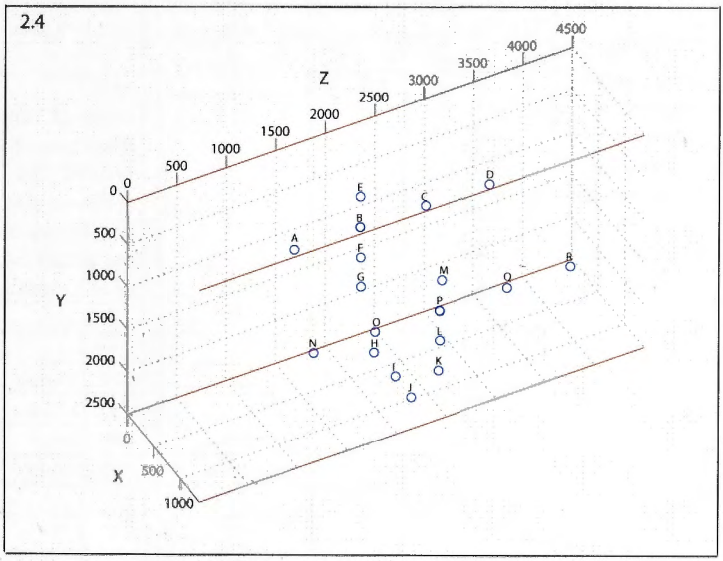

Figure 2.4 3-D plot showing the nominal positions of the test markers placed at various positions along the walls and floor of the tunnel. The tracking dots are shown in Figure 2.3. The distances between the tracking dots are computed in Table 2.1.

Table 2.1 shows a comparison of the true distances and the measured distances between various pairs of test markers, along with the RMS errors in these measurements.

Table 2.1

Tracking dot label	x	y	z		Actual distance between points	Experimentally measured distance between points
				Lengths		
A	12.92	1232	1682	AB	650 mm	669.08 mm
B	7.7	1241	2351	BC	650 mm	662.24 mm
C	7.5	1259	3013	CD	650 mm	652.089 mm
D	4.16	1269	3665			
						RMS error=13.14mm. Percentage RMS error=2.02% (expressed as a percentage of the actual value of 650 mm)
N	1342	1226	1165	NO	650 mm	617.023 mm
O	1347	1223	1782	OP	650 mm	652.11 mm
P	1349	1235	2434	PQ	650 mm	689.21 mm
Q	1350	1252	3123	QR	650 mm	639.32 mm
R	1339	1269	3762			
						RMS error=26.19mm. Percentage RMS error =4.03% (expressed as a percentage of the actual value of 650 mm)
				Height		
E	7.35	887	2354	EB	350 mm	354.01mm
B	7.7	1241	2351	BF	350 mm	354.06 mm

F	13.88	1595	2353	FG	350 mm	338.04 mm
G	17.98	1933	2356			
						RMS error=7.65mm Percentage RMS error =2.19% (expressed as a percentage of the actual value of 350 mm)
M	1357	883.5	2454	MP	350 mm	352.16 mm
P	1349	1235	2434	PL	350 mm	350.06mm
L	1354	1585	2438	LK	350 mm	349.24mm
K	1353	1934	2425			
						RMS error=1.32mm Percentage RMS error =0.38% (expressed as a percentage of the actual value of 350 mm)
				Width		
H	309.8	2476	2334	HI	370 mm	372.78 mm
I	682.2	2481	2350	IJ	330 mm	328.29 mm
J	1010	2473	2334			
					Mean=350mm	RMS error=2.30mm Percentage RMS error =0.65% (expressed as a percentage of the actual value of 350 mm)

Table 2.1 Comparison of the true 3-D co-ordinates of the calibration markers with their reconstructed co-ordinates and the Root Mean Square error for all the values.

2.5.3.2 Digitization of bird flight trajectories

The trajectories of the birds were digitized by affixing tracking dots to the head and body. Custom written Matlab programmes were used to digitize and track the head and body for the experiments in Chapter 4, and the head, body and wing tips in Chapters 5 and 6. For each set of experiments, the cameras were calibrated and the trajectories digitized and reconstructed as described above.

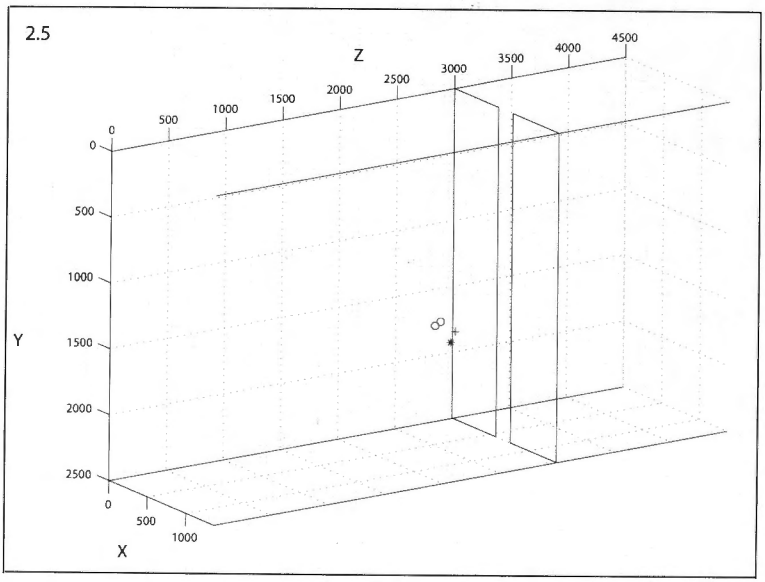

Figure 2.5 3-D plot of the position of a bird at one instant of time during flight though a tunnel before it encountered an obstacle. The plot shows the position of the head ('+'), the body ('') the left wing tip ('o') and the right wing tip ('o'). The solid red lines depict the tunnel boundaries and the solid black lines the boundaries of the obstacle.*

Figure 2.5 shows a reconstruction of the positions of the head, body, and the two wing tips of a budgerigar at one time point in a video sequence that was

captured during flight in a tunnel, in which an obstacle was placed that forced the bird to fly though a narrow vertical opening. Two examples of complete video sequences are given in Videos 2.1 and 2.2.

Chapter 3
Edge detection in landing budgerigars

3.1 Introduction

Over the past few decades, considerable effort has been devoted to investigating how vision guides insect flight, especially in flies and bees (Egelhaaf and Kern, 2002; Ibbotson, 1991; Ibbotson, 2001; Srinivasan and Zhang, 2000). As a result, we now have a reasonably good understanding of how flying insects regulate flight speed, avoid collisions with obstacles, negotiate narrow gaps and orchestrate smooth landings. However, relatively little is known about how birds perform these tasks.

This study begins to address this discrepancy by examining whether, and how budgerigars use visual features to direct and guide their landings. The budgerigar (*Melopsittacus undulatus*) is a native Australian bird found mostly in inland Australia. Budgerigars are highly aerobatic, have a well-developed visual system, and are known to be visually sensitive to the three human primary colours (Plath, 1935), as well as to ultraviolet light (Goldsmith and Butler, 2005). Thus, they provide an attractive model system in which to investigate visual guidance of bird flight, particularly in relation to the use of visual features in the environment, and of colour. Here I investigate what visual cues guide budgerigars towards a landing site.

Earlier studies of visually guided landings in birds have concentrated on identifying the visual cues that trigger various phases of the landing manoeuvre. Gannets plummeting into the sea to catch fish, consistently close their wings at a constant time prior to contact with the water surface, irrespective of the speed at which they approach the water or the height at which they commence their

dive (Lee and Reddish, 1981). When a Harris hawk (*Parabuteo unicinctus*) lands on a perch, it extends its claws in preparation for landing at a constant time (τ) prior to making contact with the perch (Davies and Green, 1990). On the other hand, pigeons (*Columba livia*) show a characteristic head bobbing during landing, which is not observed in case of the hawk (Davies and Green, 1988). This head bobbing may prevent the use of τ as a factor for timing landing in the case of pigeons (Lee et al., 1993). However, in a further study it was shown that pigeons use τ as a factor for landing under conditions of stress (Davies and Green, 1991). In a subsequent study it was shown that pigeons control braking before landing by keeping $\dot{\tau}$, (the rate of change of τ) constant (Troje, 2001).

The aim of my study is to determine whether, and how, the budgerigar uses visual features to decide where to land. I find, firstly, that landings are directed primarily at regions of the scene that carry contrasting visual features, such as the edges of objects. Secondly, I find that the process of detecting the edge appears to be mediated by a 'colour blind' system, although the budgerigar as a whole is known to possess well-developed, tetrachromatic colour vision (Goldsmith and Butler, 2005; Plath, 1935).

3.2 Methods

3.2.1 Experimental arena

All of the birds were housed indoors in a room (of length 400 cm, width 300 cm and height 240 cm), which also served as their training and experimental room. The room did not carry any extraneous visual landmarks. Indoor lighting was provided by means of Phillips daylight fluorescent tubes (Phillips Power Miser

TLD 36 W, NSW, Australia). There were two lamps in the ceiling, with two fluorescent tubes in each lamp. The lights were controlled by an automatic timer (WF, WF-60A, Hagemeyer, UK Ltd.), which provided a 12:12 L:D photoperiod. The lamps operated at the standard frequency of 50 Hz and therefore generated pulses of illumination at 100 Hz. The critical flicker fusion frequency (CFF) of budgerigars has been reported to be in the range of 40 - 75 Hz (Figure 1, (Ginsburg and Nilsson, 1971)). The CFF is in the range of 80-105 Hz for domestic hens (D'Eath, 1998; Railton et al., 2009), 55-105 Hz for African Grey parrots (D'Eath, 1998), and 73–140 Hz for pigeons (D'Eath, 1998), depending upon illumination levels and other factors. Therefore, it is likely that the 100 Hz fluorescent illumination used in our experiments was at or close to the budgerigars' CFF.

The illumination spectrum of the room in which the experiments were carried out was measured. The lights were controlled by an automatic timer (WF, WF-60A, Hagemeyer, UK Ltd.), which provided a 12:12 L:D photoperiod.

3.2.2 Apparatus

The experiments were carried out in the room described above, which did not carry any extraneous visual landmarks. A large horizontal surface was created by arranging nine tables (each of length 79 cm, breadth 79 cm and height 72 cm), in a 3 x 3 matrix. The surface of the table was covered with blue paper (Kingfisher Blue 402275036, Canford paper 150 gsm, Daler Rowney, Bracknell, England) (Figure 3.1A).

Since a single large piece of paper was not available, individual papers of A1 size were pasted breadth wise, using double-sided tape, to form a blue

background (of length 247cm and breadth 256 cm). Upon this background was placed a disc of 41.5 cm diameter, of one of several grey levels ranging from black to white. The grey papers used for the discs were Jet Black (402275004)[1] Mouse Grey (0741657)[2], Sombre Grey (999960202)[2], Dreadnought Grey (402 275 023)[1], Azure Blue Grey (402275003)[1], and Snow White (402275068)[1], ([1]Canford paper, Daler Rowney , Bracknell, Berkshire, England;[2] Canson card, Arjo Wiggins Pty.Ltd , Keysborough, Victoria, Australia).

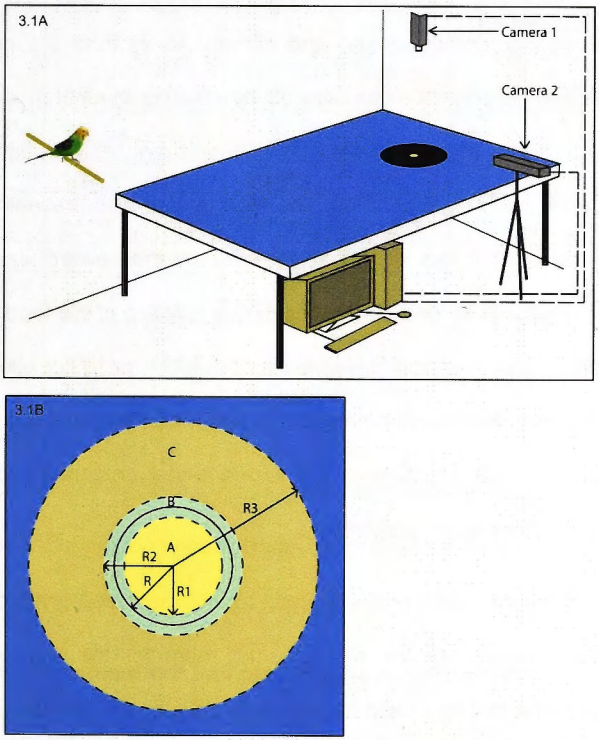

Figure 3.1 Experimental arena (A) Budgerigars were trained in the laboratory to take off from a perch and land at a Petri dish containing bird seed, placed at the centre of a grey paper disc 41.5 cm in diameter. The disc was placed over a blue background of length 247 cm and width 256 cm. The landings were video-

filmed from above and from the side. (B) Illustration of the regions A (yellow), B (blue) and C (light brown) used for the analysis of the spatial distribution of the landings.

3.2.3 Training

The budgerigars were trained to fly from a wooden perch to a feeder, placed in the middle of a grey disc (Figure 3.1A). The feeder consisted of a transparent Petri dish of 8.7cm diameter, containing budgerigar seed mix. For each trial a trained bird was randomly chosen and allowed to fly from the perch to the feeder. The bird was induced to take off by rotating the perch slowly. Upon landing, the bird was allowed to eat a few seeds from the Petri dish. The total duration of each trial was 5 minutes. The food reward was present in all of the trials. The reason for this was that removal of the reward destroyed the motivation of the birds to land near the previous location of the food source and caused them to land randomly anywhere on the table, or to not even leave the perch. During each trial the remaining birds were kept under visual isolation so that they were unable to observe the experimental procedure. None of the experiments involved food deprivation.

On a given day each bird was used for 10 trials on a given colour card, and then kept away from the experimental room for the rest of that day. However the same bird was used for the same colour card on subsequent days, again for 10 trials. Hence, for any given colour card, each bird contributed 30-35 trials. Between 100 and 201 trials were performed for each card. Data from certain trials were excluded from analysis, for the reasons detailed in Table 3.1. 3-6 birds were used in each experiment.

The grey discs as well as the Kingfisher Blue background were replaced when they had acquired a significant number of bird droppings. This was done because the bird droppings created distracting visual features that attracted landings.

Table 3.1

Disc Colour	Total flight trials	Total flights analysed	Total flights excluded	Data excluded due to landings occurring outside region C	Landings discounted due to bird droppings, seeds and visual imperfections	Data lost due to video file corruption
Kingfisher Blue	100	51	49 (49%)	46	2	1
White	100	91	9 (9%)	9	0	0
Azure blue Grey	201	152	49 (24%)	34	11	4
Mouse Grey	100	83	17 (17%)	14	2	1
Dreadnought Grey	201	104	97 (48%)	75	20	2
Sombre Grey	200	162	36 (18%)	29	7	0
Black	200	144	56 (28%)	44	11	1

Table 3.1 Composition of data, showing total flight trials conducted for each disc colour, the numbers of landings excluded from analysis for various reasons, and the number of landings analyzed.

3.2.4 Control experiment to test for colour discrimination

For reasons that will be explained in the Results section, it was necessary to test whether the budgerigars were able to discriminate the colour of the Dreadnought Grey disc from the colour the Kingfisher Blue background. To this end, 4 birds were trained to receive a food reward from a Petri dish placed on the Dreadnought Grey disc, and presented over the Kingfisher Blue

background. After 10 rewarded trials, the trained birds were tested by offering them a choice between two discs, one Dreadnought Grey and the other Kingfisher Blue, both placed side by side with their centres 90 cm apart over the Kingfisher Blue background (Figure 3.2). In the tests each disc carried a Petri dish with a food reward, but the dish was sealed with a transparent lid to prevent access to the food (This was done to avoid reinforcement during the tests). The tests were conducted in blocks of 10 trials, with 10 further training trials inserted between successive test blocks. The spatial positions of the Dreadnought Grey disc and the Kingfisher Blue disc were swapped in consecutive test blocks (It was experimentally impractical to swap the disc positions randomly from trial to trial within a test block, because the discs had to be affixed firmly to the background to prevent edge artefacts). In the tests, the birds flew toward the discs and landed on or close to one of them, thus displaying their choice preference. I measured the relative choice frequencies of the birds for the two test discs, to assess their ability to distinguish between the colours of Dreadnought Grey and Kingfisher Blue.

3.2.5 Recording of bird landings

Landings were recorded using two synchronized video cameras (Jai Pulnix TM-9701d). One camera, attached to the ceiling of the room, filmed the landings from a position above the grey disc while the second camera filmed the lateral view of the landing area. Each camera carried a Computar TV lens with a fixed focal length of 8.5 mm (M 8513; CBC Co., Ltd, Tokyo, Japan). Both cameras captured video at 30 frames per second. The videos were directly recorded on a computer (PC, AMD Athlon) equipped with an ATA Raid controller and Euresys

camera card, using software developed in-house with Visual C and Visual Basic (Microsoft Corporation, Redmond, Washington, USA).

3.2.6 Analysis of video data

The video recordings were analyzed by playing back the video recordings frame by frame and digitizing the position and orientation of the bird at the point of touchdown using a Matlab (Mathworks, USA) program developed in-house. The radial distribution of landing densities was measured by counting the landings that occurred in three concentric regions in and around the disc (described below). The landing density for each region was calculated as the number of landings per unit area in that region.

The three regions were (a) an inner circle (radius (R1) = 34.4 cm), (b) an annular region containing the boundary of the disc (inner radius (R1) = 34.4 cm, outer radius (R2) = 48.6 cm) and (c) an outer annulus (inner radius (R2) = 48.6 cm, outer radius (R3) = 101.6 cm). These regions are shown in Figure 1B as A (yellow), B (light blue) and C (beige) respectively. The disc is shown as the circle with the solid boundary, of radius (R) = 41.5 cm.

The rationale for the choice of these three regions is as follows. I wished to measure and compare the numbers of landings occurring 'inside' the disc and in the 'boundary' region. Since landings directed at the boundary of the disc seldom occurred precisely at the edge, but within a region surrounding the boundary, I defined the 'boundary region' as an annulus containing the boundary, and extending a small and equal distance on either side of it (i.e. with an inner radius R1 and an outer radius R2), and having an area equal to that of the inner circle (A) of radius R1. I defined the inner circle A to be the 'inside

region' of the disc, and the annulus B (of inner radius R1 and outer radius R2) to be the 'boundary region' of the disc. R1 and R2 were chosen such that (i) the area of the boundary region B is equal to that of the inside region A and (ii) the boundary region extends an equal distance away from the boundary on either side of it (i.e. R2-R = R-R1). This choice of equal 'inside' and 'boundary' regions for the disc allowed us to make an objective comparison of the landings occurring within the disc, with the landings occurring at its boundary. If the regions A and B elicit equal numbers of landings, we can infer that the boundary of the disc is just as attractive as the interior of the disc. If B elicits a greater proportion of landings, then the boundary is more attractive; if A elicits a greater proportion, the interior is more attractive. It can be shown that the radii R1 and R2 that describe the sizes of the inner circle and the boundary annulus to satisfy the above constraints are given by R1 = 0.828R and R2 = 1.172R. For a disk of radius R = 41.5 cm (see above) one obtains R1 = 0.828R = 34.4 cm and R2 = 1.172R = 48.6 cm, as indicated above.

The radius R3 of the outermost circle was chosen to define the largest possible area over the surface of the table that excluded regions close to the boundary of the table, and other features on the walls of the room that could potentially produce interfering effects. R3 was chosen to be 101.6 cm, which was close to the edge of the table. Landings occurring outside this region were excluded from the analysis.

The landing density for each region was calculated as the number of landings per unit area in that region. From this, two measures of landing performance were obtained: (i) The *normalized landing density* for each region was calculated by dividing the landing density in that region by the total number

of landings that had occurred within the entire area under consideration (i.e. within the circle of radius R3); (ii) The *landing density ratio* (α) for the boundary annulus was calculated as the ratio of the landing density in the annulus to the average landing density over the entire area under consideration.

Data, obtained with the six different grey discs and the control disc (of the same Kingfisher Blue colour as the background), were analyzed using the method described above.

3.2.7 Definition, measurement and calculation of contrasts

The contrast produced in each spectral class of photoreceptor was calculated as described in Lehrer et al. (Lehrer et al., 1990). The procedure is summarized briefly below.

3.2.7.1 Photoreceptor excitation

The photoreceptor excitation is given by $\int P(\lambda).I(\lambda).R(\lambda).d\lambda$

In the above expression, $P(\lambda)$ is the absorption spectrum of the photopigment. The absorption spectra were obtained from Goldsmith & Butler (Goldsmith and Butler, 2003) by digitizing the curves in the lower panel of their Figure 2 using Digitizeit software (Digital River GmbH, Cologne, Germany). This data, sub sampled and reconstructed using linear interpolation, is shown in Figure 3.3A.

3.2.7.2 Illumination spectrum

$I(\lambda)$ is the illumination spectrum. The illumination spectrum in the experimental area was measured by pointing the probe of a calibrated fibre optic spectrometer (USB 4000 Ocean Optics Inc, Dunedin, Florida, USA) directly at

one of the fluorescent lamps in the ceiling. This illumination spectrum, plotted in relative photon units, is shown in Figure 3.3B.

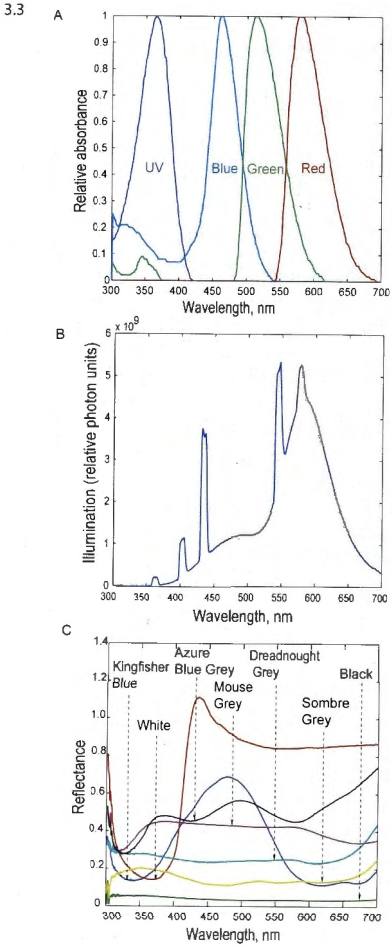

Figure 3.3 Spectral plots. (A) Absorbance spectra of the visual pigments of the budgerigar. (B) Illumination spectrum of the room in which the experiments were carried out. (C) Reflectance spectra of the various discs used in the experiments.

3.2.7.3 Reflectance spectra of papers

The reflectance spectrum (R (λ)) of each of the papers that was used in the experiment (all of the grey level papers, as well as the blue background) was measured by comparing the spectrum of the light reflected from the paper, P(λ), under a source of constant illumination (in this case, outdoors in the sun on a cloudless day) with the spectrum of light, S(λ), reflected from a white reflectance standard under the same illumination. The white reflectance standard possessed uniform reflectance throughout the spectral range of 330 nm – 800 nm. The relative reflectance spectrum of the paper was then calculated as $R(\lambda) = \frac{P(\lambda)}{S(\lambda)}$. (Note that R(λ) can assume values greater than 1.0 if P((λ) is greater than S((λ) at certain wavelengths.)

P(λ) and S(λ) were measured by pointing the probe of the spectrometer at the paper (or the reflectance standard), taking care not to cast a shadow on the surface that was being measured, and that the measured surface covered the entire field of view of the probe. The measurement of each paper was preceded and followed by a measurement of the reflectance standard. The two measurements of the standard were averaged and compared with the measurement of the paper, in order to minimize any errors due to instrumental drift or varying illumination. The relative reflectance spectra of the various papers used in the experiments are shown in Figure 3.3C.

3.4

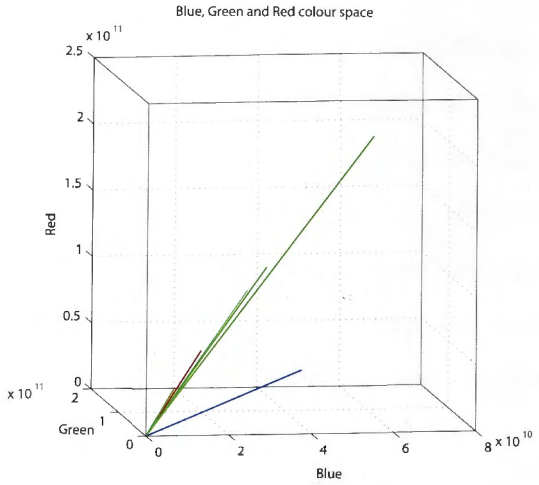

Figure 3.4 Three dimensional representations of various discs in colour space. The colours of the blue background and of the various grey discs, shown as vectors representing the relative excitations of the red, green and blue photoreceptor channels. The UV excitation is not depicted, as it is very low. The blue vector represents the blue background. The green vectors represent the various grey discs, except for one grey disc (Dreadnought Grey), which is shown in red. The vectors for all of the grey discs have almost identical directions, indicating that the hues of the grey discs (as perceived by the birds) are all very similar.

3.2.8 Experiments

Experiments were carried out using discs of 6 different grey levels, as described above. In each case, the disc was placed on a constant Kingfisher Blue background. In addition, a control experiment was carried out in which the disc had the same colour (Kingfisher Blue) as the background. This control

experiment was used to check for the presence of any artifactual edges between the disc and the background.

Figure 3.4 shows the colours of the Kingfisher Blue background and of the various grey discs, as vectors representing the relative excitations of the red, green and blue photoreceptor channels. It shows that, while all of the grey cards possess the same colour (the vectors are similarly oriented), the blue background has a different colour, represented by a vector with a substantially different orientation.

3.2.9 Statistical analysis

To quantify landing preferences, I analyzed the birds' landings on the card by measuring the density of landings within the boundary region between the disc and the background, and comparing this with the overall density of landings over all three regions (A, B and C). We define α as the ratio of the density of landings in the boundary region, to the overall landing density. Thus, a value of $\alpha=1$ would imply that birds do not prefer the boundary region at all, and land with a uniform probability density over the entire region. On the other hand, $\alpha > 1$ would indicate that the birds show a preference for the boundary region. The procedure used to determine if the measured value of α is different from random choice is based on the assumption that the binary choice behaviour of a landing bird follows a binomial distribution. An estimate of the standard error of the mean of the distribution is given by $\sigma = (\alpha(1-\alpha)/n)^{1/2}$ (Schefler, 1979; van Hateren et al., 1990). In a two-tailed test, α is significantly different from the value of 1 at the $p < 0.05$ level if α is more than 1.95σ away from 1, and at the $p < 0.01$ level if it is more than 2.57σ away.

3.4 Results

Although a few birds landed directly at the Petri dish to feed, the majority landed at the boundary of the disc (i.e. in region B) and then walked to the food -- even though there was no food at the boundary (Video 3.1). Evidently, the birds were using the visual contrast that was present at the boundary to direct and guide their landings. Figure 3.5 shows, for one typical bird, the positions and orientations of the landings and the landing densities (number of landings per unit area) in the three regions A, B and C for four of the discs: Snow White, Jet Black, Kingfisher Blue, and Dreadnought Grey. The lines indicate the position and orientation of the body axis and the dot represents the position of the head,

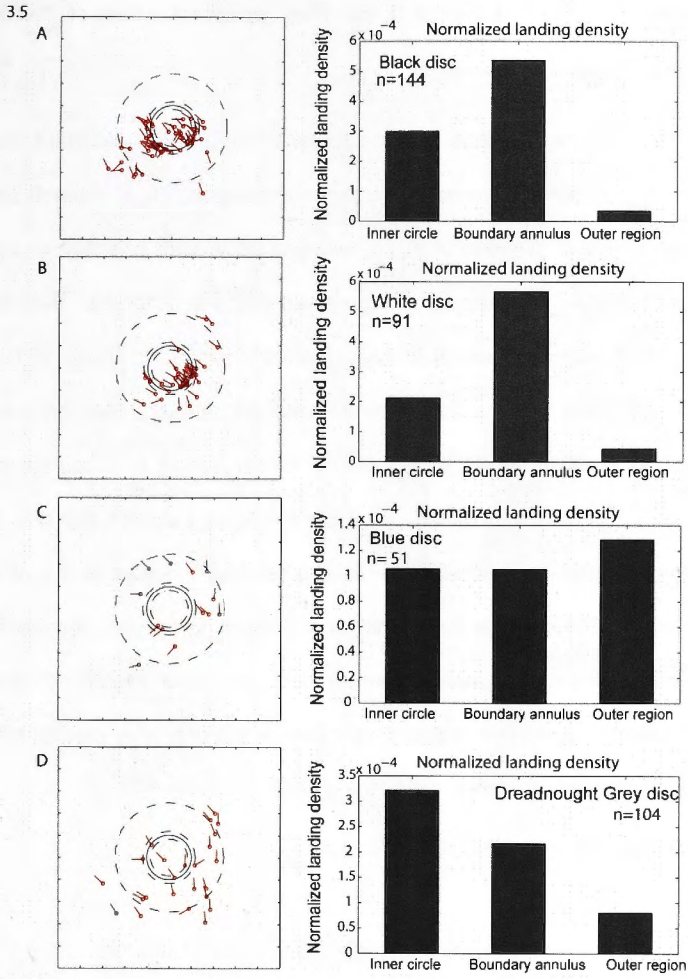

Figure 3.5 A sample of bird landings. The left hand panels show examples of the positions and orientations of landings of one bird when the disc was Snow White (A), Jet Black (B), Kingfisher Blue (C) (control) and Dreadnought Grey (D). The dot denotes the head position and the line the body orientation. The background was a constant Kingfisher blue in all cases. The right hand panels show the radial distributions of normalized landing densities for these discs in

regions A, B and C (see Figure 3.1B). They represent a total of 390 landings from 3-6 birds.

This data reveals that, with the Snow White and the Jet Black discs, the highest landing density occurs in the boundary region. Thus, in each case, the boundary between the disc and the background is very effective in attracting landings. However, in the control experiment with the Kingfisher Blue disc, the landing density in the boundary region is very similar to those in the other regions, indicating that the edge between the disc and the identically-coloured background is invisible to the birds. A similar result is obtained with the Dreadnought Grey disc, indicating that the boundary between this disc and the background is not very effective in eliciting landings. For all of the other grey discs (Mouse Grey, Azure Blue Grey and Sombre Grey) the boundary region elicits a higher landing density compared to the other regions (Figure 3.6). These results suggest that Dreadnought Grey is the only grey disc for which the boundary is nearly invisible to the landing birds.

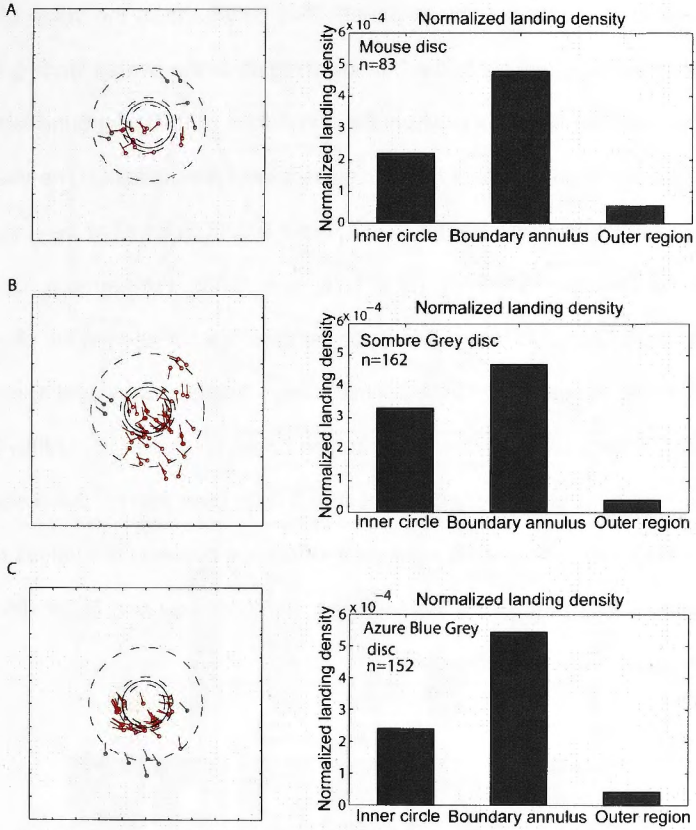

Figure 3.6 The left hand panels show examples of the distributions of landings of one bird when the disc was Mouse Grey (A), Azure Blue Grey (B), and Sombre Grey (C). The dot denotes the head position and the line the body orientation. The background was a constant Kingfisher Blue in all cases. The right hand panels show the radial distributions of landing densities for these discs. They represent a total of 397 landings from 3-6 birds.

The results for the entire data set (all experiments, all birds) are summarized in Figure 3.7 (lower panel). This panel shows the value of α, the ratio of the landing density in the boundary region to the overall landing density (as described in 'Methods'), when the Kingfisher Blue background was held constant and the grey level of the disc was varied systematically. The value of α is highly and significantly greater than 1.0 ($p < 0.00005$) for all of the grey discs, except for Dreadnought Grey ($\alpha = 1.76$, $p = 0.03$). Furthermore, α for the Dreadnought Grey disc is significantly lower than that for each of the other grey discs (White, Azure Blue Grey, Mouse Grey, Sombre Grey and Black; $p < 0.000001$ in each case; Binomial distribution z-test, [(Yates et al., (1999))]), and is only marginally statistically different ($p = 0.035$) from that for the control disc (Kingfisher Blue). There is no significant difference between the values of α for the White, Azure Blue Grey, Mouse Grey, Sombre Grey and Black discs ($p > 0.09$ for all pair wise comparisons).

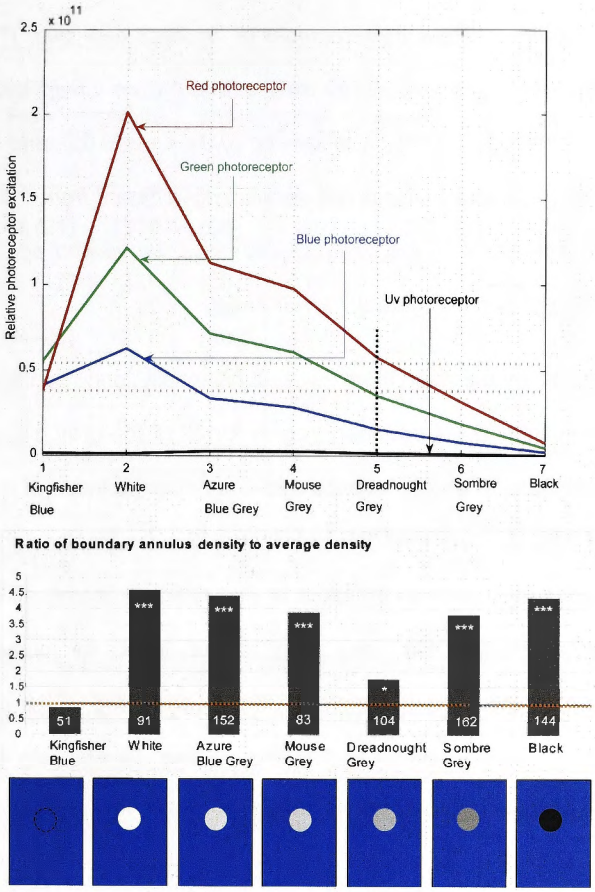

Figure 3.7 Relative photoreceptor excitations for the various colour discs. Upper panel: The vertical dotted line facilitates reading of the excitations induced by the Dreadnought Grey disc in the red, green, blue and UV photoreceptors, and comparison with the excitations induced in the red and green receptors by the Kingfisher Blue background (horizontal red and green dotted lines, respectively). Lower panel: Values of α obtained for the various grey cards. α is the ratio of the density of the landings in the boundary region (region B in Figure 3.1B) to the average overall landing density (measured over regions A, B and C

in Figure 3.1B). The data represent a total of 787 landings from 3-6 birds. The number in each bar denotes the number of landings analyzed. (***) indicates that the value of α is highly significantly different from 1.0 ($p < 0.00005$), (*) indicates a marginally significant difference ($0.01 < p < 0.05$), and the absence of this symbol indicates that α is not significantly different from 1.0 ($p > 0.3$). A pictorial representation of the various grey discs, as viewed against the blue background, is shown in Figure 3.7 lower panel.

These findings reveal that there is a substantially and significantly higher density of landings in the boundary region for all of the grey discs, except for Dreadnought Grey. With the Dreadnought Grey disc the value of α was closest to 1.0, and was different from this value at only a marginally significant level, implying that in this condition the birds landed nearly randomly all over the test surface even though this grey disc is (at least for humans) clearly distinguishable from the Kingfisher Blue background (Figure 3.4). The contribution of each individual bird to the landing density ratio (α), and the number of landings analyzed for each bird and disc colour, are given in Table 3.2.

Table 3.2

Disc colour	Kingfisher Blue	White	Azure blue grey	Mouse grey	Dreadnought grey	Sombre grey	Black
Bird Name							
Google	0.41 (21)	4.93 (30)	5.28 (66)	6.31 (29)	2.3 (53)	2.24 (80)	4.22 (66)
Drongo	1.45 (12)	4.71 (37)	4.81 (38)	2.29 (19)	1.74 (15)	2.84 (49)	5 (47)
Budgie	1.09 (26)	3.99 (24)	3.48 (30)	3.3 (29)	0.48 (18)	4.35 (32)	3.65 (31)
Acer	n/a (0)	n/a (0)	4.35 (2)	0 (2)	1.58 (11)	0 (1)	n/a (0)
Casper	n/a (0)	n/a (0)	2.18 (8)	0 (3)	1.74 (5)	n/a (0)	n/a (0)
Icarus	0 (2)	n/a (0)	1.09 (8)	0 (1)	0 (2)	n/a (0)	n/a (0)
Pooled data	0.85 (51)	4.59 (91)	4.41 (152)	3.88 (83)	1.76 (104)	3.82 (162)	4.35 (144)

Table 3.2 Summary of landing density ratios (α) for the middle annulus for different birds on various discs, with the number of landings analyzed in each case shown in parentheses. When the number of landings in a particular condition is zero, α is designated 'not applicable' (n/a).

The above results indicate that the disc boundary was clearly visible to the landing birds for all of the grey discs, except for Dreadnought Grey (Figure 3.7, lower panel). In the control experiment (Kingfisher Blue disc on an identical Kingfisher Blue background, Figure 3.7, lower panel) α was 0.85, which was not significantly different from 1.0 ($p > 0.3$). This finding demonstrates that any residual visual contrast between the edge of the disc and the background had a negligible effect in eliciting landings. Therefore, the vast majority of landings that occur within the boundary region in the other experiments must be due to the

presence of a perceptible visual contrast (to the birds) between the disc and the background, and not due to any artefacts at the boundary.

When the disc and the background are both Kingfisher Blue, the birds land on the visually uniform areas, but far less frequently. Many of these residual landings then occur completely outside the region of interest (C), or at bird droppings, seeds or small visual imperfections on the surface of the paper. Table 3.1 gives, for each disc colour, the total number of flight trials conducted, and the number of trials excluded from the analysis for various reasons, as explained in the table. It is clear that the percentage of these excluded trials is substantially larger when the disc is Kingfisher Blue (i.e. the same colour as the background), or Dreadnought Grey (little or no edge contrast). Under each of these conditions, the birds show an increased tendency to land either completely outside region C, or at bird droppings or visual imperfections. Furthermore, Table 3.1 shows a reciprocal relationship between the visibility of the disc boundary, and the tendency to land at spurious features or at locations outside region C. These findings further support the conclusion that landings are guided principally by visually contrasting features.

The relative photoreceptor excitations produced by the various grey cards in the red, green, blue and UV photoreceptors in the retina of the budgerigar were computed as described in the 'Methods' section (Figure 3.7, upper panel). When the disc is Dreadnought Grey, we see from Figure 3.7 (upper panel) that the red photoreceptor receives approximately the same excitation from the disc (0.55) as it does from the blue background (0.4). The same is true for the green photoreceptor, which receives excitations of 0.55 from the Kingfisher Blue background and 0.4 from the disc. This means that with the Dreadnought Grey

disc on the Kingfisher Blue background, neither the red receptor nor the green receptor experiences a strong contrast at the boundary. However, neither the red receptor nor the green receptor alone exhibits a perfect match of excitations from the Kingfisher Blue background and the Dreadnought Grey disc. On the other hand, the sum of the excitations of the red and green receptors produces a perfect match (Figure 3.8). We also note that a 'total luminance' signal, comprising the sum of the UV, blue, green and red signals, produces a poorer match (Figure 3.8).

3.8

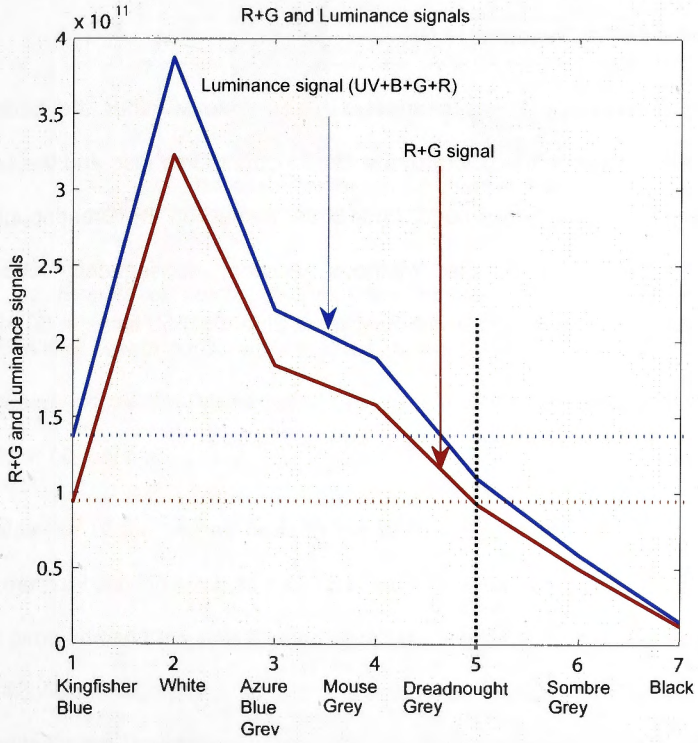

Figure 3.8 Relationship between the luminance signals for the various coloured discs. Variation of the luminance signal (UV+B+G+R) and the (R+G) signal for

the various coloured discs, calculated as described in 'Methods'. The vertical dotted line facilitates reading of the (UV+B+G+R) signal and the (R+G) signal induced by the Dreadnought Grey disc, and comparison with the corresponding signals induced by the Kingfisher Blue background (horizontal blue and red dotted lines, respectively).

Thus, if we postulate that edge detection for landing is mediated by a 'colour-blind' visual subsystem that receives input from a sum of the signals from the red and green receptors; we have an explanation for why the birds behave as though they barely detect the boundary between the disc and the background when the disc is Dreadnought Grey.

A control experiment was conducted to examine whether the birds could distinguish between the colour of the Dreadnought Grey disc and the colour of the Kingfisher Blue background. Four birds, trained on the Dreadnought Grey disc as described in the 'Methods' section, subsequently chose the Dreadnought Grey disc (over the Kingfisher Blue disc) 50 times in 60 test trials (Figure 3.2) (Video 3.2).

3.2

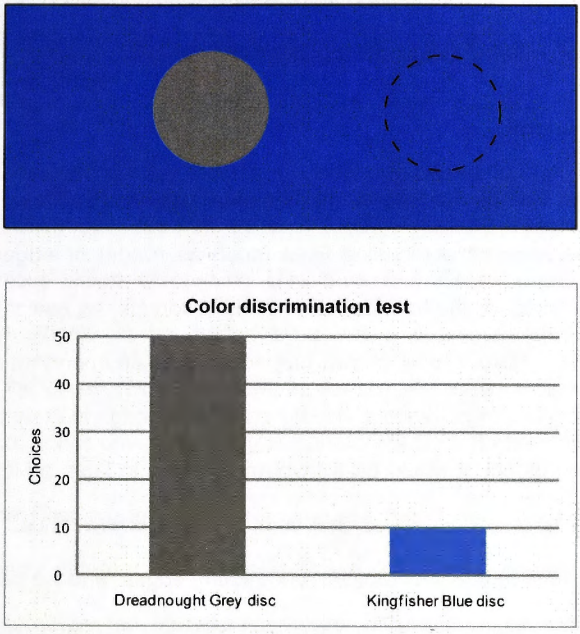

Figure 3.2 Results of colour discrimination control experiment. Four birds, trained on the Dreadnought Grey disc as described in the 'Methods' section, subsequently chose the Dreadnought Grey disc (over the Kingfisher Blue disc) 50 times in 60 test trials.

The behaviour of the trained birds in the tests did not show any evidence of spatial memory playing a role in their choices. At the start of each test block, the trained birds immediately flew to the correct disc, even though it was now in a different position compared to the previous test block. The trained birds' preference for the Dreadnought Grey disc was statistically highly significant ($p < 0.00005$, using the binomial statistics described in 'Methods'). This demonstrates that, although the visual subsystem that guides the budgerigar's

landings does not detect the boundary between the Dreadnought Grey disc and the Kingfisher Blue background, the bird's colour vision system is clearly capable of distinguishing between these two colours.

3.5 Discussion

It is known that, during long-range migration, pigeons (*Columba livia)* use visual landscape features comprising lines (such as roads) or edges (such as the shores of lakes, or the boundaries of fields or forests) as navigational aids (Lau et al., 2006). Here, I have shown that edges play an important role in directing and guiding landings. Since a visually contrasting edge is likely to represent the edge of an object, it would be a favourable place to land, as it would offer the bird's claws a good grip at the point of touchdown. Thus, it would seem advantageous to direct landings at contrasting edges; and we can conclude that the principle of 'affordance', as espoused originally by Gibson (Gibson, 1950) is used by birds to seek suitable locations for landing. The findings further suggest that the visual subsystem that detects edges and guides landings is colour-blind, and could possibly be a visual modality that predates the evolution of colour vision. The ability to detect edges almost disappears when the Dreadnought Grey disc is presented against the Kingfisher Blue background (Figures 3.5, 3.6 and 3.7 lower panel). The reason for the weak residual preference for the boundary region may be that the Dreadnought Grey disc does not offer precisely the level of grey at which the visibility of the boundary disappears.

We see from Figure 3.7 (upper panel) that, with the Dreadnought Grey disc, the excitation produced by the disc is similar to that produced by the background,

for the red as well as the green receptors. A perfect match of the excitations that are produced by disc and the background is obtained if one postulates that edge detection is performed by a colour-blind pathway that sums the red and the green signals.

Colour-blindness in edge detection and motion perception has also been observed in honeybees (Lehrer et al., 1990), which possess excellent trichromatic colour vision comprising UV, Blue and Green photoreceptors. There, landings appear to be guided by a visual subsystem that is driven exclusively by the green photoreceptors. Movement detection in honeybees is also colour blind, and is driven by the green photoreceptors (Lehrer, 1987).

Since the Dreadnought Grey disc and the Kingfisher Blue background disc possess very different colours (see Figure 3.3), these colours must be easily discriminated by the bird's colour vision system. Dual-choice training experiments reveal that budgerigars can indeed distinguish between these two colours readily (Figure 3.2). Nevertheless, the edge detection system that guides landing is evidently driven by a colour-blind signal that is incapable of this colour discrimination.

The parallel observations in the budgerigar and the bee suggest that the ability to use colour vision to distinguish between objects, but the inability to use colour information to detect edges, may be a common feature of many flying species. Budgerigars carry the so-called red 'double cone' photoreceptors, which constitute 50% of the total population of cone receptors in the retina. The absence of an oil droplet in one of the double cones endows this type of photoreceptor with a spectral sensitivity that is somewhat broader than that of a

single red photoreceptor with an oil droplet (Goldsmith and Butler, 2003). This makes the spectral sensitivity of the red double-cone photoreceptor similar to that of a system that pools signals from the red and green photoreceptors. Thus, our findings suggest that the visual subsystem that mediates edge detection during landing is driven by a colour-blind system that pools signals from the red and green photoreceptors, or, alternatively, derives its input exclusively from the red, double-cone photoreceptors. The present experiments do not allow us to distinguish between these two possibilities. If the edge-detecting system were to pool the red and green signals, it would be analogous to the 'luminance' channel in the primate visual system, which is colour-blind and known to be involved in the perception of movement (Livingstone and Hubel, 1987). On the other hand, if the edge-detection system is driven by the red double cone photoreceptors, then it is possible that the red double cones constitute the luminance channel in birds, and mediate edge detection as well as motion perception. Given the dominant presence of the red double cones in the bird retina, and the importance of accurate landing to survival, this intriguing possibility deserves to be explored.

Chapter 4

The use of optic flow by flying budgerigars

4.1 Introduction

Birds fly flawlessly between branches of trees as well as manmade structures (Daniel and Willard, 1978). In order to navigate through cluttered environments, birds depend entirely on the cues perceived by their visual system. This visual information has to be processed in real time to generate motor outputs in the form of quick reflexive wing movements that steer the bird away from the path of danger.

Earlier studies involving visually guided flight in birds have investigated the mechanism of binocular stereopsis which is essential for depth perception, and is well developed in predatory birds such as falcons and eagles (Martin, 2007). However this mechanism does not seem to play any significant role in visually guided navigation in budgerigars, as their eyes are positioned laterally. This ocular configuration precludes any binocular overlap that would provide information on the distance to objects.

Previous studies involving optic flow in birds have investigated specific behaviour like landing in pigeons and hawks, as well as diving by gannets to catch fish (Davies and Green, 1990; Lee and Reddish, 1981).

In freely flying zebra finches, it has been suggested that saccadic gaze shifts may play an important role in discrimination between rotations and translations (Eckmeier et al., 2008). It was concluded that the translational motion of the images on the retina of the flying bird help in the determination of

the three dimensional configuration of objects in the flight path (Eckmeier et al., 2008). In this case, optic flow arises due to relative motion of the flying budgerigar with respect to the surrounding environment. During flight, objects that are closer to the bird appear to move faster than objects that are more distant.

Although a lot is known about long-range navigation in birds, we know relatively little about moment-to-moment navigation, especially obstacle avoidance. This chapter describes an investigation of how budgerigars fly through narrow gaps without risk of collision. This so called 'centring response' is well known in flying insects (Kirchner and Srinivasan, 1989; Srinivasan and Zhang, 2004), but has never been investigated in birds.

Specifically, the experiments described here involve filming and analysing flights of the birds through a narrow tunnel in which the visual textures on the walls are systematically manipulated. The questions explored are: (a) Do birds fly through narrow passages in a collision-free manner, and if so, how do they achieve this? and (b) Do birds regulate the speed of their flight when flying through such passages, and if so, how do they achieve this?

4.2 Methods

The birds were maintained under controlled laboratory conditions as described in the 'General Methods' chapter (Chapter 2) of this thesis.

4.2.1 Subjects

Adult male and female wild type budgerigars (*Melopsittacus undulatus*), a native Australian desert bird (n=8, approximately 1 year old), served as subjects for this experiment.

4.2.2 Experimental setup

The birds were flown in an indoor tunnel. Technical details about the design of the tunnel are described in the 'General Methods' chapter (Chapter 2) of this thesis.

Depending upon the experiment, either wall of the tunnel was left uncovered, or decorated with black stripes that were oriented either vertically or horizontally. The stripes were 11 cm wide and spaced 11 cm apart, producing a square-wave grating of period 22 cm. The black stripes were machine-cut from paper (Elle card 135040 ERA1 Black 220 gsm). 7 different experimental conditions were tested, in which each wall was either blank, or carried stripes that were oriented either vertically or horizontally, as shown in Figure 4.1 below.

Denoting the horizontal stripes by H, the vertical stripes by V, and the blank wall by B, 'left' by L and 'right' by R, the various configurations can be denoted by LHRV, LVRH and LVRV (first row), LVRB, LBRV and LBRB (second row) and LHRH (third row).

4.1

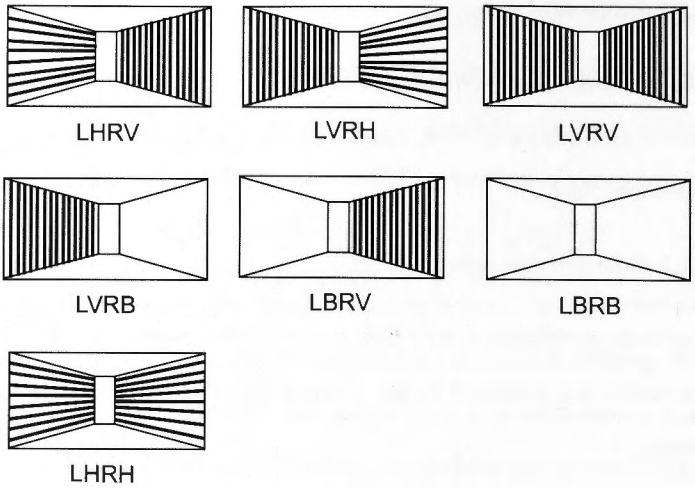

Figure 4.1 Schematic illustrations of the 7 experimental configurations used in the study. The abbreviations are: LHRV – left horizontal and right vertical, LVRH- left vertical and right horizontal, LVRV- left vertical and right vertical; LVRB- left vertical and right blank, LBRV- left blank right vertical, LBRB- left blank and right blank and LHRH- left horizontal and right horizontal.

4.2.3 Budgerigar Training

The budgerigars were trained to take off from a perch when it was slowly rotated, to fly to the end of the tunnel, and then to make a U-turn and fly back to the perch. The U-turn performed by the bird is a natural instinct of the bird to fly back to the experimenter in the absence of a perch at the far end of the tunnel.

The training lasted for one to two days. Once training was complete, the bird was flown under the 7 different experimental conditions described above. On a given day a bird was randomly chosen for the experiment and used only for ten flights for one particular experimental condition. The bird was then rested, and

another bird was used. Typically, a given bird made 10 flights through the tunnel in a day.

4.2.4 Video recording of bird flights

Video recording was carried out using two high speed cameras (DRS lightning RDT, DRS Data and imaging systems, Inc. Oakland, NJ, USA). One camera was mounted and concealed inside the ceiling, facing downwards. It was positioned halfway along the tunnel and midway between the walls. The other camera was hidden behind a curtain and positioned at the end of the tunnel, facing along its axis. Each camera was equipped with a Pentax wide-angle lens with a focal length of 6.5 mm and a visual field of 98 degrees. The optical axes of the two cameras were approximately at right angles to each other. The cameras were calibrated as described in the 'General Methods' chapter (Chapter 2).

4.2.5 Analysis of video images

The entire flight sequence, starting, from take off to the far end of the tunnel, as well as the return flight back to the perch, was recorded. The movies were converted from .avi format to a sequence of .tiff images using the MIDAS 2.0 player (Xcitex Inc, Cambridge, Mass, USA). The flights were filmed at 250 frames per second and then down sampled to 25 frames per second for plotting, visualization and analysis purposes. The image sequences thus obtained were then analyzed by using a tracking program developed in-house, using Matlab (v.R2007a; The Mathworks Inc., Natick, MA, USA). This program was used to digitize the flights and to generate 3-D plots of the flight paths taken by the birds in the tunnel. Only the flight path from the perch to the far end

of the tunnel was used for analysis. Further details are described in the 'General Methods' chapter (Chapter 2).

4.2.6 Statistical analysis

The mean position of each flight trajectory (along the x-axis) was calculated and a histogram was plotted for the population. The mean of the population was determined (shown by a red arrow head in Figures 4.3, 4.4 and 4.5) as well as the standard deviation (shown by a horizontal red error bar in Figures 4.3, 4.4 and 4.5). A t-test was used to test for a significant deviation of the mean position of the flight trajectories from the mid line of the tunnel, which was 680 mm from either wall. All of the data thus obtained are summarized in Table 4.1a.

A one-way ANOVA (Analysis of variance) (Matlab function ANOVA1 from Mathworks, USA) (Hogg and Ledolter, 1987) and a Multcompare statistical analysis (Matlab function Multcompare from Mathworks, USA) (Hochberg and Tamhane, 1987) was used to compare the mean speed and mean axial speed of three budgerigars (One, Two and Casper) that had flown in the following three conditions LVRV (Left vertical right vertical), LHRH (Left horizontal right horizontal) and LBRB (Left blank right blank). These analyses were used to check for statistically significant differences in the mean speed and mean axial speed across the three data sets. ANOVA and Multcompare were carried out using their respective Matlab functions. The results from the ANOVA test are summarised in Table 4.2.

A paired two way t-test (Matlab function t-test2 from Mathworks, USA) was carried out to check for statistically significant differences between the flight

speeds (measured as mean total speed or mean axial speed) in the various experimental conditions, namely, (LVRV versus LHRH), (LVRV versus LBRB), and (LHRH versus LBRB). The results of this test are summarised in Table 4.3.

4.3 Results

4.3.1 Flight trajectories through narrow passages

45-50 flights were filmed, digitized and analysed for each of the 7 experimental conditions, using a total of 5 birds in each condition. The experimental configurations are illustrated Figure 4.1. Figure 4.2 shows overhead views of 5 randomly selected trajectories obtained for each of the three experimental configurations. When both walls were lined with vertical stripes, the birds flew along the middle of the tunnel, never colliding with either wall (Figure 4.2A) (Video 4.1). There is no significant difference between the mean x-position of the trajectories and the midline of the tunnel ($p > 0.26$, t-test and N=50). On the other hand, when one wall carried vertical stripes and the other horizontal stripes, the birds flew significantly closer to the wall carrying the horizontal stripes (Figures 4.2 B and C; $p < 0.0001$, t-test, N=45 and N=50 respectively) (Videos 4.2 and 4.3).

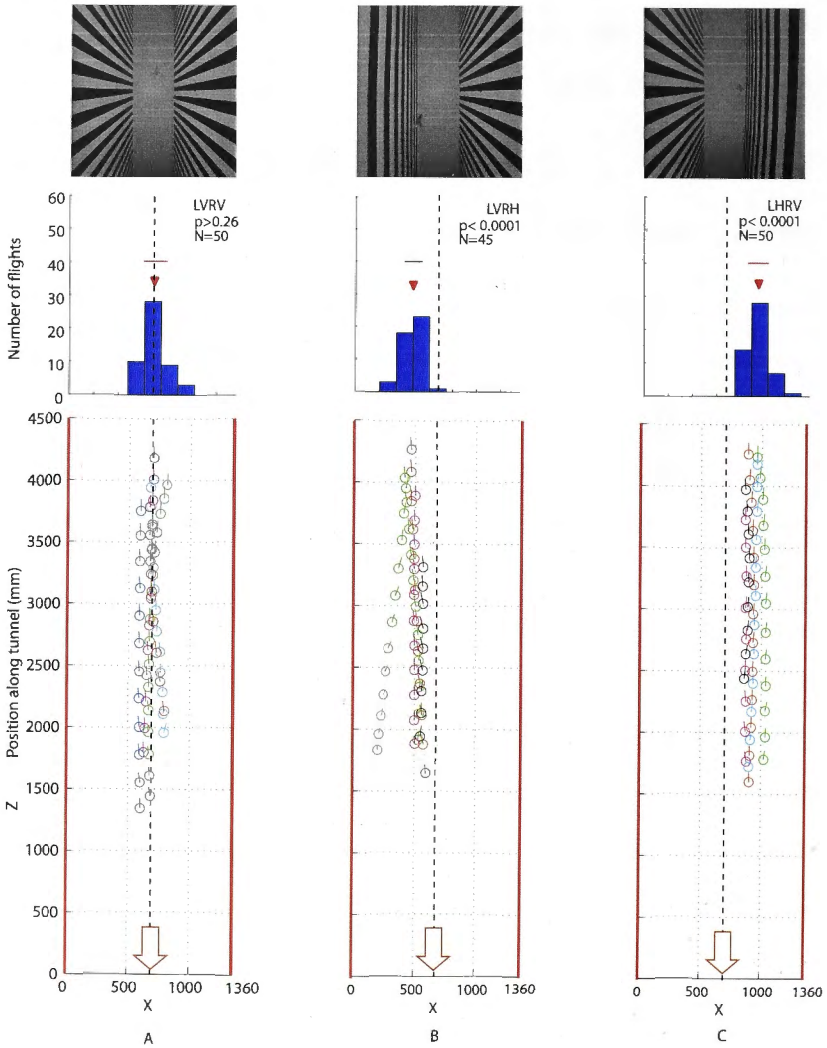

Figure 4.2 Plan views of 5 randomly chosen trajectories of budgerigars flying in a tunnel in which both walls were lined with (a) vertical stripes, (b) the left wall with vertical stripes and the right wall with horizontal stripes, and (c) vice versa. In each case flight is from the top of the image toward the bottom. (Left and right are defined from the bird's viewpoint: hence LVRH is in the middle panel).

The dashed vertical line denotes the midline of the tunnel. The histograms show the distributions of trajectory positions for the total number of flights analyzed (N), the small arrowheads indicate the mean trajectory position, and the horizontal bars show the standard deviation. Data were analyzed from 5 birds, producing a total of 45-50 flights for each condition.

Overhead views of 5 randomly selected trajectories for two further experimental configurations are shown in Figure 4.3. When one wall carried vertical stripes and the other wall was devoid of any visual texture the birds flew very close to the blank wall, occasionally grazing it (Figure 4.3 B and C) (Video 4.4 and 4.5). In either case, the bird's flight trajectories are significantly closer to the blank wall ($p < 0.0001$, t-test; N=51 in each case).

Finally, when both walls were blank, or when both walls carried horizontal stripes, the birds flew along the middle of the tunnel, displaying a mean X-position that was not significantly different from the midline of the tunnel ($p < 0.0001$, t-test; N=45, Figure 4.4 A; and $p = 0.54$, t-test; N=50, Figure 4.4 B) (Video 4.6 and 4.7)

4.3

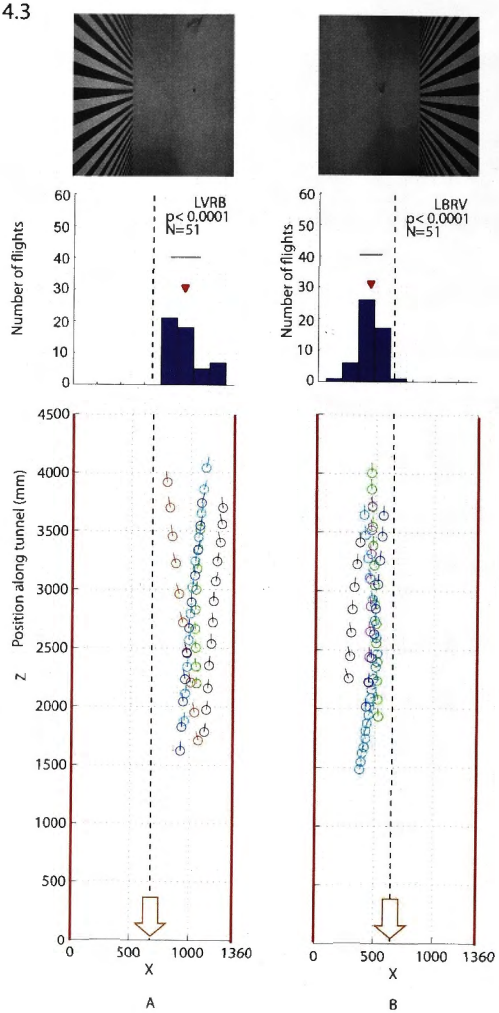

Figure 4.3 Plan views of 10 randomly selected trajectories of budgerigars flying in a tunnel in which (a) the left wall was blank and the right wall was lined with vertical stripes, and (b) vice versa. In each case flight is from the top of the image toward the bottom. The dashed vertical line denotes the midline of the tunnel. The histograms show the distributions of trajectory positions for the total number of flights analyzed (N), the small arrowheads indicate the mean

trajectory position, and the horizontal bars show the standard deviation. Data were analyzed from 5 birds, producing a total of 51 flights for each condition.

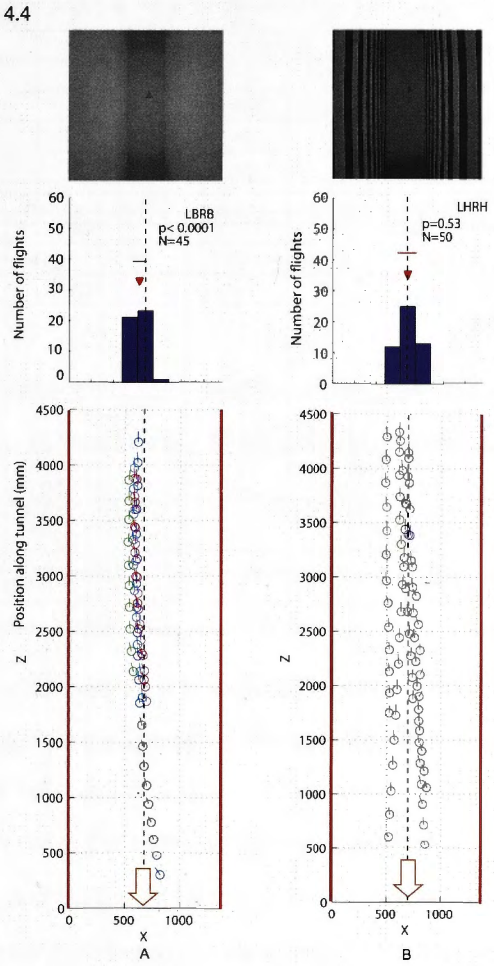

Figure 4.4 Plan views of 5 randomly selected trajectories of budgerigars flying in a tunnel in which both walls were (a) blank, (b) lined with horizontal stripes. In each case flight is from the top of the image toward the bottom. In each case flight is from the top of the image toward the bottom. The dashed vertical line denotes the midline of the tunnel. The histograms show the distributions of

trajectory positions for the total number of flights analyzed (N), the small arrowheads indicate the mean trajectory position, and the horizontal bars show the standard deviation. Data were analyzed from 5 birds, producing a total of 45-50 flights for each condition.

Table 4.1a

	LHRV	LBRV	LVRV	LVRH	LVRB	LBRB	LHRH
N (number of flights analysed)	50	51	50	45	51	45	50
Mean distance (x- position) from right-hand wall, in mm (Mean of means)	934.32	946.74	695.25	475.14	438.39	629.66	672.53
Standard deviation (mm)	84.2	127.15	95.88	72.66	97.27	59.58	84.78
Degrees of freedom	49	50	49	44	50	44	49
p value (t-test)	1.78×10^{-26}	4.03×10^{-20}	0.27	9.38×10^{-23}	3.23×10^{-23}	1.04×10^{-06}	0.54
h (significance index)	1	1	0	1	1	1	0

Table 4.1a Results of analysis of positions of flight trajectories along the width of the tunnel, for the various experimental configurations. Abbreviations as in Figure 4.

Table 4.1b

Conditions	LHRV	LBRV	LVRV	LVRH	LVRB	LBRB	LHRH
N (number of flights analysed)	50	51	50	45	51	45	50
Bird names							
One	10	10	10	13	15	10	10
Two	10	10	10	5*	15	9	10
Drongo	10	10	10	10		10	
Casper		11	10		2	6	10
Four		10					10
Spice	10		10	12	9	10	
Three							10
Rama	10			10	10		

Table 4.1b Contributions by each bird for the various experimental configurations (raw data was lost as it was not backed up and hence was not used in the analysis).*

Table 4.1a shows a summary of the analysis of the positions of the flights along the width of the tunnel (the x-positions) for the various experimental configurations: LHRV, LBRV, LVRV, LVRH, LVRB, LBRB and LHRH. The meanings of the abbreviations are: LHRV – left horizontal and right vertical; LBRV- left blank right vertical; LVRV- left vertical and right vertical, LVRH- left vertical and right horizontal; LVRB- left vertical and right blank; LBRB- left blank and right blank; and LHRH- left horizontal and right horizontal. And Table 4.1b shows the individual contributions by each bird for each experimental condition.

The second row of the table 4.1a shows the mean x-position of the flight trajectories obtained under each condition, as measured from the right-hand wall. The third row displays the standard deviations of the x-positions of the flight trajectories obtained in the various conditions. The fourth, fifth and sixth rows show the results of t-tests to check for a statistically significant difference

between the mean x-position of the flight trajectory and the midline of the tunnel (which has an x-position of 670 mm) for each experimental condition. The fourth row displays the degrees of freedom in the t-test, the fifth row the value of p obtained with the t-test ($p < 0.05$ indicates a statistically significant difference), and the sixth row the value of a significance index (h=1 denotes a significant difference, and h=0 denotes not significant difference). The procedure for this statistical analysis procedure is described in http://www.socialresearchmethods.

net /kb/stat_t.php.

4.3.2 Control of flight height

At what height do the birds fly in the tunnel? This can be determined by viewing the reconstructed 3-D trajectories from the side, i.e. in the y-z plane. The panels in Figure 4.5 show these views for all of the flights for each experimental condition.

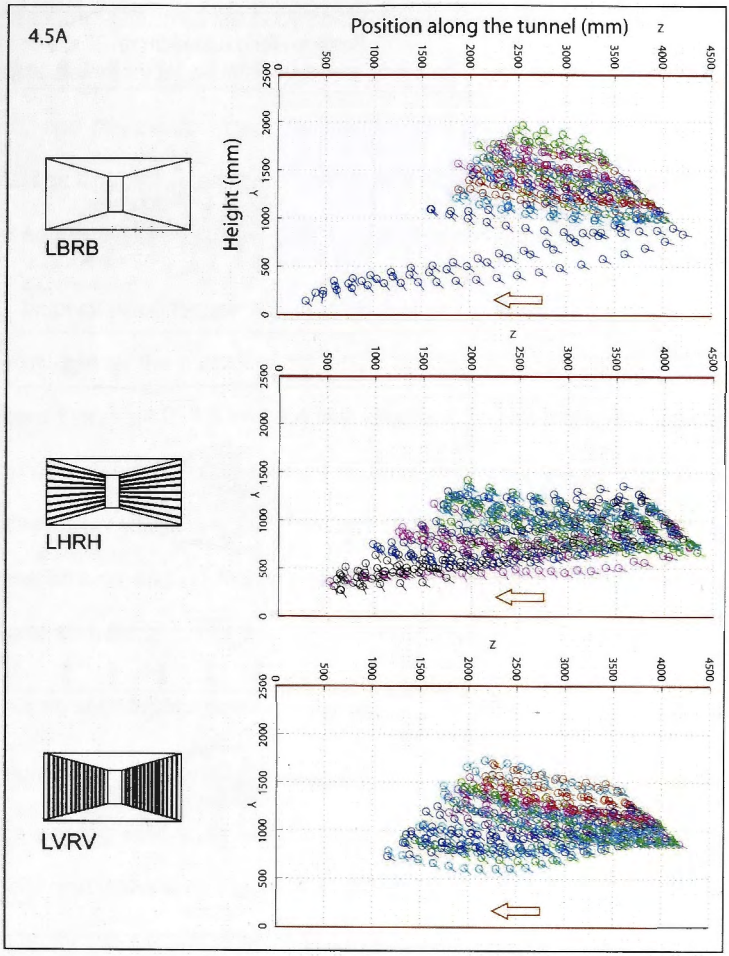
4.5A
Position along the tunnel (mm)
Height (mm)
LBRB
LHRH
LVRV

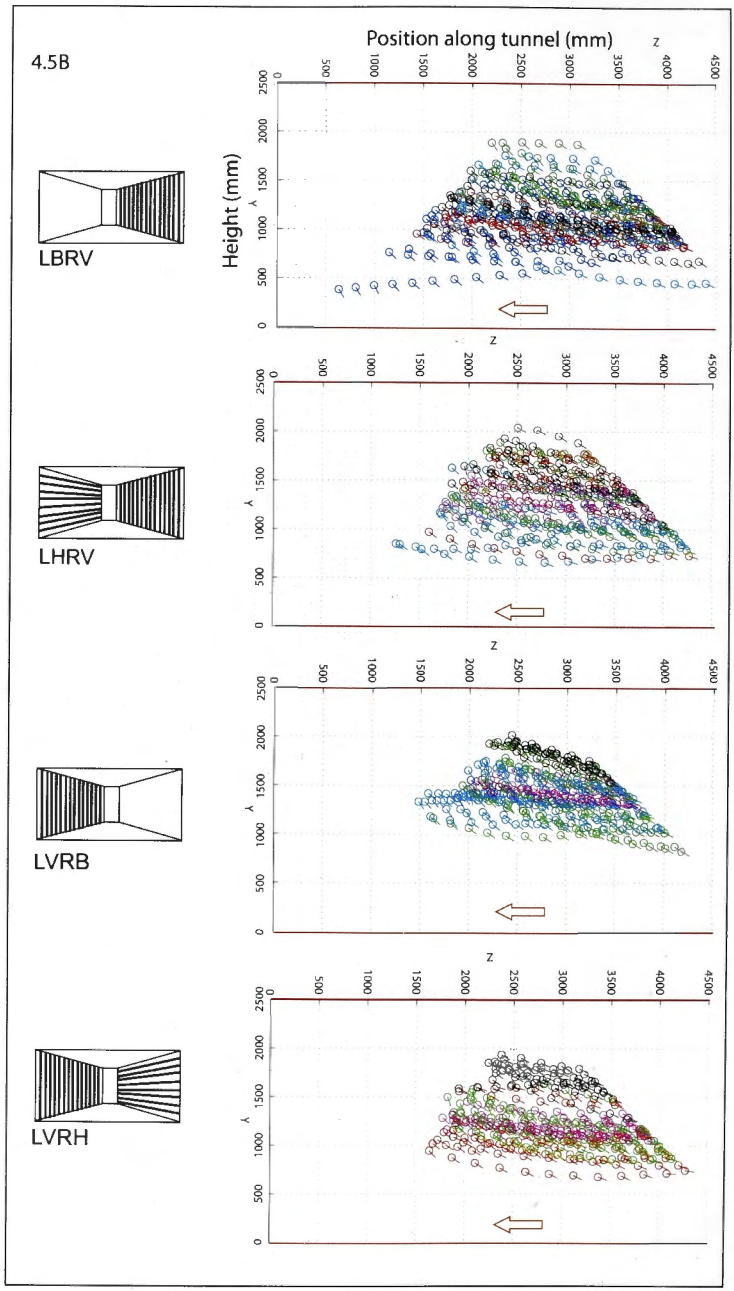

Figure 4.5 A and B Side views (views in the y-z plane) of all of the flights for each of the experimental conditions. The circle 'o' represents the position of the

head and the '-' denotes the body orientation of the bird. Each colour represents the flight trajectory of a different bird. The y-axis shows the height above the ground, and the z-axis shows the position of the bird along the length of the tunnel. The flight trajectories are shorter at a higher height and longer at a lower height because the top camera has a cone shaped field of view of 95 degrees.

Inspection of Figure 4.5 reveals that the control of height is nowhere nearly as tight as the control of the lateral position along the width of the tunnel (compare Figures 4.2, 4.3 and 4.4 with Figure 4.5). The birds vary their altitude by approximately the same amount in all of the experimental conditions. The side views shows that (i) flights that start at a higher altitude tend to stay high or increase altitude and (ii) flights that start at a low altitude tend to stay low or decrease altitude.

4.3.3 Control of flight speed

The birds' flight speeds were measured in tunnels whose walls were lined with various visual patterns, as described in the 'Methods' section of this chapter. The left-hand panels of Figure 4.6 show, for three different birds, the flight speed profiles in tunnels in which both walls were blank (red curves), lined with vertical stripes (green curves) or lined with horizontal stripes (blue curves). The dashed green, blue and red horizontal lines depict the mean flight speeds in the three corresponding conditions. In general, the speed of flight tends to increase after takeoff, reach a plateau and then decrease when the bird has neared the end of the tunnel and is preparing to land or make a U-turn and fly back to the experimenter's perch. This is true for all three birds and for all of the experimental conditions.

The right-hand panels show the mean flight speeds for the three different experimental conditions. For all three birds, the mean flight speed is lowest with vertical stripes, highest with horizontal stripes and intermediate with the blank walls.

4.6

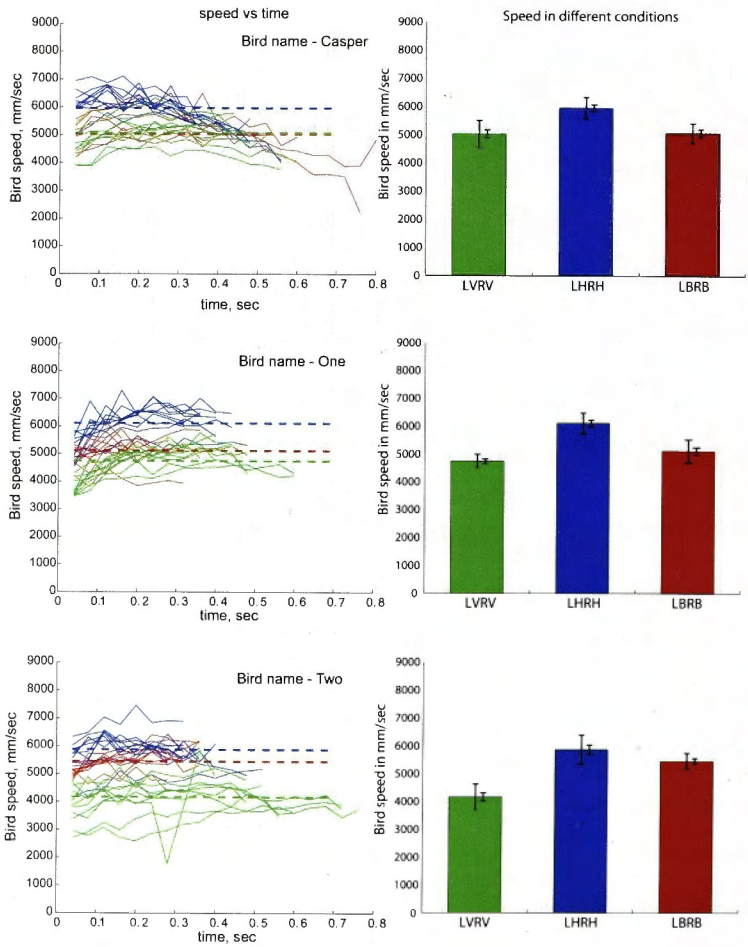

Figure 4.6 Profiles of speed versus time (left hand panels) and mean flight speeds (dotted lines in left hand panel show the mean of mean flight speed when both walls were blank (red), or carried vertical stripes (green) or horizontal

stripes (blue). Green, blue and red bars (right hand panels) show mean flight speeds when the patterns on the walls were blank (red bar - LBRB), or lined with vertical stripes (green bar - LVRV) or horizontal stripes (blue bar - LHRH). The error bars in the right hand graph show the standard deviation (left set of bars) and the standard error (right set of bars). Data are shown for three different birds: Caspar, One and Two.

4.7

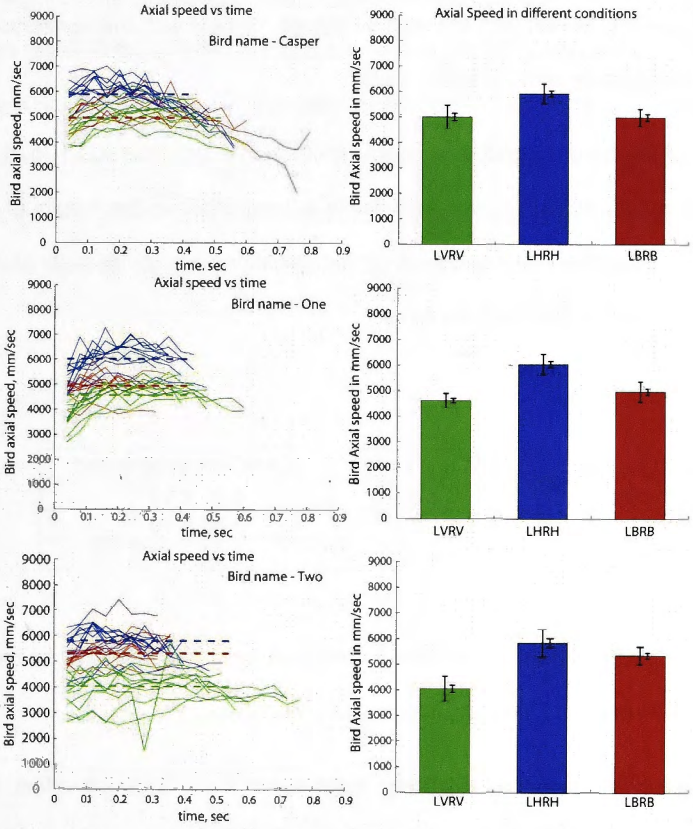

Figure 4.7 Data as in Figure 4.6, but computed for axial flight speed versus time, rather than total flight speed versus time. Green, blue and red bars (right hand panels) show mean axial flight speeds when the patterns on the walls

were blank (red bar - LBRB), or lined with vertical stripes (green bar - LVRV) or horizontal stripes (blue bar - LHRH). The error bars in the right hand graph show the standard deviation (left set of bars) and the standard error (right set of bars). Data are shown for three different birds: Caspar, One and Two.

Similar results are obtained when the data is re-plotted to show profiles of axial speed, rather than total speed, as illustrated in Figure 4.7. Again, the mean axial speed is lowest with the vertical stripes, highest with the horizontal stripes and intermediate with the blank walls.

Are the differences in flight speeds that are observed in the three conditions statistically significant? Table 4.2 summarizes the results of ANOVA tests to examine whether the observed variations are significant, or purely a result of chance, for the three birds.

Table 4.2

Bird name	p ANOVA speed	p ANOVA axial speed
Casper	6.75×10^{-05}	4.81×10^{-05}
One	9.20×10^{-09}	3.86×10^{-09}
Two	1.02×10^{-08}	1.94×10^{-08}

Table 4.2 summarises the p value for ANOVA for speed and axial speed for the three different birds, namely, Casper, One and Two.

The computed p values are very much lower than 0.05, indicating that the observed variations in speed across the three experimental conditions are highly statistically significant for all three birds, in relation to total flight speed as well as axial flight speed,

The question that then arises is: Under which conditions do the flight speeds differ? This is answered by performing a Multcompare analysis. The results are summarized in Figure 4.8 A, B and C. They show that for birds Caspar and One, the mean flight speed is (a) significantly greater in the LHRH condition than in the LVRV condition at the $p < 0.05$ level, (b) significantly greater in the LHRH condition than in the LBRB condition at the $p < 0.05$ level (c) not significantly different between the conditions LBRB and LVRV. Bird Two also flies faster in the LHRH condition than in the LVRV condition, like the other birds ($p < 0.05$). However, in the case of this bird there is also a significant difference between the mean flight speeds in the LBRB and LVRV conditions ($p < 0.05$), but not between the LBRB and LHRH conditions. These results hold for mean total flight speed as well as mean axial flight speed.

4.8 A

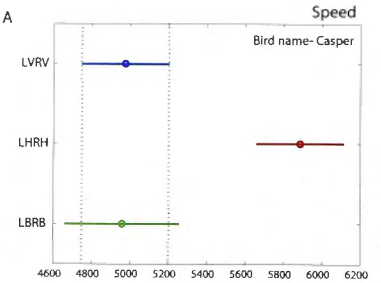

The means of groups LVRV and LHRH are significantly different

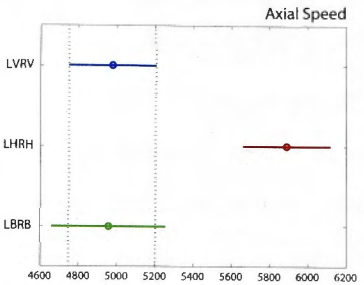

The means of groups LVRV and LHRH are significantly different

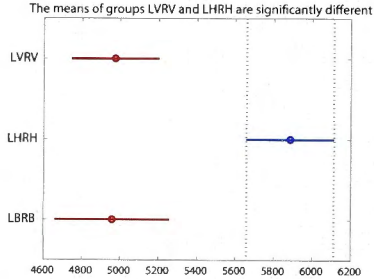

2 groups have means significantly different from LHRH

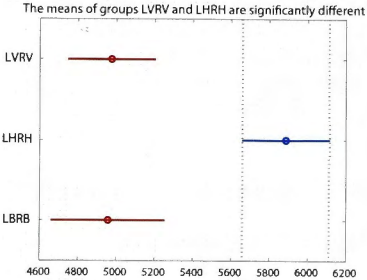

2 groups have means significantly different from LHRH

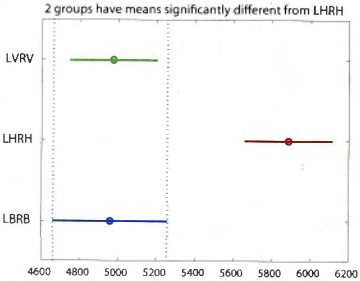

The means of groups LBRB and LHRH are significantly different

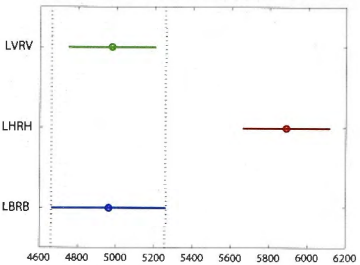

The means of groups LBRB and LHRH are significantly different

4.8 B

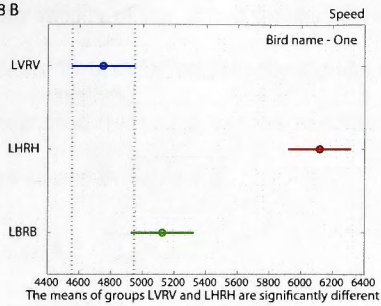

The means of groups LVRV and LHRH are significantly different

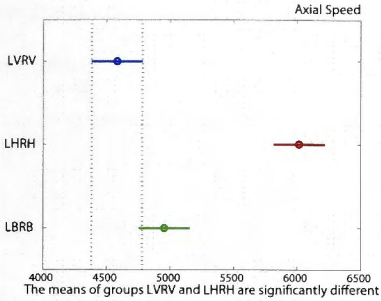

The means of groups LVRV and LHRH are significantly different

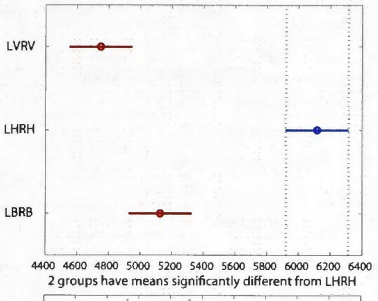

2 groups have means significantly different from LHRH

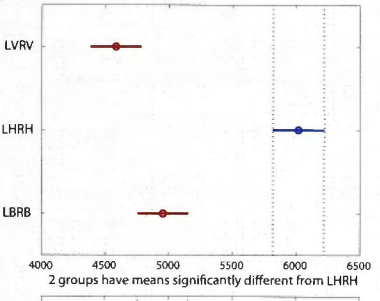

2 groups have means significantly different from LHRH

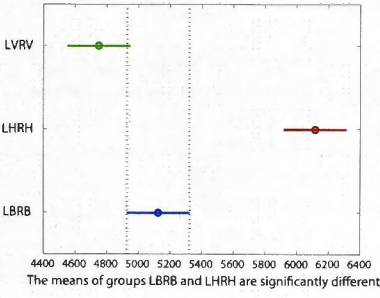

The means of groups LBRB and LHRH are significantly different

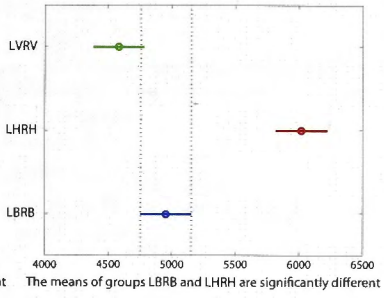

The means of groups LBRB and LHRH are significantly different

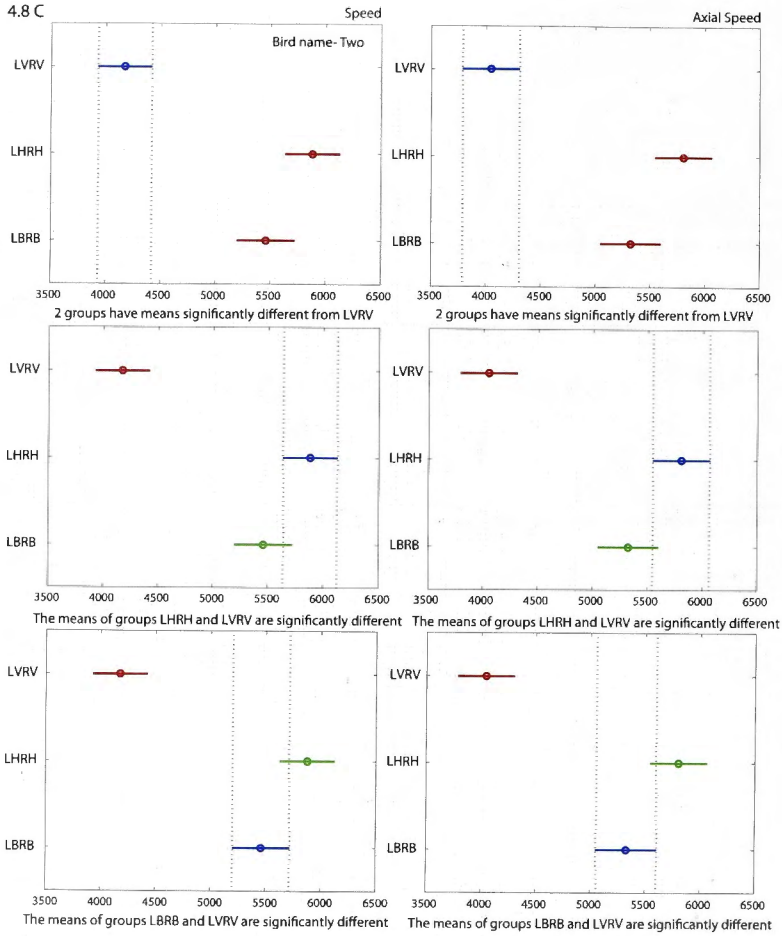

Figure 4.8 Results of Multcompare statistical analysis of mean speed and mean axial speed across the three different experimental conditions LBRB, LVRV and LHRH for three birds: Casper (A), One (B) and Two (C). The results of the statistical analysis (testing for statistical difference at the $p < 0.05$ level) are summarized below each panel.

The validity of the above results can be checked by performing paired two-way t-tests to test for statistically significant differences between the flight speeds measured under the various conditions, considered two at a time. The results are shown in Table 4.3.

Table 4.3

Bird name	Casper		
Serial number	Condition	h	p value (t-test)
1	LVRV mean speed, LHRH mean speed	1	0.0002
2	LVRV mean speed, LBRB mean speed	0	0.8791
3	LBRB mean speed, LHRH mean speed	1	0.0005
4	LVRV mean axial speed, LHRH mean axial speed	1	0.0002
5	LVRV mean axial speed, LBRB mean axial speed	0	0.9358
6	LBRB mean axial speed, LHRH mean axial speed	1	0.0003
Bird name	One		
Serial number	Condition	h	p value (t-test)
1	LVRV mean speed, LHRH mean speed	1	0
2	LVRV mean speed, LBRB mean speed	1	0.0292
3	LBRB mean speed, LHRH mean speed	1	0
4	LVRV mean axial speed, LHRH mean axial speed	1	0
5	LVRV mean axial speed, LBRB mean axial speed	1	0.0259
6	LBRB mean axial speed, LHRH mean axial speed	1	0
Bird name	Two		
Serial number	Condition	h	p value (t-test)
1	LVRV mean speed, LHRH mean speed	1	0
2	LVRV mean speed, LBRB mean speed	1	0
3	LBRB mean speed, LHRH mean speed	1	0.0431
4	LVRV mean axial speed, LHRH mean axial speed	1	0
5	LVRV mean axial speed, LBRB mean axial speed	1	0
6	LBRB mean axial speed, LHRH mean axial speed	1	0.0342

Table 4.3 Results of paired two-way t-tests to test for statistically significant differences between flight speeds measured under the various conditions, considered two at a time. Abbreviations are as in Table 4.1a. h is an indicator

of whether the difference is statistically significant at the $p < 0.05$ level (in which case h=1) or not (in which case h=0).

The results shown in Table 4.3 confirm that, for all birds, (a) flight speed is significantly higher with horizontal stripes than with vertical stripes, and (b) flight speed is significantly higher with horizontal stripes than with the blank walls. This is true for total flight speed, as well as axial flight speed. For two of the birds (One and Two), flight speed is significantly lower with vertical stripes than with the blank wall. This, again, is true for total flight speed, as well as axial flight speed. For Casper, on the other hand, there is no significant difference in flight speed between these two conditions, either for total speed or axial speed. Interestingly, Casper exhibits a behaviour that is somewhat different to the other birds: He displays a tendency to decrease his flight speed steadily from the beginning to the end of the flight (see upper left-hand panels of Figures 4.6 and 4.7.

Another way of comparing the flight speeds of the birds under the various conditions is by means of the box plots shown in Figure 4.9. The figure shows a detailed analysis of the total and axial flight speeds measured for the various conditions, for each of the birds One, Two and Casper.

4.9

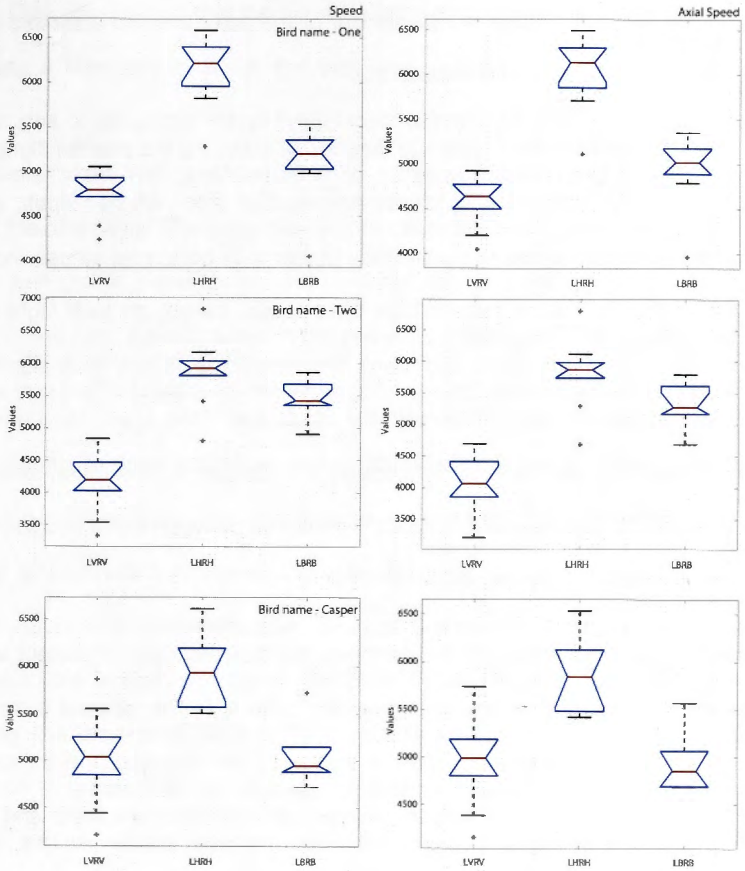

Figure 4.9 Box plot representation of mean speed and mean axial speed for the three different birds, for each of the three different conditions. In each panel of the figure, the horizontal red lines represent the median values of flight speed. The bottom and top edges of the blue boxes correspond to the 25th and 75th percentiles of the data sets. The notches in the blue boxes represent 95% confidence intervals for the median values: If the notches in two data sets do not overlap, this means that their median values are significantly different at the $p < 0.05$ level. The whiskers represent the data points that are farthest above and below the median value, and within 1.5 times the inter-quartile range (25%

to 75%), i.e. within 1.5 times the height of the box. The red asterisks denote samples that lie outside the whiskers.

We see from the Figure 4.9 that, for all birds, (a) the median flight speed is significantly higher with horizontal stripes than with vertical stripes, and (b) the median flight speed is significantly higher with horizontal stripes than with the blank walls. This is true for total flight speed, as well as axial flight speed. For two of the birds (One and Two), the median flight speed is significantly lower with vertical stripes than with the blank wall. This, again, is true for total flight speed, as well as axial flight speed. For Casper, on the other hand, there is no significant difference in median flight speed between these two conditions, either for total speed or axial speed.

Broadly speaking, therefore, the data from the box plots are consistent with the results of the statistical analysis given in Table 4.2. The general pattern that emerges from the above analyses is that (with one exception), flight speed is highest with the horizontal stripes, intermediate with the blank walls and lowest with the vertical stripes.

4.4 Discussion

4.4.1 Flight trajectories through narrow passages

When both walls are lined with vertical stripes, the birds fly close to the midline, i.e. midway between the two walls. How do the birds gauge and balance the distances to the two walls, given the fact that they do not possess stereo vision to estimate distance in the lateral fields of view?

One possibility is that the birds navigate through the middle of the tunnel by flying a trajectory in which the two eyes experience approximately equal magnitudes of optic flow. When flying closer to one wall, the corresponding eye (eye closer to the wall) would experience a greater magnitude of optic flow than would the other eye. This imbalance would cause the bird to veer away from the closer wall and to move toward the centre of the passage, where the balance between the optic flows induced in the two eyes is restored. This strategy would ensure that the bird flies a collision-free path through the middle of the passage.

Do the budgerigars adopt such a strategy? The results shown in Figure 4.3B and 4.3C suggest that this is indeed the case. When one wall carries vertical stripes (which induce strong optic flow) and the other horizontal stripes (which induce little or no optic flow, because the horizontal stripes are oriented parallel to the direction of flight), the birds fly significantly closer to the wall carrying the horizontal stripes. The results of Figure 4.4 provide further evidence in support of the strategy of balancing optic flow. When one wall carries vertical stripes and the other is devoid of any visual texture (and therefore induces no image motion and hence no optic flow), the birds fly very close to the blank wall, occasionally grazing it (Figure 4.3A, B).

These results suggest that budgerigars negotiate narrow passages safely by steering a course such that the two eyes experience similar rates of image motion, or 'optic flow'. When both walls carry visual textures that provide optic flow (as is usually the case in a natural environment), this strategy ensures that the bird flies a collision-free path through the middle of the passage.

However, optic flow cannot be the only cue that the birds use to navigate through the centre of the tunnel. This is because they fly through the middle of the tunnel even when the walls do not provide any optic-flow cues, as in the case when the walls are blank (Figure 4.4 A) or carry horizontal stripes (Figure 4.4 B). Evidently, in the absence of the optic flow cues, the birds are relying on other cues to steer a collision-free course. It is unlikely that stereo vision is used to gauge the distance to the walls, because budgerigars anatomically have little or no binocular overlap. If any overlap exists at all, is likely to be restricted to a narrow region in the front of the animal. Therefore, in order to extract stereo-based information on range, the birds would have to turn their head frequently from side to side to gauge and compare the distances to the two walls. Since I have not observed such head movements (see Chapter 6,) it is unlikely that stereo vision plays a role in guiding the flight through the tunnel. It is possible that the birds are relying on the geometrical cues that are inherent to the structure of the tunnel – for example, the positions of the two lateral boundaries of the floor in the visual field. Flight through the middle of the tunnel could be achieved by taking a trajectory in which the images of these two boundaries are located symmetrically to either side of the centre of the visual field. Further experiments are required to investigate the possibility that this is used as an additional cue.

Control of the height of flight appears to be considerably less tight than control of the lateral position of flight along the width of the tunnel (compare Figure 4.5 with Figures 4.2, 4.3 and 4.4). There could be several reasons for this, three possible explanations being:

1) There are no visual patterns on the floor or on the ceiling, hence optic flow cues for centring in the vertical plane are weak or absent. (However, this explanation is not consistent with the observation that the centring response persists in the horizontal plane even when the optic flow cues are removed - see Figure 4.4);

2) The centring response is less pronounced in the vertical plane because the height of the tunnel is greater than its width, thus making centring less critical in the vertical plane;

4.4.2 Control of flight speed

The observation that the mean flight speed through the tunnel varies with the patterns with which the walls are lined, indicates that visual cues play a significant role in controlling flight speed. For all of the birds tested, the mean flight speed is lower with the vertical stripes (which provide strong optic flow cues) than with the horizontal stripes or with the blank walls, both of which provide weak or no optic flow cues. Thus, it appears that the speed of flight is at least partly regulated by optic flow.

For birds Casper and One, the mean bird flight speed is lower with the blank walls than it is with the horizontal stripes. Why do the birds fly slower when the walls are blank – given that both of these conditions provide no horizontal image motion cues, at least in theory? It is possible that the visual system extracts weak motion cues even from the blank-walled tunnel. The contrast of the blank walls was not truly zero: rather, it was very low. Residual contrast features arising from imperfections in the surface of the wall, from the painting process, and from light and shade effects, could have contributed to

the detection of image movement. Indeed, it is known that most visual systems can sense motion even at contrasts as low as a few per cent (Dvorak et al., 1980). Furthermore, it is possible that contrast adaptation – a phenomenon whereby the contrast sensitivity of the visual system is enhanced in the presence of low ambient contrast, and suppressed in the presence of high ambient contrast (Harris et al., 2000) - plays a role in amplifying the sensitivity to low contrasts. In the case of the blank walls, the absence of high environmental contrast would have made the visual system highly sensitive to the low-contrast flaws in the stimulus, whereas in the case of the horizontal stripes the presence of a high environmental contrast would have made the system insensitive to such flaws. Since the horizontal stripes, by themselves, carry no horizontal image motion cues, it is reasonable to expect that, in the presence of contrast adaptation, the horizontal image motion signals will be weaker with the horizontal stripes than with the blank walls, causing the flight speed to be generally higher in the former case. This is indeed what occurs (Figures 4.6 and 4.7).

4.4.3 Image velocities experienced during flight

For a bird flying at an axial speed of V mm/sec through the middle of a tunnel of width D mm, the angular velocity ω of the images of the walls in the lateral fields of view (in a viewing direction at 90 degrees to the flight direction) is given by (Srinivasan et al., 2000; Srinivasan and Zhang, 2000):

$$\omega = \frac{180}{\pi}\left[\frac{2V}{D}\right] \text{ degrees/second} \qquad (1)$$

Using D = 1360 mm for the tunnel width, the average image angular velocities that would have been experienced by the three birds Caspar, One and Two during flight in the vertical-striped tunnel, as estimated from (1), are given in Table 4.4. It is evident from this table that, on average, the birds experienced an image angular velocity of about 400 degrees/second.

Table 4.4

Bird	Mean axial flight speed (V, mm/sec)	Estimated average image angular velocity (ω, deg/sec)
Caspar	5033.26	424
One	4750.84	400
Two	4174.77	351
Grand means	**4652.96**	**391**

Table 4.4 Average image angular velocities for the three birds during flight through the vertical striped tunnel, as estimated using (1).

4.4.4 Comparison with flying insects

Over the past twenty years, research on flying insects has yielded a considerable amount of information about how these creatures use visual cues to avoid collisions with obstacles, and to regulate flight speed (Baird et al., 2010; Baird et al., 2011; Barron and Srinivasan, 2006; Srinivasan and Zhang, 2004). Studies of honeybees flying through tunnels have revealed that they, too, steer a collision-free path by balancing the magnitudes of the optic flow that are experienced by the two eyes (Kirchner and Srinivasan, 1989; Srinivasan et al., 1991). Examination of the speed of their flight through tunnels of various widths, and with the patterns on the walls either stationary or moving at various speeds

in either direction, has revealed that honeybees regulate the speed of their flight by holding the image velocity in the lateral fields of their eyes constant at a value of approximately 300 deg/sec (Baird et al., 2005; Srinivasan et al., 1996). This value is not very different from the average value of around 400 degrees/second found here for the image velocity that the birds seem to maintain in their tunnel flights. Whether this similarity in image velocities is merely a coincidence, or reflects a more general principle of visual guidance, remains to be determined. Further experiments, using longer tunnels and tunnels of various widths, and displaying stationary and moving patterns on the walls, would be necessary to investigate more comprehensively the visual control of flight speed in birds.

The experiments described here show that budgerigars fly about 1.5 times faster when the tunnel is lined with horizontal stripes, as compared with vertical stripes (Figures 4.6, 4.7, 4.8 and 4.9). In the case of honeybees, this effect is more pronounced: the speed-up factor is about 2.5-3.0 (Baird et al., 2005; Barron and Srinivasan, 2006). One reason for this difference may be that the tunnels that I used for the bird experiments were not long enough to allow the birds to reach a steady-state cruising flight speed: they may have had to decelerate before cruise was fully attained, in preparation for landing at the far end or turning back. Further work, using longer tunnels, would be needed to investigate this possibility.

Notwithstanding these quantitative differences, the findings of this study seem to suggest broadly that budgerigars, like honeybees, (a) navigate through narrow passages safely by balancing the magnitudes of optic flow in the two eyes and (b) regulate the speed of their flight by holding constant the velocity of

the image of the environment. Thus, some of the principles that underlie visually guided flight may be shared by all diurnal, flying animals.

Chapter 5

Obstacle avoidance in flying budgerigars

5.1 Introduction

Short range navigation in a complex and cluttered environment relies heavily on the use of visual cues to control the direction and speed of flight, as well as to avoid collisions with intervening obstacles. This is true for most birds, with a few exceptions such as the Cave Swiftlet (*Collocalia spodiopygius*) which flies in total darkness, using acoustic echolocation to avoid obstacles (Griffin and Thompson, 1982).

Birds need to acquire three dimensional information about their environment in real time, and to avoid collisions with natural obstacles such as trees, bushes and rock faces, as well as man-made objects such as lamp posts, pylons and buildings (Erickson et al., 2001). Gos hawks display a very impressive ability to fly at high speeds through highly cluttered environments, such as a dense forest, in a collision free manner (Animal Camera BBC documentary: http://www.youtube.com/watch?v=p-_RHRAzUHM).

Obstacle avoidance has been investigated in pigeons (*Columba livia*) where it was shown that a subpopulation of neurons in the nucleus rotundus in the pigeon brain produces a strong response when a pigeon approaches an obstacle in its flight path. These neurons respond at a specific time point before collision occurs, and the response is independent of the velocity of approach or the size of the object, suggesting that these neurons may indeed be computing the time to contact, Tau. Their study, however, falls short of making a claim about the role played by these neurons (Wang and Frost, 1992).

In a separate study, freely flying tree swallows (*Tachycineta bicolor*), when confronted with a pair of apertures through which they can potentially fly, will choose to fly through the large aperture (Mandel et al., 2008).

In the context of collision avoidance, the greatest known risk to birds comes from on shore and off shore wind turbines that are located on the routes of migratory birds. Collisions with the moving wind turbine blades are usually fatal (Allan L and Rowena H. W, 2006; Allan and Rowena, 2008), particularly at night (Mabee et al., 2009). Clearly, the ability to avoid stationary and moving obstacles during flight is essential for the survival of birds.

In this chapter I begin to explore how budgerigars fly through cluttered environments safely by video-filming their flight paths as they negotiate a narrow aperture. I also examine how budgerigars choose between two apertures that are identical, or of different widths, in an attempt to understand how these birds make choices between the various paths that can be taken whilst traversing a complex environment.

5.2 Methods

5.2.1 Experimental Arena

The experimental arena was as described in 'General Methods' chapter (Chapter 2) of this thesis. Birds were flown through a tunnel, as in Chapter 4. Each of the side walls was decorated with an array of black and white vertical stripes of 11 cm width. This arrangement provided the birds with optic flow in their lateral visual fields as they flew through the tunnel. Halfway along the tunnel (3000 mm from the start) the birds encountered a transversely oriented wall, which presented either one aperture (in one set of experiments) or two

apertures (in another set of experiments). The transverse wall was made of cloth (SJS061021 Studio jet synthetic outdoor 180MIC, GBC Australia, for the single aperture experiments, SJCLOTH91418, Studio jet instant dry cloth, GBC Australia, for the double aperture experiments), which was either blank white or decorated with a black-and-white checkerboard pattern (check size 4 cm x 4 cm).

5.2.1.1. Flight through a single aperture

In the first set of experiments the transverse wall carried the checkerboard texture and presented a single, vertically oriented aperture, extending from the floor to the ceiling. Depending upon the experiment, the width of the aperture was 50%, 25% or 12.5% of the width of the tunnel. These widths were 64 cm (69.4 cm), 34 cm (34.2 cm) and 17 cm (18.5 cm), respectively (values in brackets indicate the actual values).

In a second set of experiments, the width of the aperture was held constant at the narrowest value 17 cm (18.5 cm), but the visual textures on the surfaces flanking the walls were varied systematically. Depending upon the experiment, these flanking surfaces were (a) textured on both sides (b) blank on both sides (c) blank on the left side and textured on the right side, or (d) blank on the right side and textured on the left side. These configurations are illustrated in Figures 5.1B to 5.1E. The control configuration without any obstacles is illustrated in Figure 5.1A.

5.2.1.2 Aperture preference in flight

In these experiments the transverse wall presented two apertures, each oriented vertically and extending from the floor to the ceiling, as shown in Figure

5.1F. The two apertures were created by constructing the transverse wall out of three panels. There were two outer panels, each 45 cm wide extending inwards from the side walls. In addition there was a central panel, 34 cm wide. All of the panels carried the checkerboard pattern (The error in the width of about 2 cm is observed as the tunnel is not a very symmetrical rectangular cuboid). The relative widths of the two apertures were varied systematically, in different experiments, by changing the position of the central panel along the width of the tunnel. When the central panel was positioned exactly midway between the two outer panels, each aperture was 5 cm wide. Displacing the central panel to the left caused the left-hand aperture to become narrower and the right-hand aperture to become wider, and vice versa. By varying the position of the central panel in steps of 1 cm, the relative widths of the two apertures were varied systematically from one extreme of 0cm (left) and 10 cm (right), through the symmetrical position of 5 cm (left) and 5 cm (right) to the other extreme of 10 cm (left) and 0 cm (right), as shown in Table 5.1 below. The 11 different experimental conditions were presented in random sequence, using a computer-generated sequence of random numbers using Matlab (Mathworks, USA).

Table 5.1

Aperture widths		
Experimental condition	Left	Right
1	0 cm	10 cm
2	1 cm	9 cm
3	2 cm	8 cm
4	3 cm	7 cm
5	4 cm	6 cm
6	5 cm	5 cm
7	6 cm	4 cm
8	7 cm	3 cm
9	8 cm	2 cm
10	9 cm	1 cm
11	10 cm	0 cm

Table 5.1 Widths of left-hand and right-hand apertures in the two-aperture experiment.

5 birds were used in this set of experiments. Each bird was tested on each of the experimental conditions for between 6 and 14 trials, so that each bird made a total of 106-107 choices. The data were analysed to obtain the choice frequency (expressed as a percentage of the total number of choices) for the right-hand aperture, for each experimental condition and for each bird. Thus, if a particular bird chose the right-hand aperture in 8 out of 11 trials in one particular experimental condition, its choice frequency for the right-hand aperture was

calculated as 100x(8/11)% = 73%. The choice frequency for the left-hand aperture was then 100%-73% = 27%.

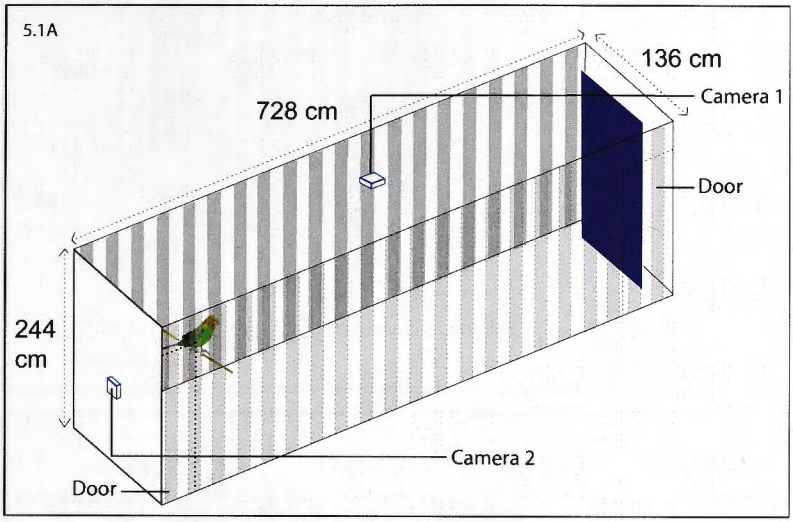

Figure 5.1A Configuration for control experiments, in which the tunnel carried no obstacles or apertures. The budgerigar was released in front of camera 2 and its flight path covered the entire length of the tunnel. The bird exited the tunnel from the door near the blue screen at the far end.

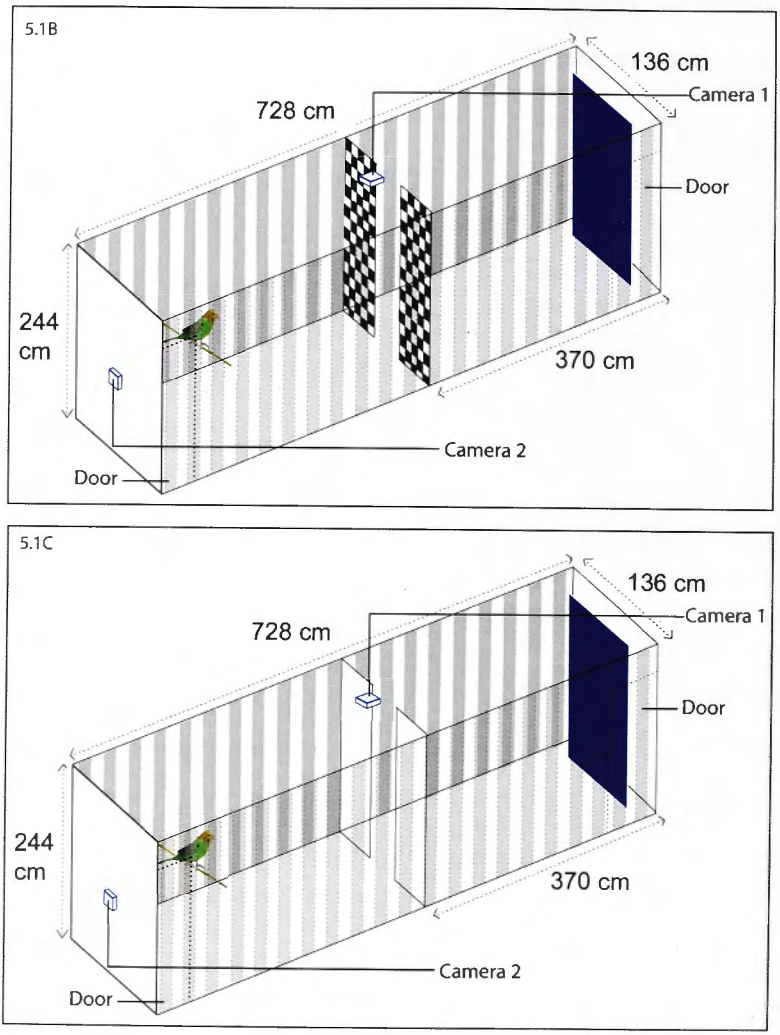

Figure 5.1B and C Illustration of the configuration for the single-aperture experiments with the flanking panels carrying a checkerboard texture (B) or no texture (C).

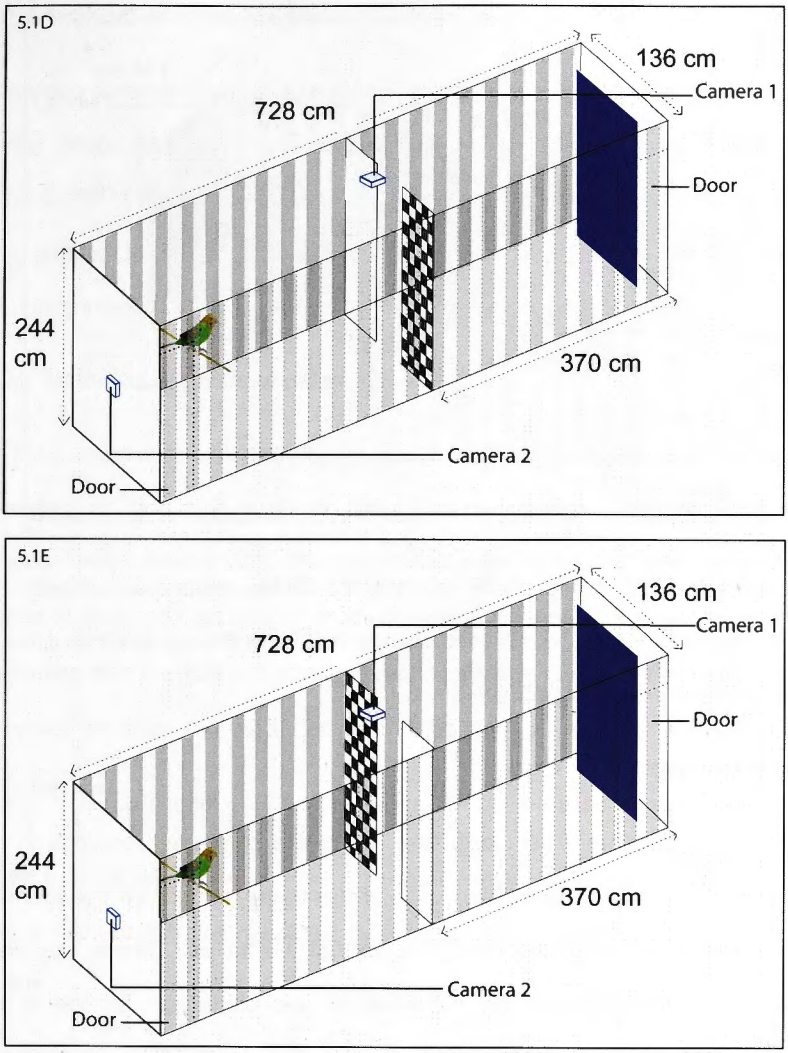

Figure 5.1 D and E Further experimental configurations in which the aperture is flanked by one textured panel and one untextured panel.

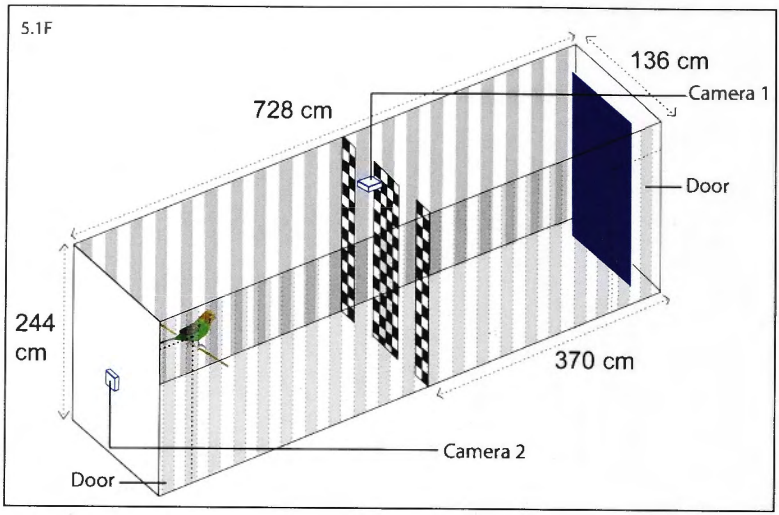

Figure 5.1F Experimental configuration for the double aperture experiments. The central panel can be moved to change the size of the apertures on either side corresponding to the Table 5.1.

5.2.2 Training

The budgerigars were trained to take off from a perch, as described in the 'General Methods' chapter (Chapter 2) of this thesis, fly through the aperture, and then leave the tunnel through a door at the far end, where they were reunited with their companions. The training was carried out for one to two days. Once training was complete (as described in the 'General Methods' chapter (Chapter 2)), the bird was flown under different experimental conditions.

5.2.3 Video Recording

Video recordings of the bird flights were carried out as described in the 'General Methods' chapter (Chapter 2) of this thesis.

5.2.4 Analysis of video images

The video cameras were run at a frame rate of 250 frames per second. Analysis of the videos was carried out as described in the 'General Methods' chapter (Chapter 2) of this thesis. Custom written Matlab code was used for analyzing and plotting the flight trajectories. Trajectories were plotted without down sampling the data.

5.2.5 Statistical analysis of data

In the two-aperture experiments, the choice frequencies for the apertures were analysed to determine whether they were significantly different from the random-choice level of 50%. If a bird chooses the right-hand aperture n times out of N trials, the probability of choosing the right-hand aperture α is n/N. Assuming that the bird's choice behaviour follows a binomial distribution, the standard error of the mean of this distribution, σ, can be calculated as $\sigma = \sqrt{\frac{\alpha(1-\alpha)}{N}}$ (Schefler, 1979). This value of σ is then used in a standard two-tailed t-test to determine whether α is significantly different from the random-choice level of 50%, as described in (Schefler, 1979) and (van Hateren et al., 1990).

5.3 Results

5.3.1 Flight through a single aperture

Experiments were conducted on 7 birds. In one series of experiments, I flew birds through a tunnel that presented a single aperture of variable width, as described above in the 'General Methods' chapter (Chapter 2) of this thesis.

The results are shown in Figure 5.3. As the aperture was progressively narrowed, the birds showed a greater likelihood to collide with or graze past the flanking walls (Figure 5.3 D). This was particularly evident when the flanking walls were blank, i.e. devoid of any visual texture (Figures 5.4 B and F). Evidently, the textural cues offered by the flanking walls are important in enabling their detection and in allowing their distance to be gauged.

A comparison of the collisions observed with flanking walls that are textured or blank is given in Table 5.2 and a bar graph showing the collision rates is shown in Figure 5.2.

Table 5.2

Both obstacles blank					
Bird name	One	Two	Casper	Saras	Drongo
Flight number					
1	Xii	Vi	I	No data	No data
2	I	vi 'C'	iii 'C'	No data	No data
3	Vi	I	I	No data	No data
4	vi 'C'	vi 'C'	Vi	No data	No data
5	Vi	I	Xiii	No data	No data
6	Xii	vi 'C'	Vi	No data	No data
7	Vi	I	I	No data	No data
8	Xii	vi 'C'	Xii	No data	No data
9	Xii	vi 'C'	Xii	No data	No data
10	Vi	Vi	Vi	No data	No data
Both obstacles checked					
Bird name	One	Two	Casper	Four	Spice
Flight number					
1	Vi	Xiii	I	Iii	Viii
2	Vi	Vi	Ii	No data	Vi
3	Vi	Ii	I	No data	Vi
4	Vi	I	I	No data	Vi
5	Vi	Vi	I	No data	Vi
6	Vi	Vi	Iii	No data	I
7	Vi	I	I	No data	I
8	Xii	Vi	I	No data	I
9	Vi	No data	I	No data	I
10	Vi	Vi	I	No data	I

Left obstacle blank and right obstacle checked					
Bird name	One	Two	Casper	Saras	Drongo
Flight number					
1	Xii	Vi	I	No data	No data
2	Xii	iii 'C'	I	No data	No data
3	xii 'C'	Vi	I	No data	No data
4	I	Vi	I	No data	No data
5	xii 'C'	Vi	I	No data	No data
6	Iii	Vi	I	No data	No data
7	Vi	Vi	I	No data	No data
8	I	Vi	No data	No data	No data
9	Xii	Vi	No data	No data	No data
10	Vi	Vi	No data	No data	No data
Right obstacle blank and left obstacle checked					
Bird name	One	Two	Casper	Saras	Drongo
Flight number					
1	Ii	Vi	Vi	I	No data
2	Vii	Vi	Viii	I	No data
3	Iii	Vi	Vi	I	No data
4	Vi	V	Vi	I	No data
5	iv 'C'	Vi	Iii	I	No data
6	Vi	Vi	Vi	I	No data
7	Vi	Vi	Ii	Vi	No data
8	Xii	Vi	Vi	I	No data
9	iv 'C'	I	Vi	I	No data
10	Vi	I	Vi	I	No data
Control (No obstacles)					
Bird Name	One	Two	Casper	Saras	Drongo
Flight number					
1	NC	NC	NC	NC	NC
2	NC	NC	NC	NC	NC
3	NC	NC	NC	NC	NC
4	NC	NC	NC	NC	NC
5	NC	NC	NC	NC	NC
6	NC	NC	NC	NC	NC
7	NC	NC	NC	NC	NC
8	NC	NC	NC	NC	NC
9	NC	NC	NC	NC	NC
10	NC	NC	NC	NC	NC

Index of symbols

(i) Both wings folded backwards
(ii) Left wing extended horizontally, right wing closed/up
(iii) Right wing extended horizontally, left wing closed/up
(iv) Right wing up, left wing down
(v) Left wing up, right wing down
(vi) Both wings up
(vii) Head on collision with obstacle but bird flies through the opening
(viii) Head on collision with obstacle and bird turns back
(ix) Right wing folds upwards and then slightly backwards is shown by 'A'
(x) 'C' denotes collision
(xi) 'NC' denotes no collisions in control flights. (xii) Barrel roll
(xiii) No collision and bird turns back

Table 5.2 Summary of the collision rates and flight patterns of budgerigars as they traverse an opening that was 12.5% of the total width of the tunnel. Different arrangements of checked and blank patterns were tested.

5.2

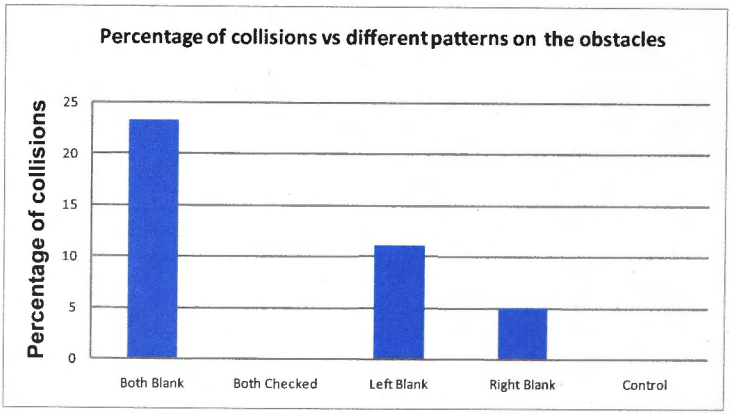

Figure 5.2 Percentage of collisions while negotiating the narrow gap between the obstacles with different types of patterns.

When the aperture was absent (control condition, Figure 5.3 A) (Video 5.1) or when it was relatively wide (e.g. 50% of the tunnel width, Figure 5.3 B, Video

5.2 and 25% of the tunnel width, Figure 5.3 C, Video 5.3), the birds flew in a straight line throughout their entire trajectory. However, when the aperture was narrowed further (e.g. 12.5 % of the tunnel width); the birds no longer flew in a straight line. Instead, they approached the aperture from the left or the right, and flew through it in an oblique direction (Figures 5.3 D and H) (Video 5.4 and 5.5).

The direction from which a narrow aperture was approached depended upon the individual bird. Among the 7 birds that were tested under different experimental conditions, three birds participated in all the experiments. Of these three birds, one displayed a strong left bias, while the other two displayed a right bias. An example of a right-biased bird can be seen in Figures 5.3 C and D (Video 5.4 and 5.6) and an example of a left-biased bird is shown in Figures 5.3 G and H) (Video 5.5 and 5.7).

The direction from which a bird approached a narrow aperture also depended upon the nature of the walls that flanked the aperture. If both of the flanking walls were identical, then this direction depended upon the bias of the particular bird – some preferring to approach from the left, and others from the right, as described above. However, if one of the walls was blank and the other was textured, all birds showed a tendency to avoid the textured wall and approach the narrow aperture from the side of the blank wall. This was true regardless of whether the bird was right-biased (compare Figures 5.4 C and D) (Video 5.8 and 5.9) or left-biased (compare Figures 5.4 G and H) (Video 5.10 and 5.11). The birds behaved as though they were avoiding the textured flanking wall, which appeared as a visible obstacle, and as though they did not detect the blank wall until they had flown very close to it. Evidently, an individual

bird's bias (preference to approach the aperture from the left or from the right) disappears when the bird is confronted with a visually asymmetrical aperture, as described above.

Other interesting behaviours that budgerigars display when negotiating apertures include (a) ceasing wing flapping and (b) increasing flight altitude slightly, just prior to passing through the aperture. These phenomena will be described in detail in Chapter 6.

5.3

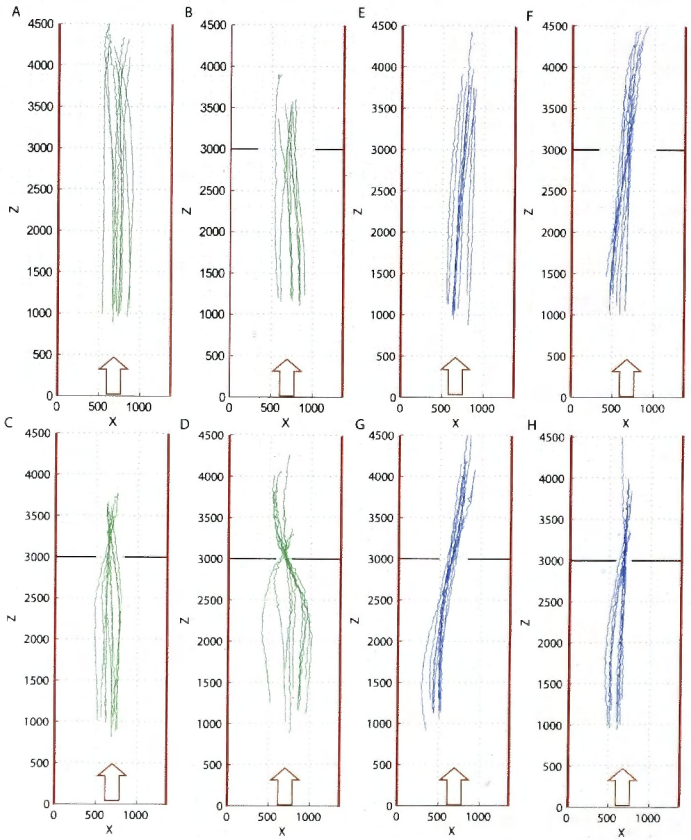

Figure 5.3 (A-D) Flight trajectories of a right-biased bird (One: shown in green) negotiating a tunnel with an aperture of variable width, positioned at 3000 mm.

The aperture is absent in (A) (control condition). Its width is 50% of the tunnel width in (B), 25% in (C), and 12.5% in (D). (E-H): Corresponding data for a left-biased bird (Casper: shown in blue).

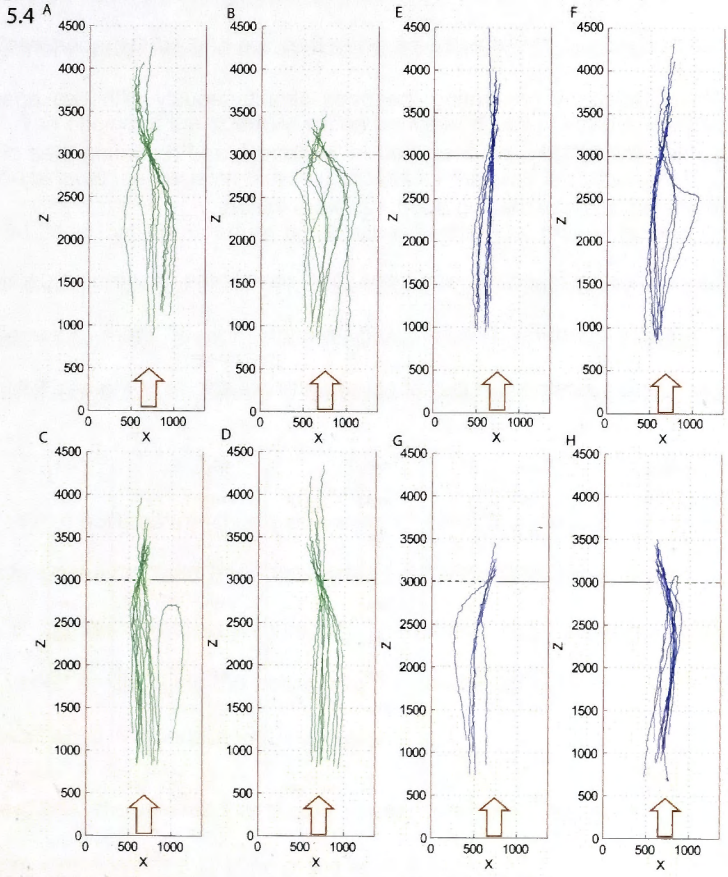

Figure 5.4 Trajectories of a right-biased bird (One; shown in green), and a left-biased bird (Casper; shown in blue) while negotiating the narrowest aperture of width 17 cm (12.5% of the tunnel width). The flanking walls are textured in A and E, and blank in B and F. In C and G, the aperture is flanked by a blank wall on the left and a textured wall on the right. The opposite is true for D and H. As

explained in the text, the bias of each bird can be overridden by a visually asymmetrical aperture.

5.3.2 Aperture preference in flight

How do budgerigars make a choice when they are offered two apertures? This was investigated by presenting the birds simultaneously with two apertures positioned side by side, as described in 'Methods', and recording their choices as the relative sizes of the two apertures were varied.

As the birds approached the apertures they sometimes flew from side to side, viewing each aperture, before flying through one of them. Examples of approach flights to two apertures of equal width are shown in Figures 5.5.

5.5

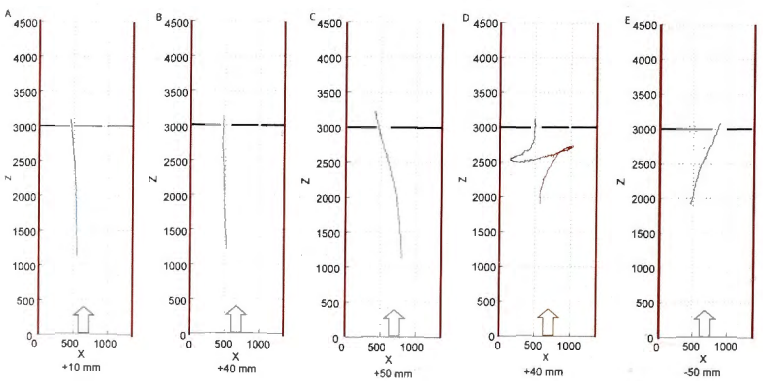

Figure 5.5 Panels A and B show trajectories of a left biased bird while making a choice between two apertures of different sizes. In panel A the right aperture is 40 mm wide while the left aperture is 60 mm wide. In panel B the right aperture is 10 mm wide and the left aperture is 90 mm wide. Panels C, D and E show trajectories of a right biased bird while making a choice between two apertures of different sizes. In Panel C the right aperture is fully blocked while the left

aperture is 100 mm wide and the right biased bird has no option but to take the left aperture. In panel D the right aperture is 10 mm while the left aperture is 90 mm wide. Here the bird tries to fly through the right aperture but is unable to do so and then changes its flight path to go through the left aperture. In panel E the left aperture is blocked and the bird flies through the right opening.

The choice of the aperture varies between different individual birds. Side bias dominates the decision making process for the choice of the opening, but if the bird finds that the aperture is too small in the final moments of approach, then it changes its flight path and flies through the larger aperture, as seen in the example of Figure 5.5 D. However when the birds do not have a choice, they fly through the only opening that is available, as in the example of Figure 5.5 C.

What governs the choice of aperture? This question was approached by examining whether, and if so, how, the bird's choices changed as the relative sizes of the two apertures was varied. The relative sizes of the two apertures were varied by changing the position of the central panel that separated them, as described in 'Methods' section of this chapter.

Figure 5.6 A shows how the choice frequency of bird One for the right-hand aperture varies with the position of the central panel.

5.6 A

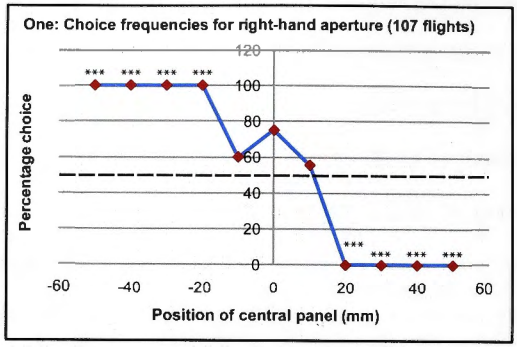

Figure 5.6 A Results of two-aperture experiment for bird One, showing percentage choice frequencies for the right-hand aperture as a function of the position of the central panel. 0 mm denotes the central position, when both apertures are of equal width. Positive values of position denote displacements of the central panel to the right (left-hand aperture wider than right-hand aperture) and negative values of position denote displacements of the central panel to the left (right-hand aperture wider than left-hand aperture). The dashed horizontal line represents the random-choice level of 50%. The symbols next to each data point indicate a statistically significant difference of the choice frequency from the random-choice level of 50%, calculated as described in 'Methods'. [$p < 0.05$: (*); $p < 0.02$: (**) and $p < 0.00001$: (***)].

When the two apertures are equally wide (or nearly so), the bird displays approximately the same preference for either aperture. However, as the central panel is moved towards the left, making the right-hand aperture wider than the left-hand one, the bird exhibits an increased preference for the right-hand aperture, eventually choosing it with 100% probability for leftward displacements of 20 mm or greater. Conversely, when the central panel is shifted progressively towards the right, the bird shows an increasing preference

for the left-hand aperture, eventually choosing it with 100% probability for rightward displacements of 20 mm or greater.

The results of a similar experiment conducted with bird Casper are shown in Figure 5.6 B.

5.6 B

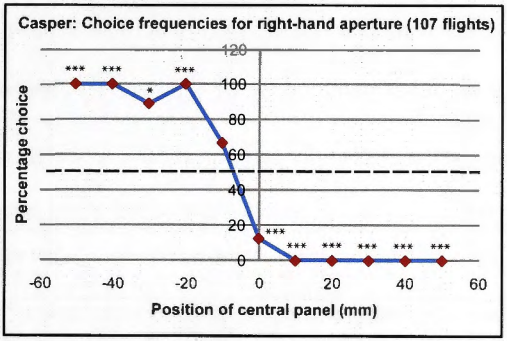

Figure 5.6 B Results of two-aperture experiment for bird Casper, showing percentage choice frequencies for the right-hand aperture as a function of the position of the central panel. 0 mm denotes the central position, when both apertures are of equal width. Positive values of position denote displacements of the central panel to the right (left-hand aperture wider than right-hand aperture) and negative values of position denote displacements of the central panel to the left (right-hand aperture wider than left-hand aperture). The dashed horizontal line represents the random-choice level of 50%. The symbols next to each data point indicate a statistically significant difference of the choice frequency from the random-choice level of 50%, calculated as described in 'Methods'. [$p < 0.05$: (*); $p < 0.02$: (**) and $p < 0.00001$: (***)].

The results are similar in that Casper, like One, shows a strong variation in the relative preferences for the two apertures when their relative widths are varied.

However, when the apertures are of equal width the bird shows a greater preference for the left-hand opening, choosing it 87.5% of the time. This choice probability is significantly different from the random-choice level of 50% ($p < 0.02$). This implies that Casper has a preference for the left-hand opening, and that this bias is superimposed upon the bird's tendency to choose the larger of the two apertures.

The results of an experiment conducted with bird Two are shown in Figure.5.6 C.

5.6 C

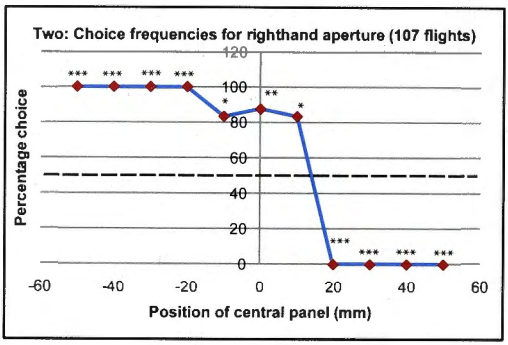

Figure 5.6 C. Results of two-aperture experiment for bird Two, showing percentage choice frequencies for the right-hand aperture as a function of the position of the central panel. 0 mm denotes the central position, when both apertures are of equal width. Positive values of position denote displacements of the central panel to the right (left-hand aperture wider than right-hand aperture) and negative values of position denote displacements of the central panel to the left (right-hand aperture wider than left-hand aperture). The dashed horizontal line represents the random-choice level of 50%. The symbols next to each data point indicate a statistically significant difference of the choice

frequency from the random-choice level of 50%, calculated as described in 'Methods'. [p < 0.05: (*); p < 0.02: (**) and p < 0.00001: (***)].

Bird Two again shows a behaviour that is essentially similar to those of One and Caspar, except that this bird possesses a preference for the right-hand aperture. This bird chooses the right-hand aperture 87.5% of the time when the two apertures are equally wide, and this preference is significantly greater than the random choice level of 50% ($p < 0.02$).

Figures 5.6 D and E show results for two other birds, Drongo and Saras. Drongo is right-biased, while Saras is left-biased.

5.6 D

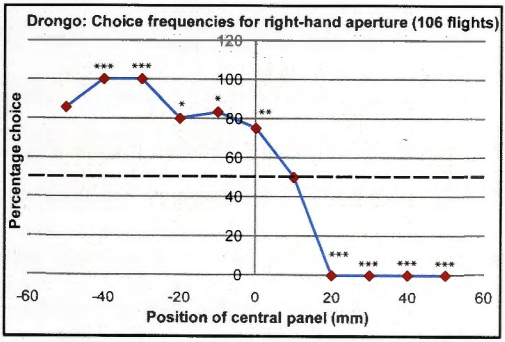

Figure 5.6 D. Results of two-aperture experiment for bird Drongo, showing percentage choice frequencies for the right-hand aperture as a function of the position of the central panel. 0 mm denotes the central position, when both apertures are of equal width. Positive values of position denote displacements of the central panel to the right (left-hand aperture wider than right-hand aperture) and negative values of position denote displacements of the central panel to the left (right-hand aperture wider than left-hand aperture). The dashed horizontal line represents the random-choice level of 50%. The symbols next to

each data point indicate a statistically significant difference of the choice frequency from the random-choice level of 50%, calculated as described in 'Methods'. [p < 0.05: (*); p < 0.02: (**) and p < 0.00001: (***)].

5.6 E

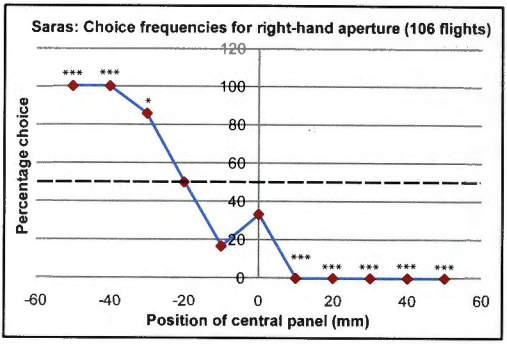

Figure 5.6 E. Results of two-aperture experiment for bird Saras, showing percentage choice frequencies for the right-hand aperture as a function of the position of the central panel. 0 mm denotes the central position, when both apertures are of equal width. Positive values of position denote displacements of the central panel to the right (left-hand aperture wider than right-hand aperture) and negative values of position denote displacements of the central panel to the left (right-hand aperture wider than left-hand aperture). The dashed horizontal line represents the random-choice level of 50%. The symbols next to each data point indicate a statistically significant difference of the choice frequency from the random-choice level of 50%, calculated as described in 'Methods'. [p < 0.05: (*); p < 0.02: (**) and p < 0.00001: (***)].

Putting aside the biases shown by the individual birds for the moment, the results reveal that each of the birds is quite sensitive to the differences in the widths of the two apertures. In each case, the bird's preference shifts from fully

in favour of the right-hand aperture to fully in favour of the left-hand aperture, when the barrier is displaced rightward by a distance of about 20 mm. This represents a 40% change in the width of each aperture from the symmetrical configuration, where each aperture is 50 mm wide.

The results also reveal that individual birds display specific biases with respect to the choice of the two apertures. Bird One displays no significant bias. Two birds (Casper and Saras) show a preference for the left-hand aperture, while two other birds (Two and Drongo) show a preference for the right-hand aperture. The above results indicate that each bird displays a characteristic bias.

What about the population as a whole? I have attempted to examine this question by averaging the data from all of the birds, point by point, for each aperture width. The results are shown in Figure 5.6 $F_{,}$ which represents the average of the results obtained for all of the five birds, shown above in Figures 5.6 A-E.

5.6 F

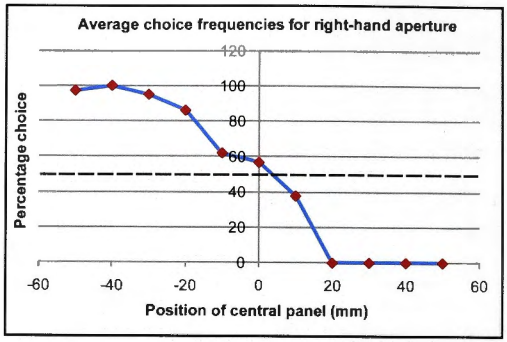

Figure 5.6 F Average preference for the right-hand aperture as a function of the position of the central panel, obtained by pooling the choice frequency curves of all 5 birds (Figures 5.6 A-E, above).

The averaged curve shows relatively little bias, as one might expect, given that in the group of birds that I tested, one bird showed no bias, two showed a right-bias and two others a left-bias. Furthermore, while the relative preferences for the two apertures change sharply as a function of their relative widths for each individual bird, the relative preferences of the population as a whole change much more gradually and smoothly. The reason for this is that the sharp transitions displayed by each bird occur at different points along the horizontal axis, because of the different biases possessed by the individual birds. This smoothing effect may have interesting implications for the behaviour of a flock of birds, as we shall see later in the Discussion section.

Figure 5.6 F suggests that the population as a whole does not possess any bias. Obviously, a larger sample of birds would need to be examined before this statement can be made with confidence. Nevertheless, the spread of biases

that I have observed, even in the relatively small number of birds that I have investigated, suggests that if there is a population bias, it is likely to be small.

5.4 Discussion

In this chapter I have examined the way in which budgerigars approach and negotiate narrow apertures, with a view to building up an understanding of how birds fly safely through cluttered environments.

The experiments investigating flight through a single aperture that is progressively narrowed reveal that, while budgerigars fly more or less in a straight line through an obstruction-free tunnel or a wide aperture, they tend to approach a narrow aperture from one side. This approach can be from the right or the left, depending upon the individual bird.

The fact that narrow apertures are approached obliquely means that the closer flanking panel will most likely be viewed only by the ipsilateral eye. This in turn implies that stereo cues are almost certainly not used during this manoeuvre, even if the bird possessed stereo vision (which is not known). It is possible, then, that the nearer flanking panel is viewed by a fovea of the ipsilateral eye (if budgerigars indeed possess a fovea, which is uncertain – see (Jeffery and Williams, 1994). There is some evidence to suggest that budgerigars do not possess a fovea (Mitkus, pers. communication). It is also possible that the birds are using lateral optic flow to avoid collision with, and keep a safe distance from, the nearby flanking panel. This would be difficult to achieve in a head-on approach because the bird would then have to rely on expansional optic-flow cues, which would be weak near the boundaries of a narrow aperture, since these boundaries are very close to the direction of flight.

So, these birds may be employing a different strategy – using one eye to measure lateral optic flow and to use this information to maintain a small, but safe distance from one of the flanking panels, as they fly obliquely through the narrow aperture. This may be a more reliable strategy for avoiding collisions, even though the effective cross-section of the aperture is lower for an oblique approach.

When one of the flanking panels is blank, the birds approach the aperture from the side on which this wall is located. The most likely reason for this is that this flanking panel is nearly invisible, so that the birds come close to colliding with this panel in the process of avoiding the other (textured) panel. Evidently the birds detect the blank panel only when they get very close to it, then turning away from it and using the impoverished flow signals from this panel to avoid and fly past it. As expected, collisions and grazes occur more frequently when both flanking panel are blank (Table 5.2), and also when only one of them is blank (in which case that is the impacted panel). The bias displayed by individual birds to approach a symmetrical, narrow aperture from the left or the right is overridden when the aperture is rendered visually asymmetrical, by making one of the flanking panels blank – the birds then consistently approach the aperture from the side of the blank panel.

When the birds are offered two equally wide apertures, some individuals show a preference to fly through the left aperture and others to fly through the right aperture. This individual bias is again overridden by a preference to choose the wider aperture, when the apertures are made unequal in width. In future experiments it would be of interest to extend the approach presented

here to determine the distance from which the birds can determine which of two apertures is wider.

Interestingly, individuals display consistent biases in the single-aperture experiment as well as the dual-aperture experiment. A bird that approaches a single, narrow aperture from the left also prefers the left-hand aperture when offered two apertures of equal width, and vice versa. This is documented in Table 5.3 below.

Table 5.3

Bird	Bias in single aperture experiment (Both obstacles checked)	Bias in dual aperture experiment (Central panel/obstacles checked)
Casper	Left	Left
Two	Right	Right
Drongo	Left	Left
Saras	Left	Left
One	Right	Right

Table 5.3 Comparison of biases in individual birds with regard to approach direction in the single-aperture experiments, and choice of aperture in the dual-aperture experiments (Some of the data used in the preparation of this table are from Tables 5.2 and 6.2).

Individual bias versus population bias

The experiments with the single and dual apertures suggest that individual birds display significant lateralization in their visually guided behaviour, but that the population as a whole does not possess a clear bias. Obviously, a larger sample of birds would need to be examined before this tentative statement can be confirmed. Nevertheless, the spread of biases that I have observed, even in the relatively small number of birds that I have examined, suggests that if there is a population bias, it is likely to be small.

What might be the selective advantage of having individually varying biases in the way in which birds use vision to guide their flight? One possibility may be an enhancement in the speed and safety with which a flock of birds can fly through dense foliage. It is clear that budgerigars confront this problem often, as is evident, for example, from the picture of a flock perched on a tree (Figure. 5.7).

Figure 5.7 A flock of twelve wild budgerigars sitting on a gum tree.

(www.eremaea.com/sightingphotos/11233.jpg, Posted by Andrew McCutcheon)

When a flock is faced with a choice of flying through one of two clear passages through a thicket of branches, it would be detrimental if all of the birds were to possess the same bias, say, toward the left. A population bias of this kind would tend to make all of the birds try to fly through the left-hand passage, thus blocking each other, and slowing down as well as endangering the passage of the flock through the thicket. (The right-hand passage would not be used at all, and therefore be wasted). It would also be detrimental to have no bias at all in each of the birds, because this would tend to make each individual vacillate in front of two equally wide apertures before making a decision, again slowing down the progress of the flock through the thicket and increasing the likelihood of bird-to-bird collisions. Furthermore, if the two passages were of unequal size, a flock of unbiased birds would all try to fly through the wider passage, overcrowding it and again slowing down progress and increasing the likelihood of bird-to-bird collisions. The narrower passage would not attract any birds even if it was wide enough to permit safe flight, and would thus be a 'waste' of a potentially useful passage for the birds. On the other hand, if, say, half the population was left-biased and the other half right-biased, two apertures of equal width would attract roughly equal numbers of birds, thus speeding up the progress of the flock through the thicket. Furthermore, the left-biased and right-biased birds would choose the left and right-hand apertures without any vacillation, leading to a quicker and safer passage of the flock through the thicket. In this case, as the right-hand aperture is gradually made wider than the left-hand aperture, the birds would not all immediately flock to the right-hand aperture: many of the left-biased birds would continue to favour the left-hand aperture until it becomes too narrow for safe passage. Thus, a hybrid flock of

left and right-biased birds would make better use of both of the available apertures, and fly through the thicket more quickly.

In Appendix 2, I describe a mathematical model that characterizes the above discussion quantitatively, and demonstrates that transit of a flock of birds through a two-passage environment will be most rapid when individual birds in the flock carry different biases, ranging from extreme left-bias, through no bias, to extreme right-bias.

It should be mentioned that, at this stage, the above discussion is only a hypothesis that makes a prediction about how a flock of birds might behave, based on my experiments with individually flown birds. This prediction can, and should, be tested in the future by flying a flock of birds through two-aperture configurations in the laboratory, as well as by observing the behaviour of flocks in the wild. Such experiments may also reveal interesting interactions between individuals, which I have not considered in the above discussion.

My findings with regard to the choices that birds make between two apertures are similar in some respects to those reported by (Mandel et al., 2008) who observed that tree swallows, when presented with two apertures of different width, choose the wider aperture. However, (Mandel et al., 2008) did not examine how this choice behaviour varied with changes in the relative widths of the two apertures – their experiments were conducted with dual apertures that were either equally wide, or that differed in width by a fixed value. While my findings indicate a clear and strong side bias in most of the individuals that I have tested, Mandel et al. found no such side bias in their birds when they were required to choose between two equally wide apertures. It remains to be

examined whether this discrepancy between their results and mine reflects an interspecies difference, or some difference in their experimental procedure, which, as far as I can tell, is very similar to that employed by me.

So far, lateralisation of vision in birds has been investigated mainly with respect to tasks that involve object detection. For example, chickens use their right eye to detect food, and their left eye to maintain a vigil against predators (Rogers, 2000). Birds that are strongly lateralised are able to perform both simple and complex tasks (Magat and Brown, 2009). Their study showed for the first time that birds that have a strongly lateralised brain are good at multitasking and are able to process more sensory information to generate effective motor outputs. For example, parrots which have strongly lateralised brains are able to process information using both their beak and feet during an experimental string pulling task, which involved acquiring a food item suspended from a string and required the use of both the beak and the foot. I believe that my study is the first to study and document lateralisation in a task that involves visual guidance in flight in birds.

Chapter 6

Head and body movements of budgerigars during complex flight manoeuvres

6.1 Introduction

Considerable scientific effort has been devoted in attempting to understand bird flight, particularly through analyzing the kinematics of wing and body movements. Previous studies of bird flight have investigated the aerodynamics of wing movements and the lift generated to keep the birds aloft (Park et al., 2001).

The wings of a bird generate the lift and thrust that is required for flight. The flow of air over the wings causes a lower pressure above the wings and a higher pressure below the wings, which causes lift to be generated. The lift enables the bird to stay in the air (Videler, 2006). But the movement of the wings through the air provides the necessary thrust to propel the bird forward.

Birds use different modes of flight, which vary according to their habits and survival strategies. The flight modes include gliding, soaring and wing flapping. The shape of the wings varies between different bird species, as well as according to their flight modes and habits (Videler, 2006).

The past two decades have witnessed increasing interest in investigating the kinematics of bird flight, in order to gain fundamental insights into the biomechanics of avian flight. These studies, undertaken in a large number of bird species, are beginning to provide a detailed understanding of how the

wings generate the aerodynamic forces necessary to overcome the forces of gravity and drag and enable sustained flight.

In addition to wing movements, movements of other parts of the avian body, like the head, have also been investigated in great detail. The head carries the visual system as well as the vestibular system, which are the primary sense organs that provide the bird with information that is essential for stable, safe and guided flight. Birds are a composite of a pilot and an airplane, embodying an excellent synergy of the sensory and motor systems that are necessary for autonomous flight.

Zebra finches use flap bounding, consisting of flapping of wings followed by flexed wing bounds, where the wings are folded back, to promote energy conservation and increased flight speeds (Tobalske et al., 1999).

Pigeons on a landing approach to a perch often display oscillatory movements of the head in the vertical plane (Frost, 1978). It has been postulated that this so-called 'head bobbing' serves to generate motion parallax cues that convey information on the distance to the target (Green et al., 1992; Green et al., 1994). Head movements during flight have been observed in Barn Owls. These movements consist of three basic movements, namely, rotations, translations and fixations, which enable a bird to estimate the distance to obstacles or prey (Ohayon et al., 2006).

Many birds possess the ability to maintain their head in a stable orientation despite changes in the orientation of their bodies during flight (Tobalske and Dial, 1996; Warrick et al., 2002). It is believed that this serves to minimize rotational movements of the head and the eyes, and enables the flying

bird to obtain a pattern of optic flow that is almost purely translational, and which therefore provides reliable information on the distances to various objects in the scene. Periods of stable head orientation are punctuated by rapid, saccadic rotations, which define a new heading (and heading orientation) that the body eventually follows. Vision is presumably compromised during the saccade, but this period is so short that the resulting momentary blindness – if this is indeed what occurs - is of no great consequence.

Saccadic head movements, interspersed by periods of stable head orientation, have been observed in freely flying Zebra finches (*Taeniopygia guttata*), when they fly through an opening. Stabilization of head orientation helps reduce the rotational components of the optic flow, thus giving the visual system more direct access to the translational component of optic flow, which carries information on the range to objects in the environment (Eckmeier et al., 2008). Stabilization of head orientation in flight has also been observed in blowflies (Schilstra and Hateren, 1999), and has been postulated to serve the same function.

The budgerigar is a desert bird found mostly in inland Australia. These birds migrate in search of food and water. When food and water are abundant, they look for nest holes in the trees and breed (Wyndham, 1981). Thus, they constitute an attractive model system in which to investigate the movements of the head, the eyes, the wings, the body and the tail while flying through open as well as constrained environments, and while evading obstacles.

Here I investigate movements of the head, body and wings of budgerigars during flight, particularly when negotiating narrow spaces and

avoiding obstacles. Some of the results described in this final experimental chapter are preliminary and are not yet conclusive. However, they suggest interesting hypotheses and point to several avenues of further investigation.

6.2 Methods

6.2.1 Experimental arena

All experiments were carried out in the bird flight tunnel described in the 'General Methods' chapter (Chapter2). Vertical strips of black paper (Elle card 135040 ERA1 Black 220 gsm), 11 cm wide, were affixed to both walls of the tunnel at 11 cm intervals. Half way down the tunnel the birds encountered an aperture consisting of a vertical slit, 17 cm (18.5 cm) wide (12.5% of the width of the tunnel) and extending from the ceiling to the floor, through which they had to fly to get to the other end of the tunnel. The aperture was produced by creating a space between two vertical panels, as illustrated in Figure 6.1B and C.

The panels flanking the aperture were made of cloth (SJS061021 Studio Jet Synthetic Outdoor 180MIC, GBC Australia), which was stretched from the floor to the ceiling. This arrangement prevented any injury to the birds when they occasionally collided with the panels.

Three different experimental conditions were used, (A) Control condition, without any aperture (Figure 6.1A) (Video 6.1A), (B) Aperture flanked by panels carrying a checkerboard pattern (4 cm X 4 cm checks) (Figure 6.1B) (Video 6.1B) and (C) Aperture flanked by white panels, carrying no visual texture (Figure 6.1C) (Video 6.1C).

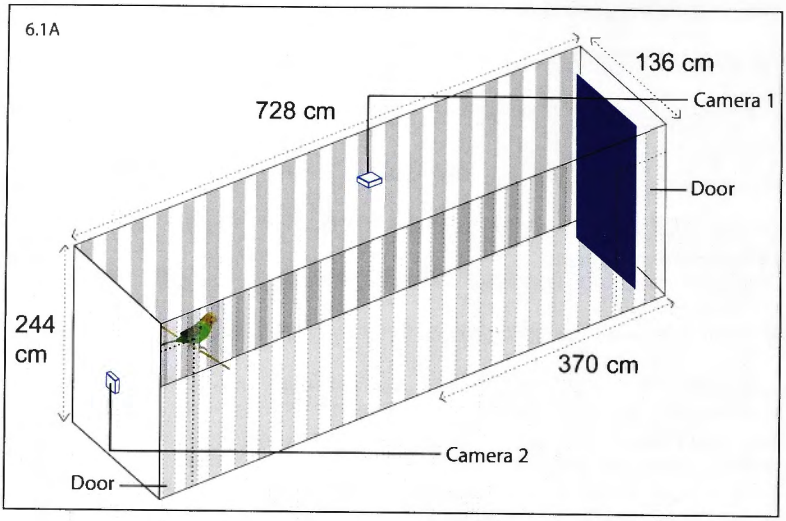

Figure 6.1A Control condition, in which the tunnel carried no aperture.

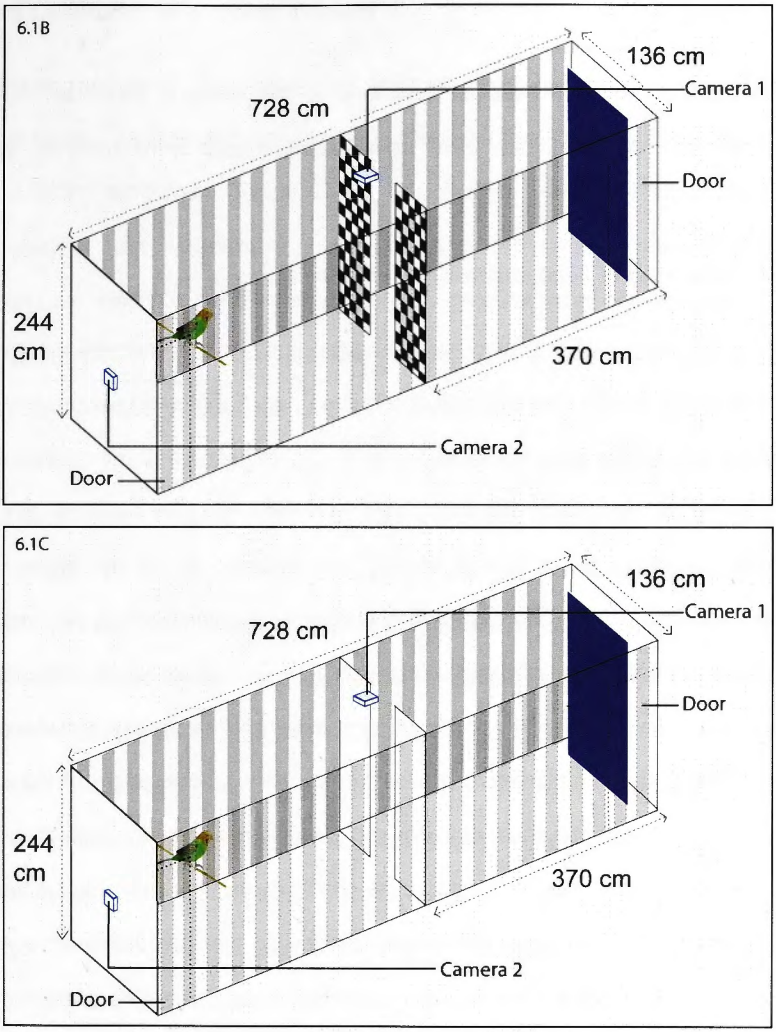

Figure 6.1B and C Experimental conditions in which the tunnel carried an aperture consisting of a vertical slit, 17 cm (18.5 cm) wide, flanked by panels that carried a checkerboard texture (6.1B), or no texture (white) (6.1C).

6.2.2 Training

The training procedure was as described in the 'General Methods' chapter (Chapter 2) of this thesis. Five trained budgerigars were used in these experiments.

6.2.3. Tracking of head and body orientations

The pitch and roll of the head as well as the body were monitored by affixing two markers, one to the head and one to the body. Each marker consisted of a white 1 cm x 1 cm square, oriented such that one diagonal (the so-called axial diagonal) was parallel to the bird's long axis and the other diagonal (the so-called transverse diagonal) was oriented perpendicular to the bird's long axis (Figure 6.2A). The markers therefore appeared as diamonds in the images acquired by the overhead camera (Figure 6.2B). The pitch and roll of the head (or body) were monitored by measuring the lengths of the axial and transverse diagonals of the corresponding marker in the image. If the length of the axial diagonal was at its maximum possible value, this implied that the axial diagonal of the marker was horizontal and that the pitch was therefore zero. If this length was smaller than the maximum value, this implied that this diagonal was not horizontal. The pitch angle was then calculated trigonometrically, as described later below. If the length of the transverse diagonal was at its maximum possible value, this implied that this diagonal was horizontal and that the roll was therefore zero. If this length was smaller than the maximum value, this implied that the transverse diagonal was not horizontal. The roll angle was then calculated trigonometrically, as described later below.

6.2.4 Calibration of tracking markers

Tracking markers in the shape of a white diamond (1 cm X 1 cm) against a black square background, one affixed to the head and another to the tail, were used for the experiment (Figure 6.2 B). The markers were calibrated by printing an array of 18 columns by 8 rows of tracking markers on a sheet of paper, affixing the sheet to a piece of plywood and filming the array of markers with the sheet oriented in the horizontal plane, at a series of different depths below the overhead camera. A small sample of a 4 by 4 array of the tracking markers is shown in Figure 6.2A. The image of the markers obtained at each height was analysed by digitizing the corners of each diamond in the array and computing the lengths (in image pixels) of the axial and transverse diagonals. These measurements were used to generate calibration tables and figures (see Figures 6.3 A and B) that gave the maximum expected lengths of the axial and transverse diagonals, in image pixels, for each height. Since the diamonds were oriented horizontally during calibration, these measurements represented the maximum length of each diagonal for each height. Any reduction of lengths from these maximum values indicated a pitch (in the case of the axial diagonal) or a roll (in the case of the transverse diagonal). The reductions in lengths of these diagonals, at any given height, were used to infer the extent of pitch and/or roll of the body and the head.

The calibration data for the axial and transverse diagonals were approximated well by second-order polynomial functions, as shown in Figures 6.3 A and B. These functions were used to interpolate the data to obtain the expected maximum lengths (in pixels) of the axial and the transverse diagonals

for any given height, by reading off the values on the ordinates of Figures 6.3 A and B.

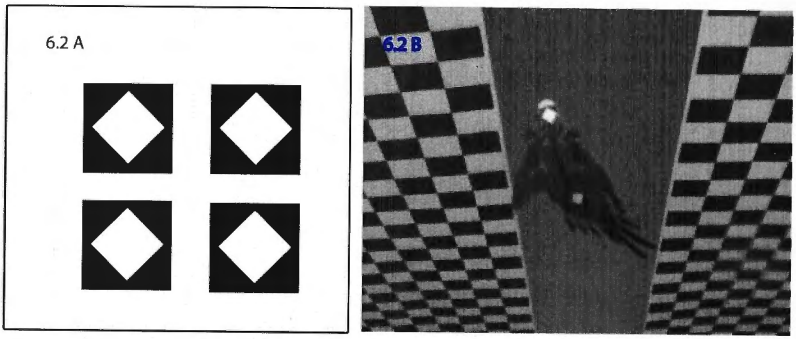

Figure 6.2 A Calibration pattern 6.2 B View of tracking markers on the head and body.

6.3

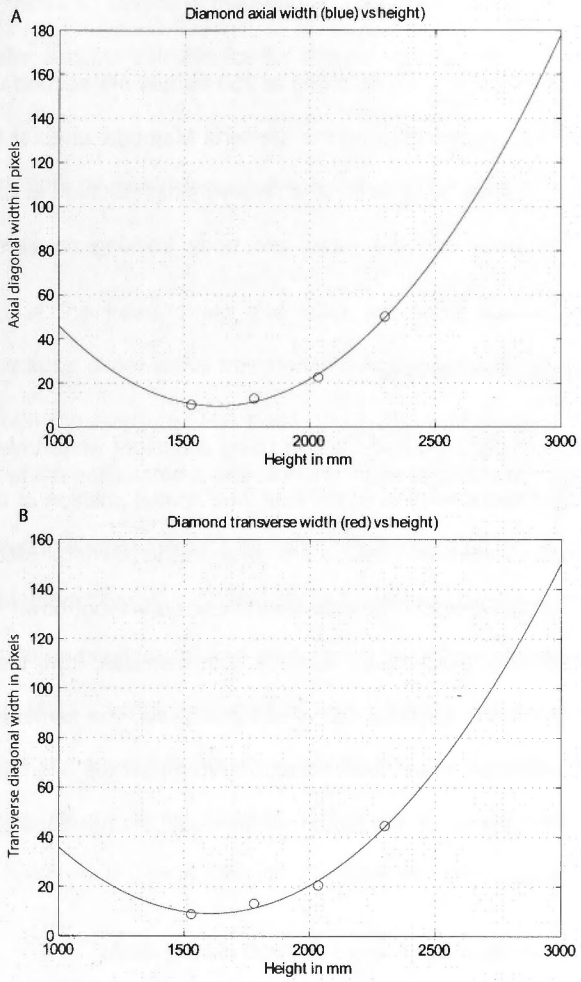

Figures 6.3 A and B. Calibration plots of the lengths of the axial and transverse diagonal widths (in pixels) of the tracking markers, versus height. The curve represents a least-square fit to a second-order polynomial.

6.2.5 Recording of bird flights

The flights of the birds were recorded at 250 frames per second using two high speed cameras, as described in the 'General Methods' chapter (Chapter 2) of this thesis. The birds were flown at a relatively high altitude in order to enable filming of the birds and the head and body tracking markers at a higher resolution.

6.2.6 Analysis of video data

The flights were digitized and tracked using a custom written Matlab program, which enabled determination of the real time spatial position of the budgerigar from the pixel coordinates (details are given in the 'General Methods' chapter (Chapter 2) of this thesis). The data was analyzed without down sampling. The entire flight path of the bird, as seen by both cameras, from the perch to the point of entry into the aperture was used for analysis. The cameras were unable to view the bird after it had flown about 500 mm past the overhead camera. In addition to the markers on the head and the body, the positions of the wing tips were also tracked.

6.2.6.1 Estimation of head and body roll during flight

For each flight the four corners of the head and body tracking markers were digitized, frame by frame, using a custom written Matlab program to determine the experimentally measured values of the lengths (in pixels) of the axial and transverse diagonals in the images of the marker, as viewed by the top camera, all along the flight trajectory. The measured axial and transverse diagonal lengths of the markers on the head and body were then compared with the theoretically expected values, as shown in the calibration data of Figure 6.3, to

compute the pitch and the roll of the head and the body of the bird. The details of the geometry and the calculations for computing pitch and roll are given in Appendix 3.

6.2.6.2 Estimation of positions of the head, body and wing tips during flight

The positions of the head, body and wing tips were tracked in order to determine their three dimensional trajectories over the entire flight, including the passage through the aperture. The head and body were tracked by digitizing the midpoints of the associated markers in the views from the two cameras.

This digitization was carried out by using the tracking program, described in the 'General Methods' chapter (Chapter 2) of this thesis. Custom-written Matlab programs were then used to plot and analyze the trajectories in various ways. A custom written Matlab script was used to make animations of the entire flight trajectory, showing the movements of the head, body and wingtips. Examples of such animations for the three different experimental conditions are given in Videos 6.2 A (Control), B (Blank walls) and C (Checked walls).

6.3 Results

I began by examining the orientations of the body and head during flight. Figure 6.4 shows six examples of the pitch of the head and the body during flight in the tunnel and passage through the aperture. These data show that the body and the head are almost always pitched upward, rather than downward. This is also evident from inspection of the video sequences captured by the camera positioned at the end of the tunnels, which show the views of the body and the head from the rear, revealing that both calibration markers are clearly visible

from this viewpoint. This confirms that both the body and the head are pitched upward, and not downward, throughout the flight. We see from Figure. 6.4 that, in general, the body is pitched at a greater angle than the head, In other words, the head is nearly horizontal, while the body trails downwards.

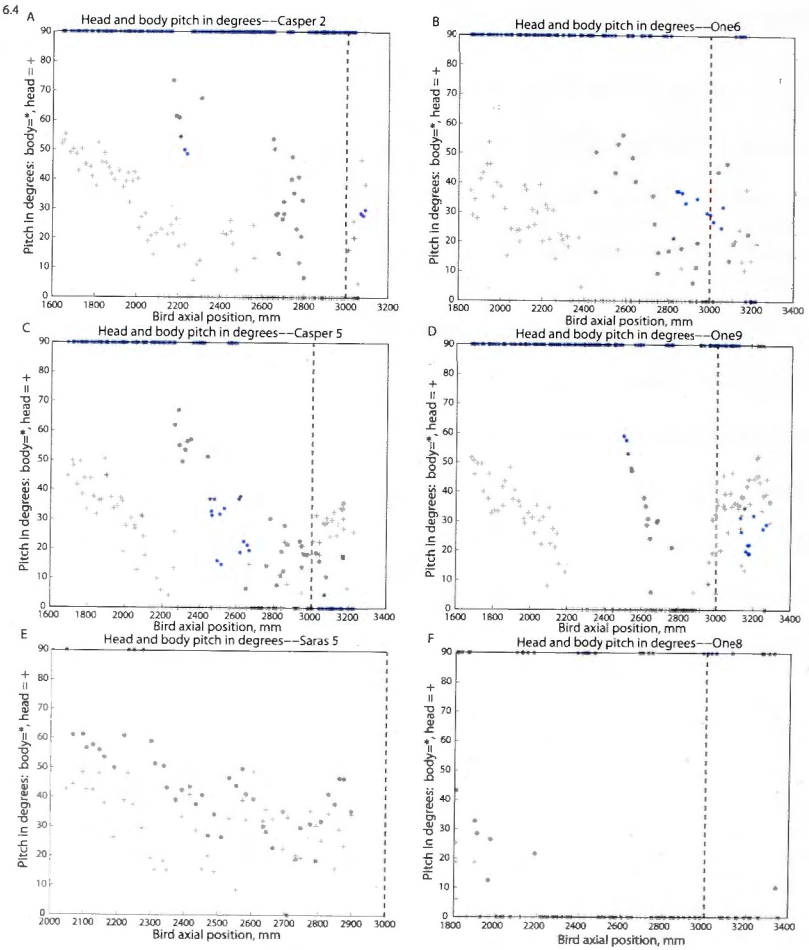

*Figure 6.4 Examples showing the head (shown with a red + symbol) and body (shown with a blue * symbol) pitch movements as a function of the axial position of the head along the tunnel. The birds flew through a tunnel with an aperture*

flanked by blank panels in (A and B), panels carrying a checkerboard texture in (C and D), and through a tunnel that had no aperture in (E and F). In each pair of panels, the left-hand panel shows data from a left-biased bird (a bird that approaches the aperture from the left) and the right-hand panel shows data from a right-biased bird (a bird that approaches the aperture from the right). In A-D the red vertical dashed line shows the position of the aperture. In E-F this line shows where the aperture would have been located, had it been present.

The roll attitudes of the body and the head are shown in Figure 6.5, as a function of the bird's axial position along the length of the tunnel. The data are shown for the three different experimental conditions – aperture flanked by textured panels, aperture flanked by blank panels and no aperture (control).

In general, we see that while the body displays substantial fluctuations in roll throughout the flight (and especially when manoeuvring through the aperture), the head is relatively stable and exhibits considerably smaller deviations from the horizontal roll attitude of 0 degrees. It is also noteworthy that, in the case of the body, the changes of roll attitude are not only larger, but are more rapid.

Bird Name	One		Table 6.1			
Control			Head roll			Body roll
	True head roll attitude	True head roll attitude	rate magnitude (deg/sec)	True body roll attitude	True body roll attitude	rate magnitude
Flight No	Mean (deg)	SD (deg)	Mean (deg/sec)	Mean (deg)	SD (deg)	Mean (deg/sec)
1	-5.71	16.97	4331.42	-18.93	38.68	8792.34
2	-10.84	35.95	6940.25	-4.72	42.45	10083.50
3	3.76	19.37	5194.14	1.29	31.33	9537.77
4	5.87	13.83	3177.79	-14.74	21.52	6456.54
5	1.24	16.09	4335.34	-5.78	28.63	7683.52
6	-6.30	22.50	5609.46	-5.84	31.42	8628.54
7	-4.39	35.94	8197.11	-3.41	36.96	10053.97
8	-3.29	15.88	4244.90	4.62	29.88	8083.71
9	21.46	36.34	5716.77	-2.48	41.61	10202.92
10	-7.49	43.78	7996.28	-15.30	43.32	12626.31
Grand means	**-0.57**	**25.67**	**5574.35**	**-6.53**	**34.58**	**9214.91**
Bird Name	**One**					
Blank obstacles			Head roll			Body roll
	True head roll attitude	True head roll attitude	rate magnitude (deg/sec)	True body roll attitude	True body roll attitude	rate magnitude
Flight No	Mean (deg)	SD (deg)	Mean (deg/sec)	Mean (deg)	SD (deg)	Mean (deg/sec)
1	4.16	28.69	3878.52	-20.29	27.90	3185.74
2	15.54	22.41	3105.95	-28.07	41.08	4806.59
3	2.28	15.31	3345.59	-50.83	26.97	4529.77

4	-2.55	16.89	3826.26	5.52	30.30	6333.61
5	7.20	17.25	3878.57	-7.18	33.85	6043.76
6	6.95	11.94	2386.38	4.04	41.21	10667.19
7	9.26	26.47	4518.11	9.17	32.38	6340.58
8	9.02	28.30	4855.40	1.13	40.61	6958.44
9	17.02	24.92	4500.41	16.55	33.19	6519.31
10	13.59	28.83	4534.75	20.39	31.80	7534.69
Grand means	**8.25**	**22.10**	**3882.99**	**-4.96**	**33.93**	**6291.97**
Bird Name	**One**					
Checked obstacles			Head roll			Body roll
	True head roll attitude	True head roll attitude	rate magnitude (deg/sec)	True body roll attitude	True body roll attitude	rate magnitude
Flight No	Mean (deg)	SD (deg)	Mean (deg/sec)	Mean (deg)	SD (deg)	Mean (deg/sec)
1	-2.00	10.39	2369.19	-28.38	32.32	5790.96
2	-19.38	21.02	3697.44	-5.89	29.27	7700.43
3	-20.37	27.02	5269.41	12.19	38.42	4765.78
4	-3.51	12.33	2312.74	-6.87	20.30	3620.60
5	1.31	9.16	1350.18	-20.55	29.41	5022.33
6	7.76	16.43	1955.28	-32.07	25.56	4271.77
7	-5.86	33.37	4645.03	0.42	37.86	5556.48
8	-3.39	14.82	2269.34	-9.18	23.12	3641.67
9	-3.02	7.98	1096.41	-1.88	28.49	6532.42
10	2.61	23.07	3056.92	0.53	36.07	7788.83
Grand means	**-4.58**	**17.56**	**2802.19**	**-9.17**	**30.08**	**5469.13**

Bird Name	**Two**					
Control			Head roll			Body roll
	True head roll attitude	True head roll attitude	rate magnitude (deg/sec)	True body roll attitude	True body roll attitude	rate magnitude
Flight No	Mean (deg)	SD (deg)	Mean (deg/sec)	Mean (deg)	SD (deg)	Mean (deg/sec)
1	10.56	28.82	5268.22	-9.89	29.78	7835.61
2	-9.82	33.84	9427.17	-10.75	36.10	8979.31
3	10.80	37.24	7364.96	-6.55	40.93	9451.02
4	0.81	39.05	7367.21	-22.25	36.84	8319.59
5	10.63	35.93	8071.57	6.59	39.56	8839.80
6	3.94	36.73	9231.42	-12.80	38.48	7557.09
7	-8.45	36.76	8959.23	-20.37	34.66	7045.63
8	-9.09	36.94	9067.60	-20.26	33.79	7813.32
9	-7.62	37.77	8082.60	-12.42	38.66	8243.78
10	4.76	37.30	10210.24	-17.45	34.87	6714.35
Grand means	**0.65**	**36.04**	**8305.02**	**-12.61**	**36.37**	**8079.95**
Bird Name	**Two**					
Blank obstacles			Head roll			Body roll
	True head roll attitude	True head roll attitude	rate magnitude (deg/sec)	True body roll attitude	True body roll attitude	rate magnitude
Flight No	Mean (deg)	SD (deg)	Mean (deg/sec)	Mean (deg)	SD (deg)	Mean (deg/sec)
1	20.48	27.21	4085.04	17.36	36.49	8561.34
2	20.96	29.28	5375.96	2.41	43.77	7140.53
3	-1.62	15.60	3756.45	-4.48	36.20	11733.01

4	24.55	24.51	4801.89	8.65	40.18	6061.59
5	25.48	20.40	3567.92	17.99	36.19	4364.67
6	25.59	24.52	3864.16	16.57	41.70	8741.78
7	14.94	32.84	5830.56	-18.94	32.98	8860.75
8	9.76	36.26	7562.77	-7.18	39.86	7883.50
9	14.36	31.15	6915.40	-23.44	30.73	6873.80
10	3.81	36.78	6482.47	-11.89	36.58	6950.28
Grand means	**15.83**	**27.86**	**5224.26**	**-0.29**	**37.47**	**7717.13**
Bird Name	**Two**					
Checked obstacles			Head roll			Body roll
	True head roll attitude	True head roll attitude	rate magnitude (deg/sec)	True body roll attitude	True body roll attitude	rate magnitude
Flight No	Mean (deg)	SD (deg)	Mean (deg/sec)	Mean (deg)	SD (deg)	Mean (deg/sec)
1	1.52	37.04	5780.66	38.42	22.73	3277.65
2						
3	7.05	27.81	7499.15	17.72	36.96	3467.18
4	23.22	23.07	2914.90	36.45	24.92	4776.56
5	8.97	10.86	2519.66	24.54	36.03	6682.29
6	-2.13	34.95	6461.53	-13.26	38.96	8181.62
7	0.13	22.73	5643.05	-1.17	41.00	7126.79
8	7.29	30.76	3599.97	28.33	41.21	8047.43
9	21.47	21.60	3120.06	26.00	43.14	7896.62
10	5.97	13.24	2856.90	4.07	38.59	9243.23
Grand means	**9.00**	**23.13**	**4326.90**	**15.34**	**37.60**	**6927.72**

Bird Name	**Casper**					
Control			Head roll			Body roll
	True head roll attitude	True head roll attitude	rate magnitude (deg/sec)	True body roll attitude	True body roll attitude	rate magnitude
Flight No	Mean (deg)	SD (deg)	Mean (deg/sec)	Mean (deg)	SD (deg)	Mean (deg/sec)
1	23.49	22.72	4115.23	5.81	38.31	8958.47
2	12.06	33.96	9381.09	-15.74	39.56	7878.87
3	-6.64	42.36	8279.29	1.51	43.29	9785.11
4	-19.95	37.46	8439.03	-23.50	40.40	7599.72
5	-1.40	40.29	11418.80	13.39	40.04	11998.19
6	-1.38	35.83	7739.41	10.26	36.99	7802.34
7	10.32	37.54	6085.91	24.97	36.18	6987.50
8	-4.11	38.44	9225.30			
9	0.30	28.55	6688.08			
10						
Grand means	**1.41**	**35.24**	**7930.24**	**2.39**	**39.25**	**8715.74**
Bird Name	**Casper**					
Blank obstacles			Head roll			Body roll
	True head roll attitude	True head roll attitude	rate magnitude (deg/sec)	True body roll attitude	True body roll attitude	rate magnitude
Flight No	Mean (deg)	SD (deg)	Mean (deg/sec)	Mean (deg)	SD (deg)	Mean (deg/sec)
1	-10.62	34.73	6139.92	-9.45	40.15	9058.73
2	-5.54	11.09	2190.28	-33.23	26.22	2738.44
3	-9.42	11.75	2641.49	-31.30	36.25	9762.28

4	-4.92	13.51	2399.81	-4.29	25.02	4473.40
5	-3.74	10.25	1551.04	4.83	24.28	3152.69
6	-10.68	18.31	3185.36	-17.54	24.40	5147.30
7	-4.43	13.73	3688.03	-21.81	39.92	6806.04
8	-5.89	10.49	2581.70	6.23	31.54	6462.45
9	-2.89	9.87	1639.01	-13.18	24.23	4200.88
10	-4.65	10.56	2134.98	-9.29	20.83	3900.10
Grand means	**-6.28**	**14.43**	**2815.16**	**-12.90**	**29.28**	**5570.23**
Bird Name	**Casper**					
Checked obstacles			Head roll			Body roll
	True head roll attitude	True head roll attitude	rate magnitude (deg/sec)	True body roll attitude	True body roll attitude	rate magnitude
Flight No	Mean (deg)	SD (deg)	Mean (deg/sec)	Mean (deg)	SD (deg)	Mean (deg/sec)
1	8.45	28.84	5413.92	24.41	28.67	5366.57
2	-0.52	30.48	2978.64	-3.51	35.05	6772.67
3	-7.41	14.92	2393.13	1.82	27.85	5128.25
4	-4.55	14.26	1704.68	4.95	26.91	5087.56
5	-1.92	11.76	2764.44	-7.92	36.39	8392.55
6	-11.26	21.88	3061.87	0.72	25.16	4518.52
7	-1.41	13.18	2311.75	-9.60	36.97	5869.74
8	-7.20	16.13	3831.60	-18.32	40.48	4235.04
9	-6.85	13.89	2781.39	-6.18	22.09	5079.74
10	-9.71	35.45	5464.63	-17.70	29.92	5356.86
Grand means	**-4.24**	**20.08**	**3270.60**	**-3.13**	**30.95**	**5580.75**

Bird Name	**Drongo**					
Control			Head roll			Body roll
	True head roll attitude	True head roll attitude	rate magnitude (deg/sec)	True body roll attitude	True body roll attitude	rate magnitude
Flight No	Mean (deg)	SD (deg)	Mean (deg/sec)	Mean (deg)	SD (deg)	Mean (deg/sec)
1	-12.24	26.80	4181.95	11.03	20.21	4952.59
2	-10.21	33.88	5071.21	-2.26	44.88	17287.64
3	-1.79	37.58	6181.54	3.27	32.49	7869.39
4	-0.72	26.48	3877.60	-0.71	34.03	7785.00
5	12.25	30.05	5265.06	12.16	36.25	10210.21
6	8.50	27.10	5464.72	-20.45	33.22	7591.09
7	17.46	30.78	7129.16	-2.63	38.69	13468.55
8	15.17	24.50	5152.19	2.98	29.74	9468.20
9	7.07	25.19	6421.78	10.41	36.98	9255.60
10	13.15	25.14	6096.88	0.40	46.53	12443.83
Grand means	**4.86**	**28.75**	**5484.21**	**1.42**	**35.30**	**10033.21**
Bird Name	**Drongo**					
Blank obstacles			Head roll			Body roll
	True head roll attitude	True head roll attitude	rate magnitude (deg/sec)	True body roll attitude	True body roll attitude	rate magnitude
Flight No	Mean (deg)	SD (deg)	Mean (deg/sec)	Mean (deg)	SD (deg)	Mean (deg/sec)
1	-11.46	30.63	6124.62	-16.33	38.07	8393.32
2						
3	-5.93	28.74	2763.67	-11.55	44.99	9233.20

4	-8.84	30.94	3658.05	18.77	35.19	5317.92
5	-7.41	29.94	3706.54	28.65	35.82	8112.95
6	-9.07	29.72	4105.84	-6.68	27.39	5355.63
7	-9.52	29.80	3492.07	-16.57	28.45	3442.01
8	-21.32	29.80	2931.98	20.86	36.00	8137.58
9	-10.14	19.39	3551.77	10.62	29.55	10681.20
10	-24.17	22.09	2605.20	-20.24	31.32	5190.55
Grand means	**-11.99**	**27.89**	**3659.97**	**0.84**	**34.09**	**7096.04**
Bird Name	**Drongo**					
Checked obstacles			Head roll			Body roll
	True head roll attitude	True head roll attitude	rate magnitude (deg/sec)	True body roll attitude	True body roll attitude	rate magnitude
Flight No	Mean (deg)	SD (deg)	Mean (deg/sec)	Mean (deg)	SD (deg)	Mean (deg/sec)
1	-23.50	28.40	2287.98	-34.18	36.69	7028.23
2	-26.22	29.01	2025.40	-27.75	30.26	8025.20
3	-23.93	26.54	2580.99	-43.47	10.49	1868.74
4	-13.97	33.09	3612.25	-29.85	35.38	8266.97
5	-14.19	29.75	4355.25	0.88	50.38	5130.68
6	-13.54	31.90	3896.54	-4.75	55.59	6524.81
7	-17.98	32.59	4378.07	-50.36	10.81	2272.26
8	-10.81	35.06	3636.93	-26.04	37.39	8107.11
9	-7.64	35.13	3680.16	-34.00	31.45	5497.55
10	-8.66	32.48	5184.46	-25.83	52.24	4676.86
Grand means	**-16.04**	**31.39**	**3563.80**	**-27.53**	**35.07**	**5739.84**

Bird Name	**Saras**					
Control			Head roll			Body roll
	True head roll attitude	True head roll attitude	rate magnitude (deg/sec)	True body roll attitude	True body roll attitude	rate magnitude
Flight No	Mean (deg)	SD (deg)	Mean (deg/sec)	Mean (deg)	SD (deg)	Mean (deg/sec)
1	7.64	37.10	3103.15	39.93	19.16	3407.59
2	-14.81	35.17	5131.69	-31.76	32.38	5189.16
3	-33.07	16.37	2966.29	-16.56	44.28	9945.24
4	-19.36	40.35	5607.93	3.18	45.04	10133.10
5	-6.26	41.08	5662.65	7.04	48.32	16590.77
6	-28.60	24.75	4344.39	18.64	45.29	7979.32
7	-12.07	38.13	8797.44	1.76	55.88	14298.12
8	10.03	35.04	5240.60	-34.44	32.16	7796.68
9	-17.94	34.36	6681.07	-5.10	44.86	9038.46
10	-16.41	41.18	3560.48	19.11	35.18	5308.40
Grand means	**-13.09**	**34.35**	**5109.57**	**0.18**	**40.26**	**8968.68**
Bird Name	**Saras**					
Blank obstacles			Head roll			Body roll
	True head roll attitude	True head roll attitude	rate magnitude (deg/sec)	True body roll attitude	True body roll attitude	rate magnitude
Flight No	Mean (deg)	SD (deg)	Mean (deg/sec)	Mean (deg)	SD (deg)	Mean (deg/sec)
1	2.14	18.59	3305.70	-4.24	37.04	5663.30
2	-3.62	24.28	5632.24	27.68	28.47	4700.89
3	-13.54	33.70	7410.68			

4	6.85	36.05	6224.28	22.43	30.75	4839.98
5	-8.56	14.68	2415.12	36.74	32.55	4845.24
6	-10.37	15.49	2166.25	30.86	35.98	5818.38
7						
8	-1.04	28.17	2437.24	-14.41	32.11	5156.58
9	18.60	24.25	3502.53	2.94	37.61	5006.30
10	-9.99	31.73	2731.17	-35.32	24.63	3855.44
Grand means	**-2.17**	**25.22**	**3980.58**	**8.34**	**32.39**	**4985.76**
Bird Name	**Saras**					
Checked obstacles			Head roll			Body roll
	True head roll attitude	True head roll attitude	rate magnitude (deg/sec)	True body roll attitude	True body roll attitude	rate magnitude
Flight No	Mean (deg)	SD (deg)	Mean (deg/sec)	Mean (deg)	SD (deg)	Mean (deg/sec)
1	6.47	32.15	5384.13	28.92	28.29	5659.63
2	-20.51	23.50	4467.89	31.81	33.37	7248.28
3	-4.89	32.78	6650.47	-7.72	41.07	6645.03
4	-6.92	31.58	3204.86	-9.52	39.28	3905.71
5	-1.65	20.08	4688.02	-29.01	38.80	5732.25
6	-10.04	34.53	1421.93	-28.81	30.21	4569.38
7	-15.62	27.01	6065.67	7.35	40.32	8178.86
8	-0.86	24.81	5814.56	5.70	48.06	7718.05
9	-6.93	16.48	3506.31	0.72	41.79	6947.15
10	0.05	28.67	1981.53	-18.03	30.79	2306.29

Grand means	**-6.09**	**27.16**	**4318.54**	**-1.86**	**37.20**	**5891.06**

Table 6.1 Mean values of the true head roll attitude, standard deviations of true head roll and head roll rate magnitudes, and the corresponding values for the body.

The rate of change of roll of the head and body was compared during the entire flight path for the three different conditions namely, no obstacles present in the tunnel, checked pattern on obstacles and white obstacles with no patterns. The results are shown in Table 6.1.

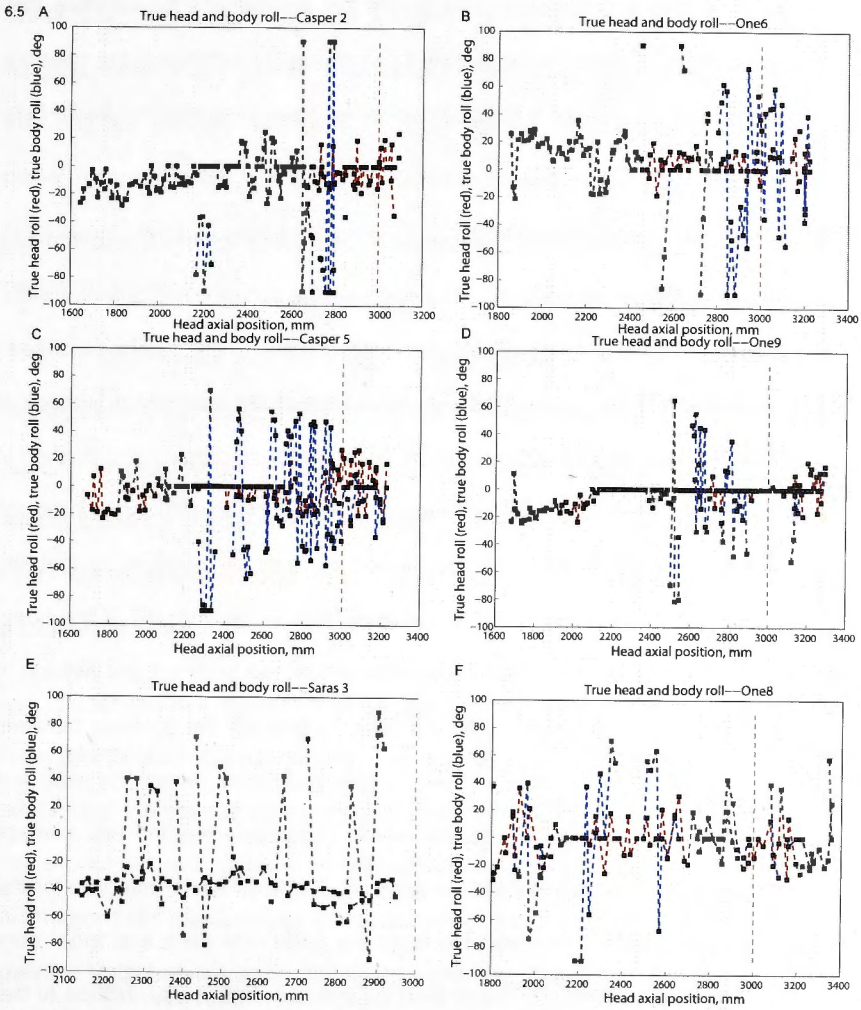

Figure 6.5 Examples showing the roll of the head (red) and body (blue) as a function the axial position of the head along the tunnel, for birds flying through a

tunnel with an aperture flanked by blank panels (A and B), panels carrying a checkerboard texture (C and D), and through a tunnel that has no aperture (E and F). In each pair of panels, the left-hand panel shows data from a left-biased bird (a bird that approaches the aperture from the left) and the right-hand panel shows data from a right-biased bird (a bird that approaches the aperture from the right). In A-D the red vertical dashed line shows the position of the aperture. In E-F this line shows where the aperture would have been located, had it been present.

A comparison of the birds' behaviour in the three different experimental conditions is shown in Table 6.1. The table shows data for five different birds, each contributing about 10 flights under each condition. The amplitude of head roll, as seen from the values of the grand means of the standard deviations of the head roll attitudes for different birds, is higher in the control flights, than in the flights with blank or checked obstacles. Second, the amplitudes of head roll are consistently lower than the amplitudes of body roll, indicating that the attitude of the head is more tightly stabilized than is the attitude of the body, except for bird Saras. Third, the rates of head roll and body roll are highest in the control flights and lowest when the birds fly through the aperture between the checked obstacles, except for birds Casper and Saras, where the head and body roll rates are lowest with the blank obstacles. Fourth, the average magnitude of the rate of head roll (in deg/sec) is always lower than that for the body, indicating that, throughout the flight the body rolls back and forth more rapidly than does the head. These findings indicate that (i) stabilization of the head is under tighter control when birds negotiate an obstacle, and (ii) the head is stabilized more tightly than is the body.

6.3.1 Wing motions and flight speed

Some examples of the motion of the wingtips during flight are shown in Figure 6.6 (plan views) and Figure 6.7 (side views). During cruise, the motion of the wingtips is primarily in the horizontal plane (front-to-back and back-to-front), rather than in the vertical plane (up and down). The axial positions of the wingtips, relative to the head, are shown in Figure 6.8. This figure reveals that the wing tips oscillate with more or less constant amplitude in the horizontal plane, extending from about 50mm - 100mm in front of the head at the end of the forward stroke, to about 100mm – 150mm behind the head at the end of the backward stroke.

It also reveals that the speed of the wingtips in the horizontal plane is highest during the second half of the backstroke, when the wingtips trail the head. Presumably, this is when the forward thrust is largest in magnitude – although one cannot be certain about this, because this thrust will also depend upon the precise orientation of the plane of the wing stroke and the angle of attack of the wings.

Changes in the instantaneous speed of the bird during the wing stroke cycle can be inferred by examining the relative separations between successive positions of the head in the trajectories shown in Figures 6.6 and 6.7. The larger the separation, the higher the instantaneous speed. We see that the forward flight speed (as measured by the axial speed of the head) is highest not at the putative instant of maximum thrust, but some time thereafter - during the middle of the forward stroke. Paradoxically, the speed of flight is lowest during the backward stroke, and highest during the middle half of the forward stroke. This

is evident in all of the examples shown in Figure 6.6. I shall consider the implications of these findings in the Discussion section.

6.3.2 Wing manoeuvres during transit through the aperture

The wing beat ceases just before the bird passes through the aperture (Figures 6.8 and 6.10). This cessation occurs earlier when the flanking walls are textured and are therefore clearly visible (compare Figure 6.8 A and B with Figure 6.8 C and D).

To examine the postures of the wings during the transit through the aperture, I have plotted the axial positions (Figure 6.6) and the heights (Figure 6.7) of the head, and the left and right wing tips, as a function of the axial position of the head. In effect, these figures show the plan and the side view, respectively, of 6 different flight trajectories. In the example of Figure 6.6 A and 6.7 A the left wing is partially extended in the horizontal direction, while the right wing is folded back. In the example of Figures 6.6 B and 6.7 B the bird raises one wing and lowers the other while passing though the aperture. In the example of Figure 6.6 D and 6.7 D the right wing is partially extended in the horizontal direction, while the left wing is folded back. In the example of Figure 6.6 C and 6.7 C both wings are folded back during the transit through the aperture. Thus, there appear to be a variety of wing manoeuvres that birds use to minimize the risk of damage to their wings when flying through narrow passages.

In the control flights where there are no obstacles (Figures 6.6 E and 6.7 E and Figures 6.6 F, and 6.7 F) the wings continue to beat throughout the flight in their normal 'cruising' mode.

Table 6.2

Blank obstacles					
Bird Name	One	Two	Casper	Saras	Drongo
Flight Number					
1	v 'C'	Vi	i	I	Vi
2	v 'C'	iv 'C'	i	I	iii 'C'
3	iv 'C'	vi 'C'	i	I	I
4	Vi	Vi	i	I	Vi
5	vii 'C'	vi 'C'	i	Iii	Vi
6	iv 'C'	vi 'C'	iii	I	Vi
7	Ix	I	iii	I	Vi
8	Vi	ii 'C'	i	No data	I
9	Ix	I	i	Vi	I
10	Vi	viii 'C'	i	I	Vi
Checked obstacles					
Bird Name	One	Two	Casper	Saras	Drongo
Flight Number					
1	Vi	Vi	i	I	Vi
2	I	No data	i	I	Iv
3	Iv	I	i	I	I
4	V	Vi	i	I	Iv
5	Vi	Vi	i	I	Iv
6	Vi	Vi	i	I	Iv
7	Vi	Vi	i	I	Vi
8	Vi	V	i	I	Vi
9	V	Vi	i	I	Vi
10	Vi	vi 'C'	i	I	Vi
Control					
Bird Name	One	Two	Casper	Saras	Drongo
Flight Number					
1	NC	NC	NC	NC	NC
2	NC	NC	NC	NC	NC
3	NC	NC	NC	NC	NC
4	NC	NC	NC	NC	NC
5	NC	NC	NC	NC	NC
6	NC	NC	NC	NC	NC
7	NC	NC	NC	NC	NC
8	NC	NC	NC	NC	NC

9	NC	NC	NC	NC	NC
10	NC	NC	NC	NC	NC

Index of symbols
(i) Both wings folded backwards
(ii) Left wing extended horizontally, right wing closed
(iii) Right wing extended horizontally, left wing closed,
(iv) Right wing up, left wing down
(v) Left wing up, right wing down
(vi) Both wings up
(vii) Head on collision with obstacle but bird flies through the opening
(viii) Head on collision with obstacle and bird turns back
(ix) Right wing folds upwards and then slightly backwards is denoted by 'A'
Collision is shown by 'C' beside the number
No collisions in control flights is denoted by 'NC'

Table 6.2 Wing orientations while negotiating the different obstacles and during the control condition.

6.3.3 Collisions

In general, there is a greater tendency for the wing tips to collide with the panels flanking the aperture when the panels are blank, as compared to when they textured. When one panel is textured and the other is blank, more collisions occur with the blank panel. Evidently, the greater visibility of the textured panels tends to make the birds more likely to steer away from them, and more likely to make contact with the blank panels. Consequently, (a) the collision rate is lower when both panels are textured, than when both panels are blank, and (b) when one panel is textured and the other is blank, it is the blank panel that receives the larger frequency of collisions.

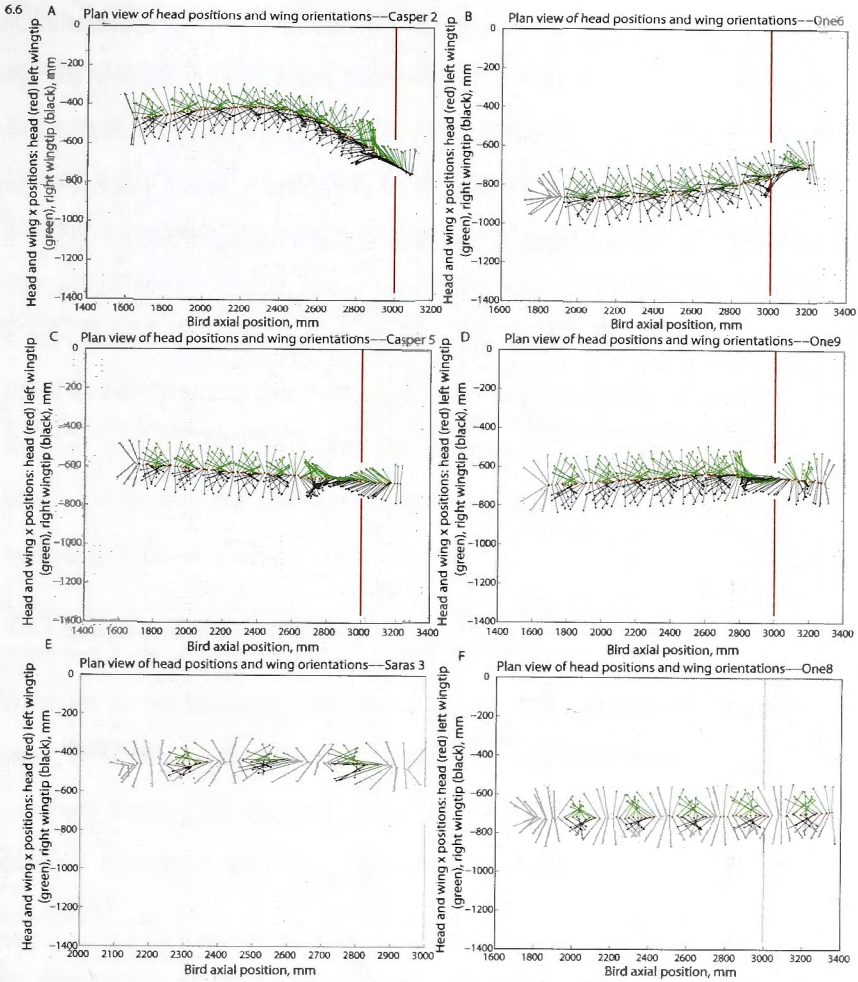

Figure 6.6 Examples showing the trajectories of the head (red dots) and left and right wings (green and black lines, respectively) as viewed from above, as a function of the axial position of the head along the tunnel. The birds flew through a tunnel with an aperture flanked by blank panels (A and B), panels carrying a checkerboard texture (C and D), and through a tunnel that had no aperture (6 E and F). In each pair of panels, the left-hand panel shows data from a left-biased bird (a bird that approaches the aperture from the left) and the

right-hand panel shows data from a right-biased bird (a bird that approaches the aperture from the right). (The full video shows that it approaches from the right hand side even though this is not very evident on the graph.) In A-D the red vertical dashed line shows the position of the aperture. In E-F this line shows where the aperture would have been located, had it been present.

6.7

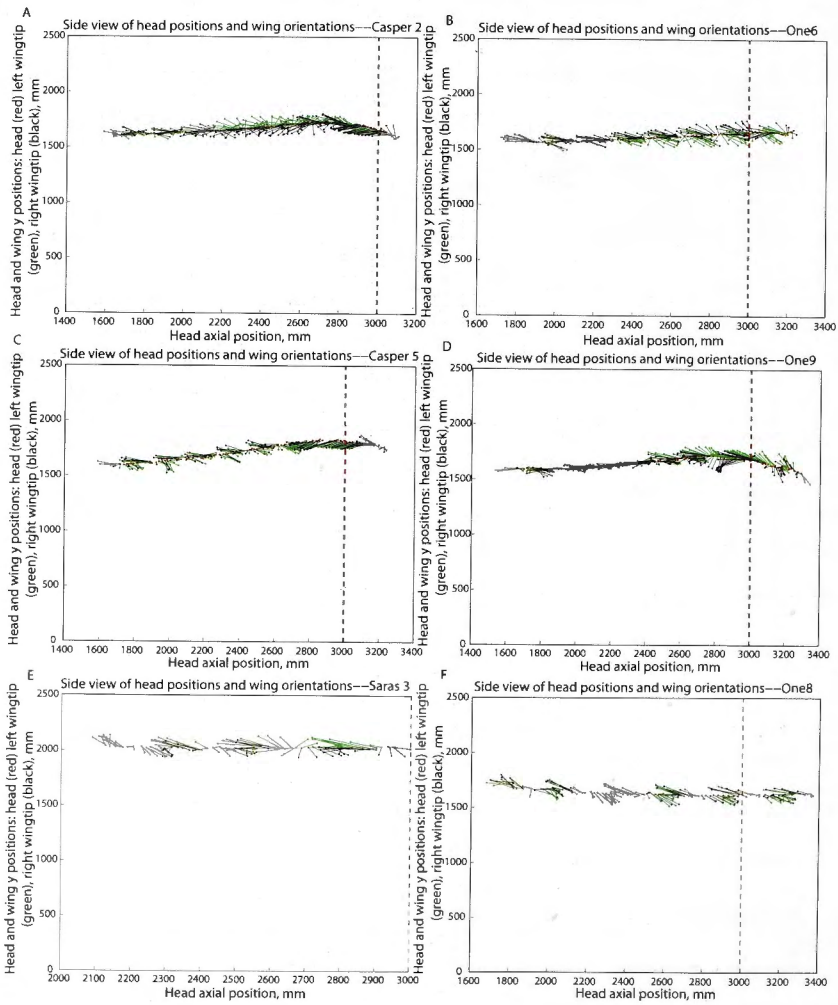

Figure 6.7 Examples showing the trajectories of the head (red dots) and left and right wings (green and black lines, respectively) as viewed from the side, as a function of the axial position of the head along the tunnel. The birds flew through a tunnel with an aperture flanked by blank panels (A and B) panels carrying a checkerboard texture (C and D) and through a tunnel that had no aperture (E and F). In each pair of panels, the left-hand panel shows data from a left-biased bird (a bird that approaches the aperture from the left) and the right-hand panel shows data from a right-biased bird (a bird that approaches the aperture from the right). In A-D the red vertical dashed line shows the position of the aperture. In E-F this line shows where the aperture would have been located, had it been present.

6.3.4 Speed and height of flight

When the tunnel carries no aperture the birds fly at a higher speed, and require fewer wing strokes to reach the position of the (now non-existent) aperture (compare Figures 6.8 A-D with E-F). The altitude of flight is more or less constant throughout the flight, regardless of whether the tunnel carries an aperture or not.

Even though wing flapping ceases when the birds pass through the aperture, there is only a small loss of altitude, if any. There is some indication that the birds pre-compensate for the slight loss of altitude by gaining some height during the approach to the aperture (see Figures 6.7 A-D). This is supported by the observation that this pre-compensation is absent in the control condition, when there is no aperture in the tunnel (see Figures 6.7 E and F).

6.8

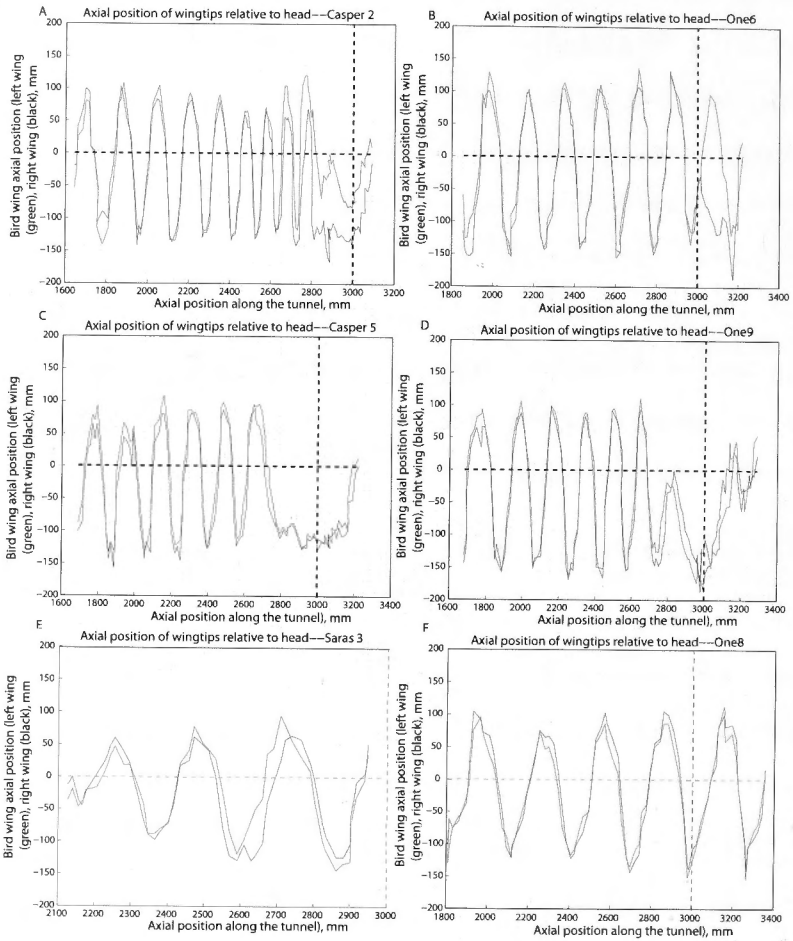

Figure 6.8 Plots of axial position of wing tips relative to the head, as a function of the axial position of the bird in the tunnel. The green and black curves correspond to the left and right wing tips, respectively. The aperture is flanked by blank panels (A and B) and by checkerboard panels (C and D). In E and F the tunnel carries no aperture (control condition). In each pair of panels, the left-hand panel shows data from a left-biased bird (a bird that approaches the

aperture from the left) and the right-hand panel shows data from a right-biased bird (a bird that approaches the aperture from the right). In A-D the red vertical dashed line shows the position of the aperture. In 6.8 E-F this line shows where the aperture would have been located, had it been present.

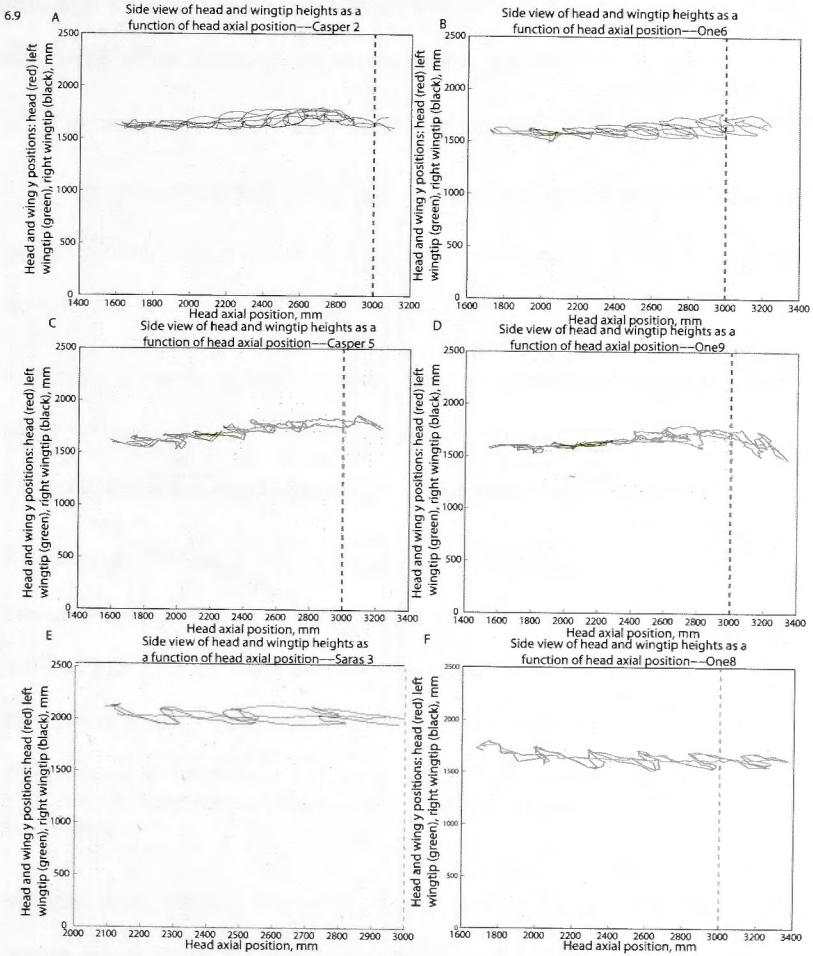

Figure 6.9 Plots of head, body and wing tip heights as a function of head axial position when the aperture is flanked by blank panels (A and B), or checkerboard panels (C and D). In E and F the tunnel carries no aperture

(control condition). The green and black curves correspond to the left and right wing tips, respectively. In each pair of panels, the left-hand panel shows data from a left-biased bird (a bird that approaches the aperture from the left) and the right-hand panel shows data from a right-biased bird (a bird that approaches the aperture from the right). In A-D the red vertical dashed line shows the position of the aperture. In E-F this line shows where the aperture would have been located, had it been present.

6.10

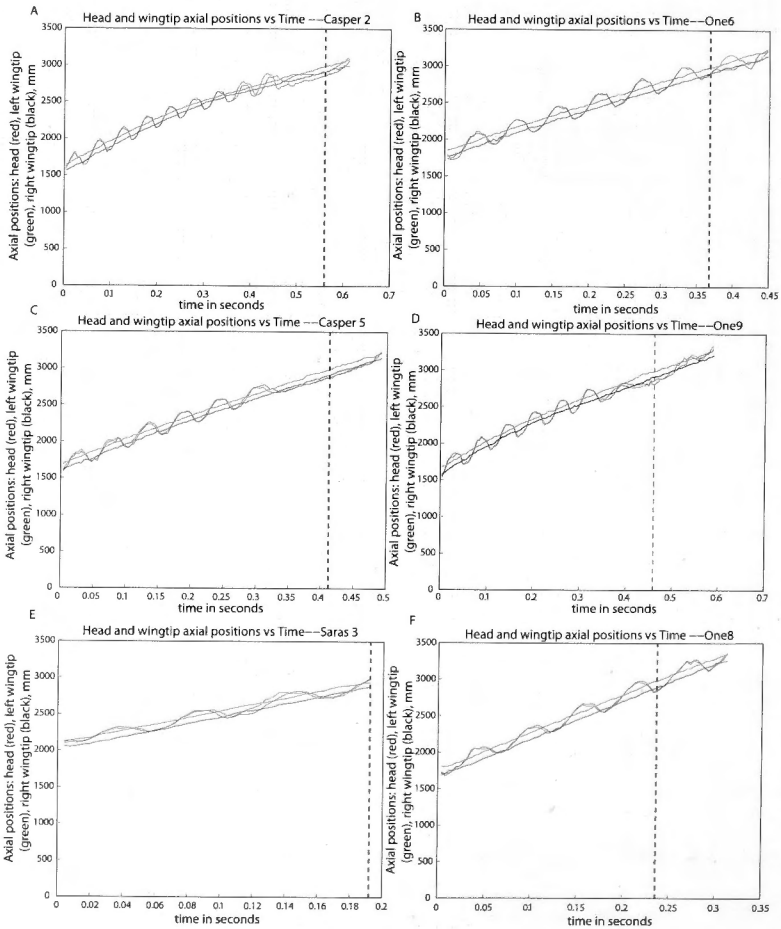

Figure 6.10 Plots of head and wing tip axial positions as a function of time when the tunnel carries an aperture flanked by blank panels (A and B) or checkerboard panels (C and D). In E and F the tunnel carries no aperture (control condition) In A-D the red vertical dashed line shows the position of the aperture. In E-F this line shows where the aperture would have been located, had it been present.

6.3.5 In summary, the above results indicate that:

i) The wing motion during cruise in the tunnel occurs primarily in the horizontal plane (front-to-back and back-to-front) rather than in the vertical plane (up-and-down).

ii) Wingtip speed is highest during the second half of the backstroke, when the wingtips trail the head. Forward flight speed, as measured by the axial speed of the head, is highest shortly thereafter, during the middle of the forward stroke.

iii) Although the body rolls substantially during flight, and especially while manoeuvring through the aperture, the head is held horizontal and exhibits minimal roll. This contrast between the movements of the head and body is particularly striking when the flanking walls are blank and therefore difficult to detect visually until they are very close, thus forcing rapid and extreme manoeuvres.

iv) Birds cease flapping the wings prior to entering the aperture. This cessation occurs earlier when the flanking walls are textured and are therefore clearly visible.

v) Usually the wings are held closed (swept back) while passing through the aperture, but occasionally one wing is extended vertically upwards or horizontally outwards.

vi) Birds lose only a small amount of altitude – if at all- when they cease flapping their wings and pass through the aperture. There is some suggestion that they pre-compensate for this loss of altitude by gaining some height during the approach to the aperture.

vii) The birds fly at a higher speed when the tunnel carries no aperture, and require fewer wing strokes to reach the position of the (now nonexistent) aperture.

6.4 Discussion

As described in the general introduction to this thesis, there is a considerable amount of knowledge in the literature about how insects use their vision to guide flight. However, these questions have not yet been explored systematically in birds. Here I have described the motions of the head, body and wings of budgerigars when they fly through narrow passages, in an attempt to obtain some insights into the processes that underlie these complex flight manoeuvres.

6.4.1 Wing kinematics and flight

Motion of the wings during flight in the tunnel appears to be mostly in the horizontal plane, rather than in the vertical plane. We have seen that the backward stroke takes up relatively little time, compared to the forward stroke. This means that the wings move much more rapidly during the backward phase of the stroke as compared to the forward phase, and implies that the wings

generate maximum thrust during the backward phase. However, the data indicate, somewhat paradoxically, that the speed of flight is a maximum in the middle of the forward stroke, which occurs later in time.

The instantaneous forward flight speed is highest toward the end of the backward stroke. One possible interpretation of these observations is that (i) the backward stroke is the primary generator of the thrust, with the bird's inertia presumably causing the flight velocity to peak some time after the peak thrust has been generated; (ii) Relatively little thrust is produced during the forward stroke, which apparently constitutes a predominantly 'gliding' phase in which the bird makes any necessary adjustments to its attitude through appropriate deflections of the wings and tail. Another possible interpretation is that the maximum forward thrust actually occurs during the middle of the forward stroke (when the head moves forward at the highest velocity), that the bird's inertia introduces a negligible delay in the translation of wing thrust into the bird's forward velocity, and that the maximum thrust is generated at this point in the wing beat cycle through an appropriate orientation of the stroke plane and the angle of attack of the wings. A more detailed kinematic analysis, combined with quantitative modelling, is necessary in order to distinguish between these two possibilities.

6.4.2 Stabilization of head roll

My results show that budgerigars hold their heads in a remarkably stable, horizontal orientation, despite the fact that the body exhibits substantial and rapid changes in roll attitude.

Presumably, the large changes in roll attitude of the body are related to the control of the relatively complex flight manoeuvres that the birds are executing in the tunnel – accelerations, decelerations, sharp yaw turns and other steering actions.

The finding that the head remains stable during the entire flight is consonant with the notion that budgerigars navigate safely through narrow passages by extracting translational optic flow to obtain information on the distances to various obstacles. Given that budgerigars have laterally placed eyes whose visual fields are likely to have minimal binocular overlap, it is unlikely that they use stereo vision for depth perception. Instead, these birds probably rely on stabilization of the head (and the eyes, although my experiments have not monitored eye movements) to enable extraction of depth cues from translational optic flow.

In pigeons, it has been shown that fixing the head to the body, which destroys the ability of the head to stabilize its orientation independently of the body, causes the birds to crash (Warrick et al., 2002). This demonstration highlights the importance of holding the head horizontal for achieving stable, visually-guided flight.

The experiments described here raise the important question as to how the roll attitude of the head is held level and stable, even though the body exhibits large roll excursions. Gravity on its own is not a reliable cue of verticality because, even if the bird were to use vestibular signals to sense gravity, the direction of the net acceleration vector, as sensed by the vestibular organs, would be influenced not only by gravity, but also by the bird's

accelerations in three-dimensional space. However, vestibular signals that sense angular rotations could be used, in principle, to compensate for the roll of the body. Such compensation would work for short time scales, but would be increasingly susceptible to drift over longer periods, because the vestibular system does not have access to an absolute orientation reference.

Directed illumination in the room, as provided by the ceiling lighting, can, in principle, provide brightness cues that help stabilize roll and maintain a horizontal roll attitude, if the bird were to maintain an attitude such that the brightness is a maximum in the dorsal field of view. Such a cue would provide an absolute orientation reference, and avoid drift. In principle, the birds could also make use of salient visual edges and other geometrical features in the tunnel to ensure that the head remains horizontal.

Head stabilization in budgerigars is analogous in some ways to that observed in insects. When mantids and locusts execute peering movements to estimate the ranges of objects through motion parallax cues, they actively counter-rotate the head relative to the thorax so as to maintain a constant head orientation in space (Boeddeker and Hemmi, 2010; Collett, 1978; Sobel, 1990; Wallace, 1959). Schilstra and Hateren (Schilstra and Hateren, 1999) showed that blowflies maintain a constant head orientation (in roll as well as yaw) during flight, despite the fact that the rest of the body (thorax and abdomen) do not do so.

In blowflies, the roll of the head is stabilized by inputs from the visual system and possibly additionally by gyrosensory inputs from the halteres (Hengstenberg, 1988). Similarly, honeybees compensate for rotations of the

thorax by counter-rotations of the head (Boeddeker et al., 2010). This eliminates the rotational component of optic flow and leaves just the translational component, which provides information on the three-dimensional structure of the world. Exactly how the compensatory head rotations are achieved remains to be discovered, in insects as well as birds.

6.4.3 The timing of wing closure

We have seen that the birds consistently cease to flap their wings when they pass through the aperture. Cessation occurs earlier when the panels flanking the aperture are clearly visible (as when they carry a checkerboard pattern), compared to when they are indistinct (as when they are blank). Further work is required to determine the variables that control the precise timing of the cessation of the wing beat, and to ascertain whether this cessation occurs at a constant time or a constant distance prior to entering the aperture, or according to some other function of these variables. It has been established that gannets, plunging into the ocean to catch fish, close their wings at a specific time prior to contacting the water surface, rather than at a specific distance from the surface (Lee and Reddish, 1981).

6.4.4 Wing postures during passage through the aperture

We have seen that budgerigars adopt a variety of different wing postures when passing through the aperture. These range from both wings fully closed, to one wing closed and the other extended horizontally, to one wing extended upward and the other downward. It would be of interest to examine, in a more detailed study, whether these postures are characteristic of particular individuals, and also to investigate whether the propensity to extend one wing or the other

depends upon the bias of the individual bird, i.e. its tendency to approach the aperture from the left-hand side or the right-hand side.

Chapter 7
General Discussion

Birds have devised elegant strategies in order to achieve mastery in the aerial domain. However, to be successful, birds have to rely on various sensory inputs that their brain has to process accurately, and in real time, to generate appropriate motor outputs. For flights over short distances, guidance is provided primarily by the visual system.

Budgerigars in the wild are found in central Australia. They live in large flocks of up to about 50-500 birds (Wyndham, 1982). Budgerigars fly through scrubland as well as woodland during their seasonal migration, avoiding obstacles and landing flawlessly on the branches of trees.

The highly precise flight manoeuvres of these birds persist even under extreme conditions like high winds, or the low light levels that prevail during dawn and dusk. Observations of wild bird populations in a wide variety of birds (Video 7.1) led me to carry out an investigation into the mechanism of edge detection in landing budgerigars. My studies have shown for the first time that budgerigars are able to detect and target visually contrasting edges when they come in to land. Presumably, such contrasting edges indicate the presence of a surface boundary that will afford a firm foothold upon touchdown and ensure a safe landing. This is essential, as a safe landing is important for survival.

My results show that the edge detection mechanism operates either through a combination of the colour blind photoreceptor channel composed of the red and green single cones, or, alternatively, through the red double cones (Chapter 3, and (Bhagavatula et al., 2009)). The role of the red double cones in motion perception has been speculated on in previous studies (Hart, 2001).

However it would be interesting to investigate the role of double cones and develop a theoretical model to elucidate the functional significance of double cones in motion perception and contrast detection. This could be achieved by careful measurement and analysis of the spectral properties of various visually mediated behaviours in the budgerigar, and correlating these sensitivities with that of the red double-cones and those of the other photoreceptors.

Some of the shortcomings of the above study were that the experiments were carried out under laboratory conditions on solitary, domesticated budgerigars. These results could therefore be different from those obtained from a wild population, in which the birds live under more natural conditions and in large flocks. It would be interesting to repeat the edge detection experiments on a wild population of budgerigars under natural sunlight. Similar experiments can also be carried out on various bird species living in different habitats, to investigate the generality of the role of edge detection in guiding landings.

Birds fly flawlessly through dense forests and between tree branches. They are able to negotiate narrow gaps and manoeuvre through extremely tight spaces. In order to do so, birds evidently rely on information derived from lateral optic flow. The importance of optic flow information in guiding locomotion has been extensively investigated in flies (Hengstenberg, 1988; Kern et al., 2006) honey bees, zebra finches, ants, and human beings, (Eckmeier et al., 2008; Ronacher et al., 2000; Srinivasan et al., 2006). The importance of translational (lateral) and rotational optic flow has been investigated in zebra finches (Eckmeier et al., 2008). There is some evidence to suggest that zebra finches may extract lateral optic flow information while flying through narrow spaces, although it does not indicate how that information is used to guide flight

(Eckmeier et al., 2008). Optic flow field variables have been shown to control landing in hawks, but not in the case of pigeons (Davies and Green, 1990). Films of the landing trajectories of hawks and pigeons revealed that, while hawks extend their feet at a specific time point (τ = 160 ms) prior to landing, pigeons do not use time-to-contact in the same way. Pigeons control their braking while landing on a perch by holding the rate of change of τ ($\dot{\tau}$) constant. (Refer to the 'tau' hypothesis previously discussed in the introduction chapter). The experiments presented in this thesis show for the first time that lateral optic flow is used by birds to navigate safely through narrow spaces and corridors.

My experiments to investigate the use of lateral optic flow cues were carried out by keeping the spatial period of the vertical stripes constant during the course of the experiments. In future experiments, it would be interesting to vary the spatial period of these stripes, to investigate the extent to which the budgerigar's visual system computes image velocity independently of the spatial texture of the retinal image.

All of the experiments described in this thesis were carried out in a relatively short tunnel of length 728 cm. However, it would be ideal to carry out these experiments in a longer tunnel, to investigate cruising behaviour. 3-D tracking of the birds could then be accomplished by one video camera at an end wall and a row of video cameras along the ceiling, with the ceiling cameras being used in conjunction with the end-wall camera to reconstruct successive segments of the flight trajectory along the tunnel.

It would be interesting to test my conclusions on the role of optic flow cues in the centring response by observing the behaviour of birds in the long

tunnel when the side walls display patterns that move in different directions and/or at different speeds. This would be a direct test of the hypothesis, arising as a result of my present study, that birds negotiate narrow passages safely by balancing the optic flow that is experienced by the two eyes.

It would also be interesting to investigate whether cruising birds regulate the speed of their flight, and, if so, to explore the mechanisms by which they might do this. My experiments to investigate this question in the short tunnels (with vertical or horizontal stripes lining both walls, as described in Chapter 4) suggest that flight speed is regulated by holding constant the overall magnitude of optic flow that is experienced by the two eyes. It would be important to test this hypothesis more rigorously by flying birds in a long tunnel – in which they are more likely to reach stable, cruising speeds – and directly manipulating the motion of patterns displayed on the side walls.

Longer tunnels would also be ideal to investigate whether birds use visual odometry to estimate how far they have flown. A bird could be trained to fly to food placed at location that is a fixed distance into the tunnel. The ability of the bird to gauge the distance that it has flown into the tunnel to get to the food can then be tested by removing the feeder and examining where the trained bird searches for the (now missing) food. One can then examine the importance of optic flow cues in gauging distance travelled by (a) varying the width of the tunnel in the tests or (b) moving visual patterns projected on the walls in or against the birds' flight direction.

Future developments could also involve the construction of a wind tunnel where flight behaviour is studied in the presence of controlled air flow. One

could investigate, for example, whether birds regulate the speed of their flight visually even in the presence of wind, by adjusting their flight thrust to compensate for headwinds or tailwinds. One way that birds might accomplish this would be to hold constant the magnitude of the optic flow that is generated by the environment. This possibility can be tested by flying birds in a wind tunnel in which the optic flow cues are manipulated.

Birds show lateralization in different aspects of their behaviour. For example, chicks are more likely to detect food, such as seeds on a floor, with their right eye (Rogers, 1990). Cockatoos show a preference for using their left foot to grab and raise food to their beak (Magat and Brown, 2009). On the other hand, Tree Swallows prefer to fly through a larger opening when two apertures of unequal sizes are presented to them, but show no lateralization in this behaviour (Mandel et al., 2008).

My observations have shown for the first time that individual birds show a lateralization with respect to avoiding obstacles during flight. Some birds fly consistently to the left of the obstacle, while others fly consistently to the right. However, this side bias is overridden when the birds encounter asymmetrical lateral optic flow information, for example a blank obstacle on one side of an aperture and a chequered obstacle on the other. My results show that when a right-biased bird, which would normally approach a symmetrically decorated aperture from the right side, encounters a blank obstacle on the right hand side of the aperture, then it approaches the aperture from the left side, i.e. away from the chequered obstacle, presumably to glean more reliable lateral optic flow information. When the birds encounter two apertures presented side by side, then if the apertures are of the same size, the choice of the aperture is

determined by the bird's lateralization. However, if the apertures are unequal in size, the birds show a tendency to prefer the larger aperture, overriding their lateralization-induced bias. However, the strategy employed to decide on which aperture to fly through varies from one individual to another. Some birds appear to make this decision before they take off from the perch, while others make the decision during their flight and make the necessary adjustments in real time. Clearly, the entire operation involves very quick reflexes.

All of my experiments used a vertically oriented aperture. In future investigations it would be interesting to carry out similar experiments using (i) a single horizontal aperture of variable height, carrying the same or different visual textures at the upper and lower ends; and (ii) two apertures of different heights, to investigate the role of aperture height in determining aperture choice.

Flying animals show six degrees of freedom of movement in three-dimensional space. These are composed of three translational movements: forward motion, lift, and sideways slip, and three rotational movements: yaw, pitch and roll. All flying animals need to maintain a more-or-less stable attitude with respect to gravity during flight. While yaw movements have little influence on flight attitude, roll and pitch movements do. Therefore, roll and pitch have to be stabilized and carefully controlled in order to promote stable flight.

In insects, vision plays an important role in stabilization of the head during flight (Hengstenberg, 1988). Honeybees in flight hold the orientation of their head relatively constant in absolute space (Boeddeker et al., 2010), interspersed by fast saccadic head and body yaw movements. During the periods of constant head orientation, the rotational components of optic flow are

kept at a minimum, thus allowing the perception of depth and the three-dimensional structure of the environment from the (purely) translational optic flow that prevails during these flight segments (Boeddeker et al., 2010). Head stabilization has also been observed in blowflies (Kern et al., 2006).

In the experiments presented in this thesis, I have shown that budgerigars keep the orientation of their head stable whilst avoiding obstacles, and flying through narrow spaces. The head shows relatively little roll movement in comparison to the body. The roll oscillations of the body increase in frequency as the bird approaches the narrow aperture but the amplitudes of the head roll oscillations are low compared to those of the body. The rates of body roll and the manoeuvres of the body are more extreme when the flanking walls are blank as compared to when they are textured. The pitch of the head is also low and it remains close to horizontal during the entire flight trajectory, whereas the body shows a greater degree of downward pitch while approaching the aperture.

Other interesting observations are that the wings beat in a roughly horizontal plane during level flight. Birds avoid flapping their wings while passing through the aperture. Most of the time the wings are held close to the body during transit through the aperture, but sometimes one wing is extended upwards and the other downwards. The birds also gain some altitude before entering the aperture in order to pre-compensate for the loss in altitude before entering the opening. When the tunnel carries no obstacles, the speed of bird flight is higher and the entire traverse through the tunnel is completed with fewer wing strokes.

My experiments to investigate head stabilization were carried out using high-speed cameras that had a high frame rate, but a relatively low spatial resolution (1 megapixel).

Thus, in order to be able to resolve the tracking dots with adequate precision I had to fly the birds relatively high (i.e. close to the camera in the ceiling). In future experiments a higher resolution colour camera, along with the use of holographic tracking dots (whose apparent colour changes with viewing angle), could be used to track the positions and orientations of the head and body more accurately.

In future work, a miniature gyroscope and accelerometer could be harnessed to the birds. The data from these devices could be combined with the information provided by the tracking dots to get more precise estimates of the orientation, and yaw, pitch and roll rates of the head and body.

Since birds occupy a wide variety of ecological niches and habitats, they display a range of anatomically different shapes of the head, eyes and beak that are suited to these different habitats. Hence it would be interesting to investigate how the visual system helps the birds generate motor outputs under such widely varying conditions. These adaptations have evolved over millions of years of selection pressure that have promoted the development of highly efficient strategies and neural algorithms for visuomotor control, which are not yet fully understood. It would also be interesting to compare the strategies and algorithms used by birds with those used by other flying organisms like insects - which are equally diverse, and occupy diverse ecological niches. Some of these

algorithms could be investigated for implementation on robotic airplanes and helicopters in order to enable them to take off, fly and land autonomously.

At present we know relatively little about the genetic basis of avian behaviour. It would be interesting to investigate the molecular players that are involved in the regulation and synthesis of the opsins in various bird species. It would also be interesting to investigate naturally occurring mutants among the bird population and the effects that these mutations may have on visually guided behaviour, as seen in case of albino zebra finches, for example, which are unable to produce an optokinetic response (Eckmeier et al., 2008). Such studies would allow us to identify the molecular pathways involved in a variety of visuomotor reflexes in birds.

The future of avian research looks extremely promising. With more advanced tools becoming available for measuring and quantifying behaviour and with the recent publication of the zebra finch genome and the chicken genome there is a renewed scientific interest in avian biology. Moreover, with newly emerging fields like biorobotics, and the successful implementation of insect visual navigation algorithms on robotic platforms, it is very likely that these robotic platforms will eventually implement avian visual algorithms as well.

Appendix 1

Further preliminary observations of budgerigar flight

In addition to the studies described in the previous chapters, I have made a number of brief observations during the course of the experiments, which I believe are interesting and worthy of pursuit in the future. Here is a brief description of them.

A1.1.1 Landing on a moving perch

Budgerigars were trained to take off from a perch and land on another perch, which was swinging in a plane roughly parallel to the bird's trajectory of approach towards it. The experimental set up is shown in Figure A1.

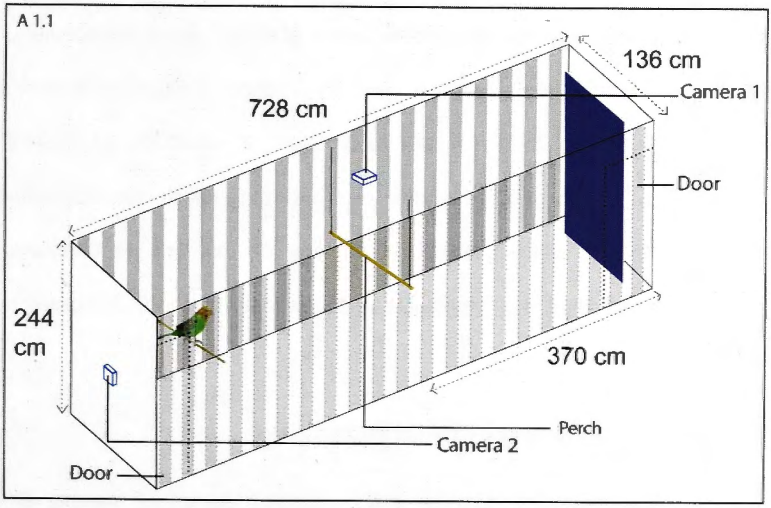

Figure A1.1 Schematic diagram of the tunnel with a swinging perch. The budgerigars take off upon slow rotation of the perch to land on the swinging perch.

My preliminary observations indicate that the birds land preferentially at the extreme ends of the swinging trajectory of the perch, i.e. at the closest or the farthest point of the arc traced by the perch. During such landings, birds hover just above the (momentarily) stationary perch before landing on it. This suggests that budgerigars prefer to touch down at the instants of time when the perch is nearly stationary, and there is little or no relative motion between the perch and the bird. A few landings also occur when the perch is moving in the same direction as the bird. This again represents a situation in which the perch is almost stationary relative to the bird. This landing strategy could be important when touching down on a branch that is swaying in the breeze. Only rarely do birds land when the perch is moving against them. In such cases the birds would flap their wings strongly in the horizontal plane just before touchdown, effectively generating a reverse thrust that reduced the speed of flight quickly to make the bird's motion more compatible with that of the perch. Presumably, the periodic, predictable, simple harmonic motion produced by the perch facilitates the planning and the timing of the touchdown. It would be of interest to investigate this phenomenon of landing on a swinging perch quantitatively and in greater detail. It would also be interesting to examine touchdowns on motorized perches that are programmed to execute aperiodic, unpredictable motions.

A1.1.2 Landmark following by flying budgerigars

Budgerigars were trained to fly through a tunnel that had a long, narrow strip of masking tape (2 cm wide) affixed to the surface of the floor, Experiments were conducted with the masking tape placed in three different configurations:

1) Close to the left wall of the tunnel (Figure A1.2).

2) Close to the right wall of the tunnel (Figure A1.3).

3) Along the diagonal of the floor area (right to left) (Figure A1.4).

In all three cases it was observed that the budgerigars used the masking tape as a guiding landmark while flying through the tunnel (Video AV2, AV3 and AV4), That is, they tend to fly above the landmark, along the direction in which it was oriented.

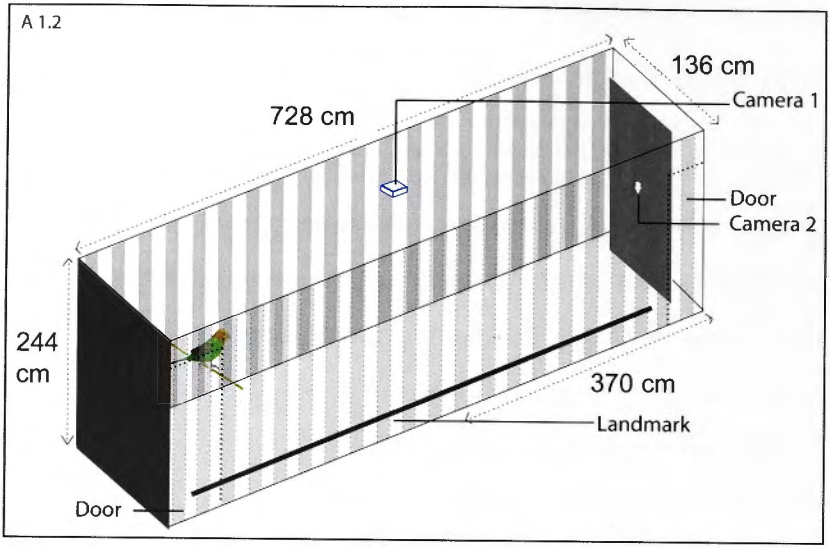
A 1.2
136 cm
Camera 1
728 cm
Door
Camera 2
244
cm
370 cm
Landmark
Door

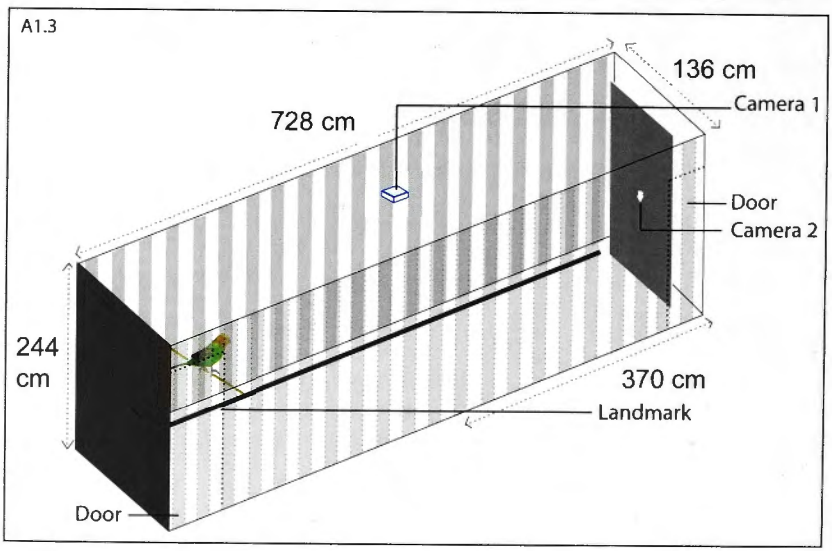
A1.3
136 cm
Camera 1
728 cm
Door
Camera 2
244
cm
370 cm
Landmark
Door

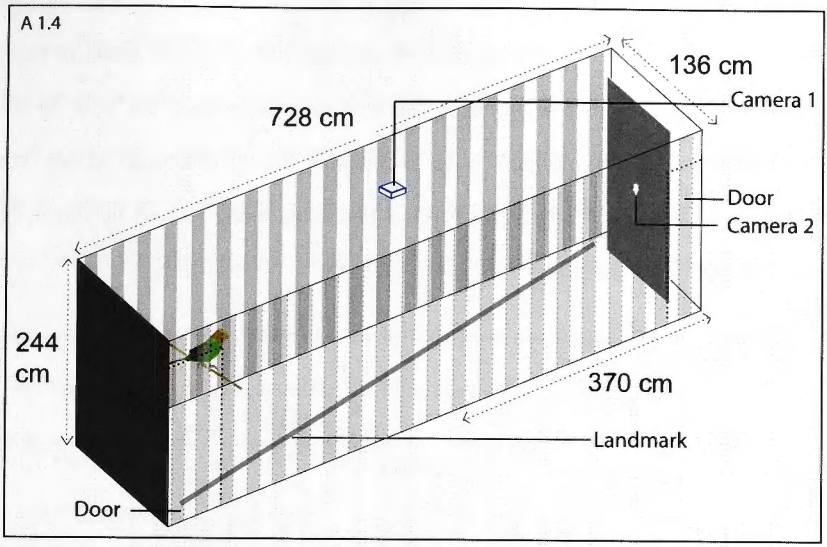

Figures A1.2, A1.3 and A1.4 Illustration of three different configurations of a landmark stripe on the floor.

Landmark following has been documented in homing pigeons, in the context of long-range navigation outdoors where these birds tend to follow highways and other visually contrasting edges on the ground (Lau et al., 2006). But those studies were carried out under field conditions where it is difficult to change the different experimental parameters. In contrast, my preliminary observations, which were conducted in a laboratory under controlled conditions, should permit manipulation of the shape, colour and contrast of such ground-based visual features in future studies to gain a better understanding of how they affect or guide flight.

A1.1.3 Multiple obstacle avoidance in flying budgerigars

Budgerigars were trained to fly a course that presented two obstacles. The obstacles were presented one after the other in a 'chicane' arrangement, as

shown in Figure A1.5. The first obstacle consisted of a vertical sheet of black cloth perpendicular to the tunnel's axis and stretching from the floor to the ceiling. The second obstacle was a similar sheet, coloured white. The background against which both of these obstacles were viewed by the flying bird (the end wall) was black.

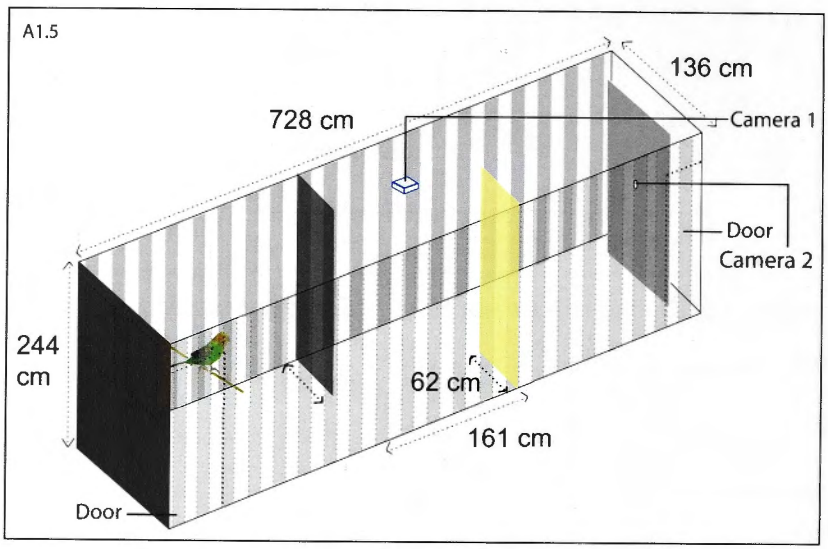

Figure A1.5 'Chicane' arrangement of obstacles used for the multiple obstacle avoidance experiment.

Each obstacle was nearly half the width of the tunnel, i.e. it obstructed nearly 50% of the tunnel opening. Recordings of the flights of birds through this 'chicane' arrangement showed that the budgerigars would close their wings as they passed through the first opening, flap their wings during the flight between the two obstacles, and then close their wings again when flying through the middle of the second opening (Video AV5).

This controlled study has interesting parallels with the flight of budgerigars while negotiating obstacles in the wild, where two successive obstacles can have contrasting differences. The above experiment could also be modified to investigate obstacle avoidance strategies adopted by birds in flight when there is no contrast between two or more successive obstacles.

Wild birds encounter obstacles every day during flight. Dexterity in negotiating obstacles is essential for their survival.

A1.2 Further suggestions for future research

A1.2.1 Scientific questions

A1.2.1.1 Optic flow experiments

The experiments involving lateral optic flow in flying budgerigars in Chapter 4 of this thesis have shown for the first time that birds rely on lateral optic flow information in order to navigate through tight spaces. However, I would like to investigate this problem more comprehensively by carrying out experiments in which patterns could be projected on to the walls of the tunnel using computer controlled video (LCD) projectors. This would enable precise control of the visual stimuli that the birds experience with regard to pattern, colour and movement.

The mechanism of the centring response can then be examined more thoroughly by systematically varying the speed and /or contrast of the pattern on one (or both) walls, to develop a full understanding and a quantitative model of this behaviour.

A detailed investigation of visual odometry has been carried out in honey bees (Srinivasan et al., 1997). However, there is as yet very little information on

how birds estimate distance travelled. This question can be addressed by training budgerigars to find food at various points along a long tunnel, which carries visual patterns projected on the side walls to provide optic flow cues. In subsequent tests, the projected stripes can be moved at various speeds in order to manipulate the extent of optic flow that the birds experience en route to their goal. If movement of the patterns changes the location at which the trained birds search for the food, systematically and predictably, these experiments would indicate that the birds use optic flow cues to estimate distance travelled.

A1.2.1.2 Avoidance of moving obstacles by flying birds

All of the experiments on obstacle avoidance presented in this thesis have investigated obstacle avoidance with respect to stationary objects. However, it would be interesting to investigate how birds detect and avoid moving obstacles. Birds in the wild are able to fly between the branches of trees even when they are swaying. But these avoidance manoeuvres are not always successful, as evidenced by the considerable numbers of fatalities caused by collisions with wind turbine blades. A systematic investigation of the ability (or otherwise) of birds to avoid of moving obstacles would enable us to develop deterrent measures that can prevent or reduce collision related fatalities.

A1.2.1.3 Real time object tracking and insect hunting by Pacific Swifts (Apus pacificus)

Motion camouflage is a type of a dynamic camouflage in which the pursuer appears to remain stationary to the organism that is being pursued. Hoverflies are known to use motion camouflage while looking for prospective mates while in flight (Srinivasan and Davey, 1995).

Pacific Swifts are agile fliers. They are known to track and hunt insects. However, the mechanism by which these and other insectivorous birds hunt the insects in flight remains to be explored. There is a strong possibility that they use motion camouflage in order to fool the prey and hence successfully catch them. This could be studied with the aid of high-speed stereo videography.

A1.2.1.4 Obstacle avoidance in Gos hawks (Accipiter fasciatus)

Gos Hawks (*Accipiter fasciatus*) are known to be very agile fliers, particularly when hunting for prey in densely wooded forests. However, little is known about how these birds avoid collisions while dodging obstacles in flight. A miniature video camera can be attached to the bird along with an attitude and heading reference system (AHRS). Such an arrangement would provide live streaming video of the bird's flight through the forest, as well as information about the attitude of the head and the body and the direction of flight while the bird is pursuing its prey and avoiding obstacles.

A1.2.1.5 Visually guided docking and hovering in honey eaters, sun birds and humming birds

Small birds like the Eastern Spinebill, (*Acanthorhynchus tenuirostris*) (a species of honey eater) (Pyke, 1981; Scoble and Clarke, 2006), the Olive Backed Sun Bird (*Nectarinia jugularis*) and the Ruby Throated Humming Bird (*Archilochus colubris*), (the first two being native to Australia and the last to the Eastern United States), are agile fliers and have a unique ability to hover during flight. This enables them collect nectar from flowers whilst airborne. The mechanism by which birds 'dock' to the flower appears to be under visuomotor control, and has not been systematically investigated. The docking behaviour can be

investigated by training the birds to feed at a sugar water feeder, and filming the birds' approach trajectories using high-speed stereo video cameras. To investigate the possible role of optic flow information in the control of approach and landing, approach trajectories can be measured when a rotating spiral stimulus is placed behind the feeder, in order to augment or reduce the apparent rate of expansion of the target.

A1.2.1.6 Establishment of a laboratory-reared genetically characterized strain of a wild type budgerigar

All the budgerigars that are currently being used for laboratory investigations are sourced from local breeders. Such budgerigars are bred for their vivid colours. The breeding is carried out randomly. However, it would be ideal to establish a genetically characterized population of budgerigars for future experiments involving animal behaviour. A Karyotype of the chromosomes should be prepared (Dongen and Boer, 1984; Rothfels et al., 1963) and all the known genes should be mapped on to the chromosomes. The establishment of a wild type laboratory strain of budgerigar would help in all future experiments involving budgerigar genetics.

A1.2.1.7 Sequencing the budgerigar genome and functional and behavioural characterization of budgerigar mutants

The first step towards budgerigar genomics would be to sequence the entire genome of the budgerigar, followed by complete annotation of all the genes. This data would be useful to characterize various genes involved in behaviour as well as to build transcriptional networks to show the interaction between the

genes and the various regulatory elements involved in the expression of a behavioural phenotype.

A1.2.2 Technical developments

A1.2.2.1 Development and standardization of an organic motion capture system to digitize motion of flying birds

Motion capture is a technique in which the movement of an object is recorded using two or more high speed cameras, after which the movement is incorporated into a previously-established model of the object. The technique has wide ranging applications in defence, entertainment, gaming and sports medicine. It is also widely used by researchers for the analysis of human and animal locomotion. Presently, the technique involves the use of active or passive tracking dots which act as markers or as reference points for digitization of a point on the object whose movement is to be recorded and measured. Once the video image sequences are acquired, they are processed by custom made-algorithms that convert the 2-D information acquired by all of the synchronized cameras into 3-D animations of the object, and which provide data on the kinematics of various body parts. While this technique is simple and straightforward, it has the disadvantage that the tracking dots placed on the subject can occasionally be displaced or dislodged, leading to inaccuracy or loss of measurements.

An approach that overcomes the above disadvantage involves the so-called 'organic motion capture'. This technique enables the tracking of static or dynamic body parts that have been filmed from different angles using multiple synchronized cameras, without the aid of any markers or tracking dots. In

essence, the approach involves fitting 3-D models of the various body parts to the recorded video sequences, in order to establish the position and orientation of each body part. Organic motion capture, also known as marker less motion capture, is gaining popularity because it is more accurate in determining the motion of the subject.

These endeavours would, of course benefit from the use of video cameras with a higher spatial resolution than the ones that I have used for my study. For example, the Viacom high-speed high-resolution digital cameras have a 5-megapixel image sensor, which should enable the experimenter to resolve and analyze data in greater detail and with higher accuracy.

A1.2.2.2 Integration of motion capture video with data from an AHRS (Attitude and Heading Reference System)

The data generated from high speed motion capture technology could also be integrated with data from an IMU (Inertial Measurement Unit) that is attached to the subject (or body part) under observation. An IMU consists of a three axis gyroscope, three accelerometers and three magnetometers. The three gyroscopes provide real time information about rates of yaw, pitch and roll. The magnetometers provide information on absolute orientation, relative to the earth's magnetic field. The accelerometers provide real time information about the acceleration along three mutually perpendicular axes. Commercially available IMUs are equipped with onboard filters that process and integrate the information from all the three types of sensors to generate real time data about the movement of the subject under investigation. The resulting IMU data could

be integrated with the data generated from stereo motion capture cameras to get a very accurate picture of how birds behave during rapid flight.

Appendix 2

Model of twin-aperture choice

Here I present a simple mathematical model that captures the behaviour of the birds when they are confronted with the task of choosing between two apertures, and incorporates the factors and tradeoffs that could influence the passage of a flock of budgerigars through the two apertures.

We assume that the width of the left-hand aperture is *d*, and that of the right-hand aperture is (*D*-*d*), where *D* is the total width of the two apertures. When $d = \frac{D}{2}$, the two apertures are of equal width. We assume that the time T taken for a single bird to fly though a passage is inversely proportional to the width of the passage. While we do not know if this assumption is exactly true, it is a reasonable first approximation, given that (a) the narrower the passage, the greater the difficulty in negotiating it, and the longer the bird will take to pass through it; and (b) if visually guided flight dynamics of budgerigars are similar to bees, the speed of their flight through a passage will be proportional to the width of the passage (Srinivasan et al., 1996), so that the time required to fly through the passage will be inversely proportional to its width.

Thus, the times T_L and T_R taken by a bird to fly through the left- and right-hand apertures will be given respectively by

$$T_L = \frac{K}{d} \qquad (1)$$

and $$T_R = \frac{K}{D-d} \qquad (2)$$

When the two apertures are of equal width, we see that

$$T_L = T_R \frac{2K}{d} \qquad (3)$$

If a flock of N budgerigars encounters the two apertures, and if N_L of them choose to fly through the left-hand aperture and N_R through the right-hand aperture ($N_L + N_R = N$), the time required for the N_L birds to transit the left-hand aperture will be

$$T_L = N_L \frac{K}{d} \qquad (4)$$

and the time required for the N_R birds to transit the right-hand aperture will be

$$T_R = N_R \frac{K}{(D-d)} = (N - N_L) \frac{K}{(D-d)} \qquad (5)$$

Let us now consider, in turn, a number ways in which the birds might choose between the two apertures and examine, for each case, the time taken by the entire flock to pass through the twin-aperture obstacle.

Strategy A: *All birds choose to fly through the left-hand aperture, irrespective of its width*

This situation would prevail if all of the birds had a strong left-bias.

In this case, the total transit time T_T taken by the entire flock will be (from equation (4)):

$$T_T = N \frac{K}{d} \qquad (6)$$

Figure A2.1 shows how the total transit time T_T for this strategy will vary as a function of the width d of the left-hand aperture (blue curve). Always choosing to fly through the left-hand aperture is unlikely to be an efficient strategy, because the right-hand aperture is never used by any bird.

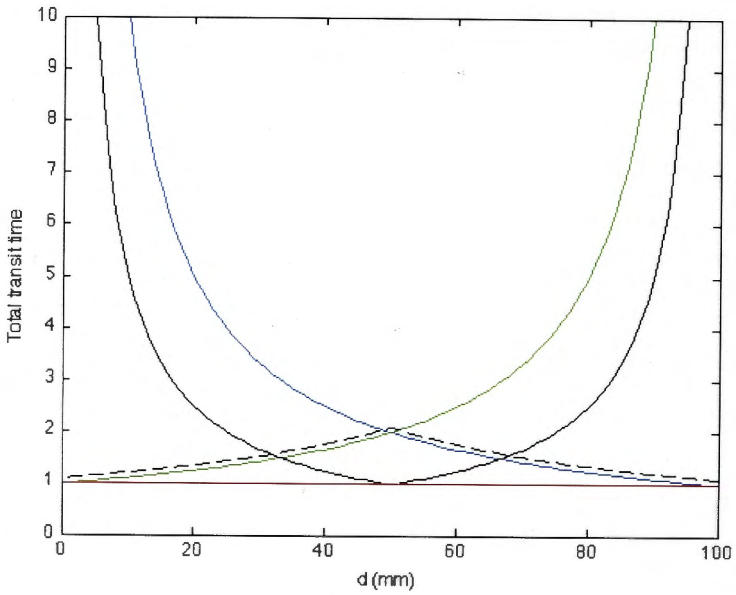

Figure A2.1 Illustration of total transit times as predicted by a model of a flock of budgerigars negotiating two simultaneously presented apertures of width d mm (left-hand aperture) and (D-d) mm (right-hand aperture), where D, the sum of the widths of the two apertures, is 100 mm. The curves show the variation of the total transit time with d for strategies A (blue), B (green), C (black), D (dashed black) and E (red), as described in the text. For clarity, the curve for strategy D is shown displaced slightly upwards.

Strategy B: *All birds choose to fly through the right-hand aperture, irrespective of its width*

This situation would prevail if all of the birds had a strong right-bias.

In this case, the total transit time T_T for the entire flock will be (from equation (5)):

$$T_T = N\frac{K}{(D-d)} \qquad (6)$$

Figure A2.1 shows how the total transit time T_T for this strategy will vary as a function of the width d of the left-hand aperture (green curve). Always choosing to fly through the right-hand aperture is unlikely to be an efficient strategy, because the left-hand aperture is never used by any bird.

Strategy C: *Birds choose randomly between the two apertures, irrespective of their size.*

This strategy would prevail either if (a) each bird were to choose randomly between the two apertures or (b) half the flock of birds had a strong left-bias and the other half a strong right-bias.

If the size of the flock is N, each aperture would be chosen by (N/2) birds, on average.

The transit time for the birds taking the left-hand aperture would be (from equation (4)):

$$T_L = \frac{N}{2}\frac{K}{d} \qquad (7)$$

and the transit time for the birds taking the right-hand aperture would be (from equation (5)):

$$T_R = \frac{N}{2}\frac{K}{(D-d)} \qquad (8)$$

The transit time T_T for the entire flock to pass through the twin-aperture obstacle would be the greater of the two transit times, T_L and T_R.

If $d < \frac{D}{2}$, then it is clear that T_L will be greater than T_R; and if $d > \frac{D}{2}$, the opposite will be true.

Therefore, the total transit time T_T for this strategy will be:

$$T_T = \frac{N}{2}\frac{K}{d} \quad \text{if } d \leq \frac{D}{2} \qquad (9)$$

i.e. if the right-hand aperture is wider than the left-hand one,

and

$$T_T = \frac{N}{2}\frac{K}{(D-d)} \quad \text{if } d > \frac{D}{2} \qquad (10)$$

i.e. if the left-hand aperture is wider than the right-hand one.

Figure A2.1 shows how the total transit time T_T for this strategy will vary as a function of the width d of the left-hand aperture (continuous black curve). This

strategy is not necessarily optimal, because it chooses wide apertures just as frequently as it does narrow apertures.

Strategy D: *Birds always choose the larger of the two apertures.*

If the left-hand aperture is wider, i.e., if $d > \frac{D}{2}$, the total transit time will be

$$T_T = N\frac{K}{d} \qquad (11)$$

If the right-hand aperture is wider, i.e., if $d \leq \frac{D}{2}$, the total transit time will be

$$T_T = N\frac{K}{(D-d)} \qquad (12)$$

Figure A2.1 shows how the total transit time T_T for this strategy varies as a function of the width *d* of the left-hand aperture (dashed black curve). This strategy is not necessarily optimal, because the narrower aperture is never used by any bird.

Strategy E: *Birds choose the two apertures with probabilities proportional to their relative widths.*

In this scenario the aperture of width *d* is chosen with probability $\frac{d}{D}$, and the aperture of width (*D*-*d*) is chosen with probability $\frac{D-d}{D}$. If the size of the flock is *N* (where N is a large number) then, on average, $N\frac{d}{D}$ birds would choose the aperture of width *d*, and $N\frac{D-d}{D}$ birds would choose the aperture of width (*D*-*d*).

The transit time for the aperture of width *d* would then be $N\frac{d}{D}\frac{K}{d}$, or $N\frac{K}{D}$. The transit time for the aperture of width (*D-d*) would be $N\frac{D-d}{D}\frac{K}{D-d}$, which is also equal to $N\frac{K}{D}$. We note that, with this strategy (a) the transit times are the same for both apertures, which means that both groups of birds will finish flying through their respective apertures at the same time; and (b) the transit times are independent of the relative widths of the two apertures. This is because the load (the number of birds) at each aperture is matched to the speed at which the birds can fly through that aperture. Since both apertures become clear at the same time, neither aperture is under-utilized, and this is the most efficient way to route traffic through the two apertures. The total transit time T_T for this strategy is $N\frac{K}{D}$, and is shown by the red curve in Figure A2.1. This represents the best (lowest) total transit time among all of the strategies. Importantly, in this case the transit time is not only minimal, but is independent of the relative widths of the two apertures.

The optimum strategy for minimizing the overall transit time, therefore, is to ensure that the *probability of choosing each aperture is proportional to the width of that aperture*. This leads to the optimum choice probability function shown in Figure A2.2. The probability of choosing the left-hand aperture is $\frac{d}{D}$, and the probability of choosing the right-hand aperture is $\frac{D-d}{D}$ where *d* is the width of the left-hand aperture and *D-d* is the width of the right-hand aperture.

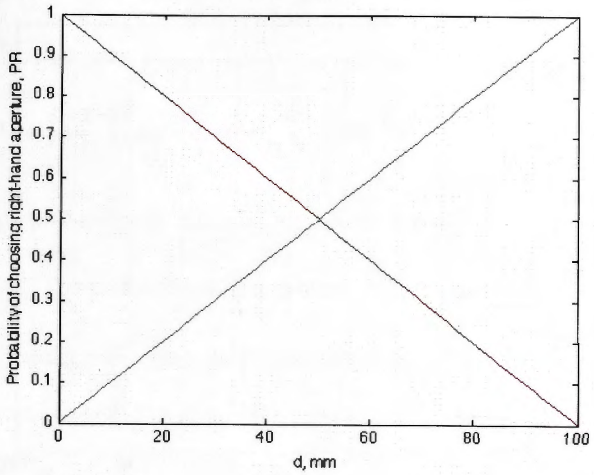

Figure A2.2 Probability functions for the choice of the right-hand aperture (red curve) and the left-hand aperture (blue curve) as a function of the width d of the left-hand aperture, for the optimum strategy (E) described in the text.

Are the budgerigars indeed realizing this optimal strategy? To investigate this, we can begin by modelling each bird's choice behaviour by a unit step function, as a simple first approximation. This step function is described by $u(B-d)$, where u, the probability of choosing the right-hand aperture when the left-hand aperture has a width d, is equal to 1 when $d \leq B$, and 0 when $d > B$. B is a parameter that represents the bird's bias. The bird is unbiased if B=(D/2), left-biased if B < 50 mm, and right-biased B > 50 mm. A family of choice probability functions, for birds with different biases, is shown in Figure A2.3.

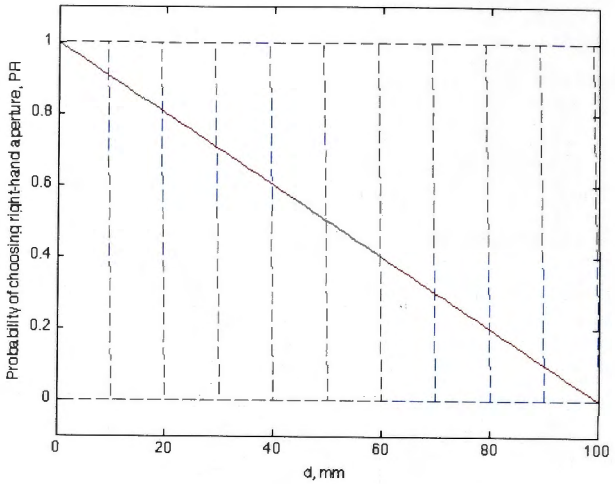

Figure A2.3. Choice probability functions for individual birds with a range of different bias parameters (B) varying from 0 mm to 100 mm in steps of 10 mm The choice probability for each bird is modelled by a step function (dashed blue curve). The continuous red curve shows the resulting average choice probability function for the entire flock.

The desired optimum choice probability function for the entire flock can be realized by having a different bias parameter for each bird. If B varies uniformly over the range [0 - D], it can be shown that the choice probability function for choosing the right-hand aperture for the entire flock will be $\frac{D-d}{D}$, as illustrated by the continuous red curve in Figure A2.3.

The proof of this is as follows:

The probability of choosing the right-hand aperture, averaged over a large number of birds with biases distributed uniformly over the range [0,D], is given

by the expected value of the function $u(B-d)$. Denoting this expected value by P_R, we have

$$P_R = E[u(B-d)] = \frac{1}{D}\int_0^D u(B-d)dB = \frac{1}{D}\int_d^D 1.dB = \frac{D-d}{D} \qquad (13)$$

The average probability of choosing the left-hand aperture, P_L, is given by $1-P_R$, which is $\frac{d}{D}$. These functions are exactly those illustrated in Figure A2.2. Therefore, the optimum strategy illustrated in Figure A2.2 can be realized by a flock of birds in which the individual biases are distributed uniformly over the range [0,D].

In reality, we see that the choice probability curves for the individual birds are not exactly step functions. Rather, they are approximately sigmoidal in shape, as is evident from the data in Figures 5.6 A-F in Chapter 5. They can be approximated by the logistic function

$$\frac{1}{1+e^{-\alpha(B-d)}} \qquad (14)$$

where B is the bias parameter (as before), and α is a parameter which defines the sharpness of the bird's transition between the left-hand aperture and the right-hand one. The larger the value of α, the steeper the transition; when $\alpha=\infty$, we have a step function, as above.

Choice probability functions modelled according to the logistic function, with $\alpha=0.15$, for birds with various bias parameters (B) ranging from 0 mm to 100 mm in steps of 10 mm, are shown by the dashed blue lines in Figure A2.4.

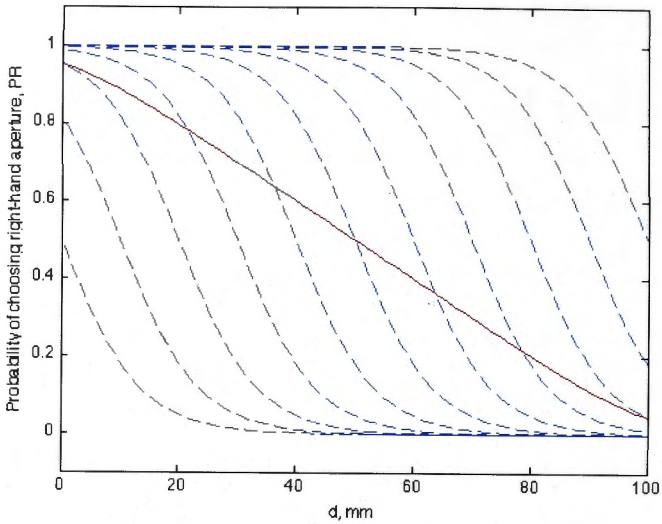

Figure A2.4. Choice probability functions for individual birds with a range of different bias parameters (B) varying from 0 mm to 100 mm in steps of 10 mm. The choice probability for each bird is modelled by a logistic function (dashed blue curve). The continuous red curve shows the resulting average choice probability function for the entire flock.

Proceeding as before, we can calculate the probability of choosing the right-hand aperture, averaged over a large number of birds with biases distributed uniformly over the range [0, D]. This is done by evaluating the expected value of the function $\frac{1}{1+e^{-\alpha(B-d)}}$. Denoting this expected value by P_R, we have

$$P_R = E\left[\frac{1}{1+e^{-\alpha(B-d)}}\right] = \frac{1}{D}\int_0^D \frac{1}{1+e^{-\alpha(B-d)}}\,dB \qquad (15)$$

The integral in (15) can be evaluated by setting

$$1+e^{-\alpha(B-d)}=p \tag{16}$$

which leads to

$$dB=\frac{-dp}{\alpha e^{-\alpha(B-d)}}=\frac{dp}{\alpha(1-p)} \tag{17}$$

Thus, we have

$$P_R=\frac{1}{D}\int_{1+e^{\alpha d}}^{1+e^{-\alpha(D-d)}}\frac{dp}{\alpha p(1-p)}=\frac{1}{\alpha D}\int_{1+e^{\alpha d}}^{1+e^{-\alpha(D-d)}}\left[\frac{1}{p}+\frac{1}{1-p}\right]dp \tag{18}$$

$$\text{i.e. } P_R=\frac{1}{\alpha D}\left[\log(p)-\log(1-p)\right]_{1+e^{\alpha d}}^{1+e^{-\alpha(D-d)}}=\frac{1}{\alpha D}\left[\log\left(\frac{p}{1-p}\right)\right]_{1+e^{\alpha d}}^{1+e^{-\alpha(D-d)}} \tag{19}$$

$$\text{which gives } P_R=\frac{1}{\alpha D}\left[\log\left\{\frac{1+e^{-\alpha(D-d)}}{-e^{-\alpha(D-d)}}\right\}-\log\left\{\frac{1+e^{\alpha d}}{-e^{\alpha d}}\right\}\right] \tag{20}$$

This can be simplified to read

$$P_R=\frac{1}{\alpha D}\log\left\{\frac{1+e^{-\alpha(D-d)}}{e^{-\alpha D}+e^{-\alpha(D-d)}}\right\} \tag{21}$$

P_R is the probability for choosing the right-hand aperture as a function of the width of the left-hand aperture (d). It is plotted as the continuous red curve in Figure A2.4. We see that this function is very similar in shape to the optimal choice probability function for strategy E, illustrated by the red curve in Figure A2.2.

Therefore, we can say that the desired optimal strategy can be approximated well by a flock of birds in which the choice probability function for each bird is characterized by a sigmoidal function, and where the biases of the various birds vary over a wide range, going from extreme left, through zero, to extreme right. The data from the birds that I have tested suggest that this is indeed what occurs.

Of course, we do not know as yet whether this is indeed the reason for the variation in bias that is displayed by the birds, but it brings up an attractive hypothesis that merits further investigation.

Appendix 3

Geometry of Tracking Markers

Here we describe the procedure for calculating the pitch and the roll of the head or the body, by analyzing the shape of the image of the corresponding diamond tracking marker.

Figure A3.1 shows a view of a diamond marker (in brown), the four corners of which are labelled 3 (front), 4 (rear), 1 (left), and 2 (right). In this illustration the diamond is depicted as when viewed from below (which does not occur in the filming), but this does not compromise the validity of the trigonometric calculations. In this illustration the diamond is pitched upward by an angle φ, and has rolled counter clockwise about this pitch axis, through an angle θ, to take on the orientation illustrated by the blue, dashed line figure. In executing this roll, corner 1 moves to position 1', corner 2 moves to position 2', and points 3 and 4 remain stationary because they are on the roll axis.

We wish to calculate the pitch (φ) of the diamond marker, and the angle θ through which it has rolled about the 3-4 axis. The calculation proceeds as follows.

Referring to Figure A3.1, let r denote the half-width of the diagonal of the diamond. This is read off from the calibration table shown in Figure 6.3 of Chapter 6, for the particular height of the bird. That is,

$$O1=O2=O3=O4=r, \quad (1)$$

and

$$O1'=O2'=r. \quad (2)$$

Let us now consider Figure A3.2, which shows two views of the diamond marker as captured by the overhead camera. Assuming that the diamond is pitched upwards (as is almost always the case), then the image of corner 1' will lead that of corner 2' if the roll is left-side-downward (as shown in Figure A3.2b), and will trail behind that of corner 2' if the roll is left-side-downward (as shown in Figure A3.2a). The illustration in Figure A3.2a corresponds to that shown in Figure A and we shall continue the analysis for this case, without any loss of generality. In Figure A3.2, A, B, C and D refer to the projections of the corners 1,2,3 and 4 of the diamond marker on the horizontal plane.

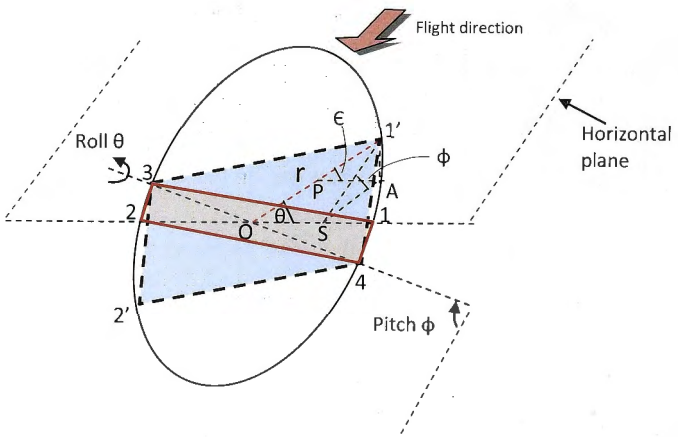

Figure A3.1. Illustration of the geometry of the diamond marker, and the effects of a change in roll attitude. The long axis of the marker is 3-4, and is pitched upward by an angle φ (brown figure). The blue figure shows the new view of the marker when it has rolled right-side-down, about the 3-4 axis, by an angle θ.

In Figure A3.2a, we can calculate the lengths of the various sides and the longitudinal diagonal as:

$$AC = \sqrt{[(x_1 - x_3)^2 + (y_1 - y_3)^2]} \quad (3)$$

$$AD = \sqrt{[(x_1 - x_4)^2 + (y_1 - y_4)^2]} \quad (4)$$

$$CD = \sqrt{[(x_3 - x_4)^2 + (y_3 - y_4)^2]} \quad (5)$$

If the pitch is zero, the expected length of the longitudinal diagonal of the marker in the image captured by the overhead camera will be 2r. If this diagonal is pitched upward by an angle φ, the projection of this diagonal on the horizontal plane will be $2r\cos\phi$. Setting this equal to CD, we obtain

$$CD = 2r\cos\phi, \quad (6)$$

giving, for the angle of pitch, φ,

$$\phi = \cos^{-1}\left[\frac{CD}{2r}\right] \quad (7)$$

Where CD is computed from equation (5) above. As indicated in the text, the pitch of the head as well as the body is almost always upward throughout the flight. Thus, computing the polarity of the pitch is never an issue.

Let us now turn to the computation of the roll angle θ.

Referring to Figure A3.2a, we begin by calculating the angle α_1 in the triangle APD from:

$$\cos\alpha_1 = -\frac{AC^2 - AD^2 - CD^2}{2(AD)(CD)} \quad (8)$$

whence

$$\alpha_1 = \cos^{-1}\left[-\frac{AC^2 - AD^2 - CD^2}{2(AD)(CD)}\right] \quad (9)$$

We also note from Figure A3.2a that

$$AP = AD\sin\alpha_1$$

(10)

where $\sin\alpha_1 = \sqrt{1 - \cos^2}\alpha_1$. (11)

In general, the triangles APD and BCQ will be congruent, because the figure ACBD is a parallelogram which implies that$\alpha_1 = \alpha_2$. Nevertheless, we can calculate α_2 independently of α_1 to obtain a more robust estimate of this angle, which we will call α. α will then be used to compute the calculate the roll angle θ, as described later below.

From triangle BCQ, we can proceed as above to obtain

$$\cos\alpha_2 = -\frac{BD^2 - BC^2 - CD^2}{2(BC)(CD)} \quad (12)$$

$$\alpha_2 = \cos^{-1}\left[-\frac{BD^2 - BC^2 - CD^2}{2(BC)(CD)}\right] \quad (13)$$

and $BQ = BC\sin\alpha_2$ (14)

where $\sin\alpha_2 = \sqrt{1 - \cos^2}\alpha_2$. (15)

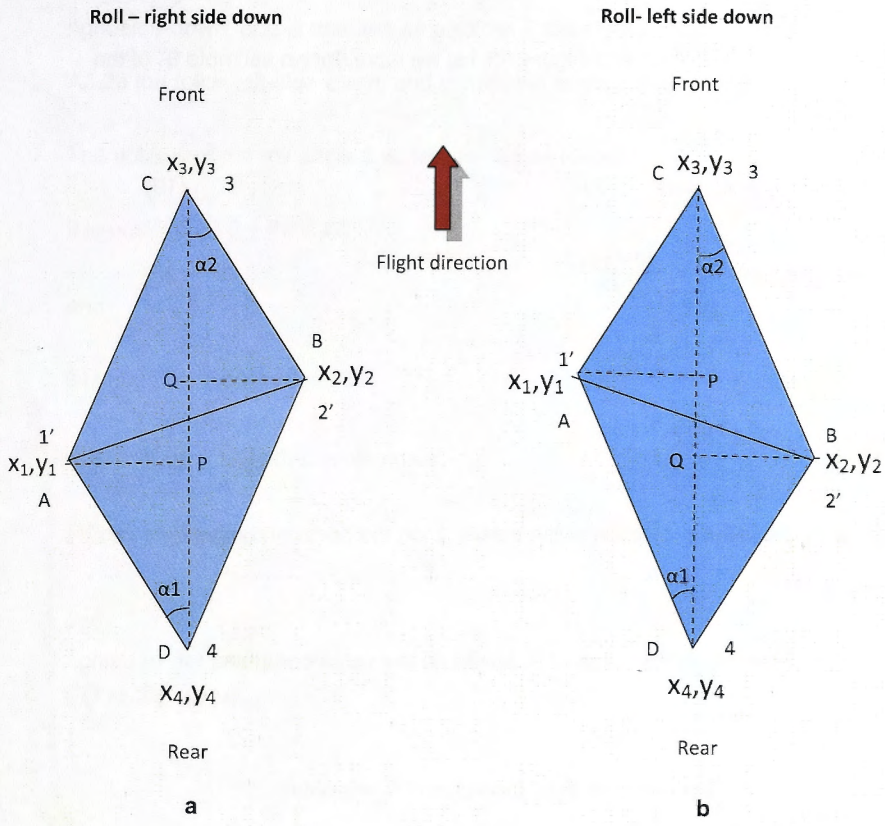

Figure A3.2. Two overhead views of the diamond marker. In ***a*** *the roll is right-side-downward, and in* ***b*** *the roll is left-side-downward. In both cases, the pitch is assumed to be upward, i.e. corner 3 is higher than corner 4.*

From the geometry of Figure A3.1, we see that

$$OS = AP = r\cos\theta; \tag{16}$$

$$1'S = r\sin\theta; \tag{17}$$

Defining A as the projection of corner 1' on the horizontal plane passing through O, we have

$$AS = 1'S.\cos\emptyset = r\sin\theta\cos\emptyset \quad (18)$$

Referring to Figure A3.1 and Figure A3.1a, we have, for an estimate θ_1 of the value of θ,

$$AP = r\cos\theta_1 = AD\sin\alpha_1 \quad (19)$$

which gives $\cos\theta_1 = \frac{AD\sin\alpha_1}{r}$, (20)

or

$$\theta_1 = \cos^{-1}\left[\frac{AD\sin\alpha_1}{r}\right]. \quad (21)$$

(Note that A is the projection of the corner 1' on the horizontal plane passing through O)

θ_1 is one estimate of the value of θ, based on the value computed for α_1 using equation (x) above.

Analogously, for the estimate θ_2 of the value of θ, we obtain

$$\theta_2 = \cos^{-1}\left[\frac{BC\sin\alpha_2}{r}\right] \quad (22)$$

where B is projection of the corner 2' on the horizontal plane passing through O.

The final estimate of the roll angle θ, about the axis 3,4, is taken to be the average of θ_1 and θ_2:

$$\theta = \frac{\theta_1+\theta_2}{2} \quad (23)$$

The direction (polarity) of the roll angle θ is determined by whether the shape of the overhead view of the diamond marker corresponds to that shown in Figure

A3.2a or Figure A3.2b. If the shape corresponds to Figure A3.2a the roll is right-side-down, and is denoted as positive. If the shape corresponds to Figure A3.2b the roll is left-side-down, and is denoted as negative.

The polarity of the roll angle θ is determined as follows:

θ is positive if $CQ + PD < CD$ (24)

and

θ is negative if $CQ + PD > CD$ (25)

where PD and CQ are calculated as

$$PD = AD\cos\alpha_1 \quad (26)$$

and

$$CQ = BC\cos\alpha_2 \quad (27)$$

Note that θ is angle of roll about the longitudinal axis of the marker, i.e. about the axis 3,4.

The effective angle of roll about the horizontal axis is a different angle – it is denoted by Є in Figure A3.1.

We see from Figure A3.1 that

$$\tan\epsilon = \frac{1'A}{AP} = \frac{1'S\sin\phi}{r\cos\theta} = \frac{r\sin\theta\sin\phi}{r\cos\theta} \quad (28)$$

which gives

$$\epsilon = \tan^{-1}[\tan\theta \sin\phi] \quad (29)$$

Є is the roll angle that is plotted in the data shown in Chapter 6.

We can also calculate the effective angle of yaw, which is the angle AOS in Figure A3.1. Denoting this angle by δ (not shown in Figure A3.1, in order to avoid excessive clutter), we see that

Tan delta = AS/OS= (1'S cos phi)/(rcos theta)= (rsin theta cos phi)/(rcos theta)= tan theta cos phi

$$\tan\delta = \frac{AS}{OS} = \frac{1'S\cos\phi}{r\cos\theta} = \frac{r\sin\theta\cos\phi}{r\cos\theta} = \tan\theta\cos\phi \quad (30)$$

which gives

$$\delta = \tan^{-1}[\tan\theta\cos\phi] \quad (31)$$

Appendix 4

List of Matlab Programmes

The Matlab programmes that were used in this thesis are listed below. While a few of these were available on the internet, most of the programs were developed in-house for specialized purposes. The programmes are included as an electronic copy in the digital media.

1) Chapter 2

a) Camera Calibration tool box

b) Tracking programmes (Trackman and cords 7)

2) Chapter 3

a) Bird landing density Graphical user interface

b) Digitization programme

c) Plot programme

d) Stats programme

3) Chapter 4

a) Trackman- Tracking programme (same as chapter 2)

b) Coords programme (same as chapter 2)

c) Plot programme

d) Stats programme

e) Speed plot and Stats programme

4) Chapter 5

a) Plot Programme

b) Animation programme

5) Chapter 6

a) Diamond Calibration digitization programme

b) Diamond Calibration plot programme

c) Bird height to Diamond theoretical axial transverse programme

d) Diamond tracking programme

e) Diamond analysis programme

f) Bird body orientation programme

Bibliography

Alerstam, T., Gudmundsson, G. A., Green, M. and Hedenstrom, A. (2001). Migration Along Orthodromic Sun Compass Routes by Arctic Birds. *Science* **291**, 300-303.

Allan L, D. and Rowena H. W, L. (2006). Assessing the impacts of wind farms on birds. *Ibis* **148**, 29-42.

Allan, L. D. and Rowena, H. W. L. (2008). Collision Effects of Wind-power Generators and Other Obstacles on Birds. *Annals of the New York Academy of Sciences* **1134**, 233-266.

Arnold, K. E., Owens, I. P. F. and Marshall, N. J. (2002). Fluorescent Signaling in Parrots. *Science* **295**, 92-.

Baird, E., Kornfeldt, T. and Dacke, M. (2010). Minimum viewing angle for visually guided ground speed control in bumblebees. *J Exp Biol* **213**, 1625-1632.

Baird, E., Kreiss, E., Wcislo, W., Warrant, E. and Dacke, M. (2011). Nocturnal insects use optic flow for flight control. *Biology Letters*.

Baird, E., Srinivasan, M. V., Zhang, S. and Cowling, A. (2005). Visual control of flight speed in honeybees. *J Exp Biol* **208**, 3895-3905.

Barron, A. and Srinivasan, M. V. (2006). Visual regulation of ground speed and headwind compensation in freely flying honey bees (Apis mellifera L.). *J Exp Biol* **209**, 978-984.

Bennett, A. T. D., Cuthill, I. C., Partridge, J. C. and Maier, E. J. (1996). Ultraviolet vision and mate choice in zebra finches. *Nature* **380**, 433-435.

Berthold, P., Gwinner, E. and Sonnenschein, E. (2003). Avian migration. Berlin; New York: Springer.

Bhagavatula, P., Claudianos, C., Ibbotson, M. and Srinivasan, M. (2009). Edge Detection in Landing Budgerigars (*Melopsittacus undulatus*). *Plos One* **4**, e7301.

Biro, D., Freeman, R., Meade, J., Roberts, S. and Guilford, T. (2007). Pigeons combine compass and landmark guidance in familiar route navigation. *Proceedings of the National Academy of Sciences* **104**, 7471-7476.

Boeddeker, N., Dittmar, L., Stürzl, W. and Egelhaaf, M. (2010). The fine structure of honeybee head and body yaw movements in a homing task. *Proceedings of the Royal Society B: Biological Sciences* **277**, 1899-1906.

Boeddeker, N. and Hemmi, J. M. (2010). Visual gaze control during peering flight manoeuvres in honeybees. *Proceedings of the Royal Society B: Biological Sciences* **277**, 1209-1217.

Borst, A. and Egelhaaf, M. (1993). Detecting visual motion: Theory and models. In *Visual Motion and its Role in the Stabilization of Gaze*, (ed. F. A. M. a. J. W. (eds)), pp. 3-27: Elsevier, Amsterdam.

Bowmaker, J. K., Heath, L. A., Wilkie, S. E. and Hunt, D. M. (1997). Visual pigments and oil droplets from six classes of photoreceptor in the retinas of birds. *Vision Research* **37**, 2183-2194.

Boyle, W. A. (2008). Partial migration in birds: tests of three hypotheses in a tropical lekking frugivore. *Journal of Animal Ecology* **77**, 1122-1128.

Burkhardt, D. (1982). Birds, berries and UV. *Naturwissenschaften* **69**, 153-157.

Carsten Egevanga, I. J. S., Richard A. Phillipsd, Aevar Petersene, James W. Foxd, and Janet R. D. Silkd. (2010). Tracking of Arctic terns *Sterna paradisaea* reveals longest animal migration. *Proceedings of the National Academy of Sciences-New York* **107**, 2078-2081.

Church, S. C., Merrison, A. S. L. and Chamberlain, T. M. M. (2001). Avian ultraviolet vision and frequency-dependent seed preferences. *J Exp Biol* **204**, 2491-2498.

Collett, T. (1977). Stereopsis in toads. *Nature* **267**, 349-351.

Collett, T. S. (1978). Short Communication: Peering-A Locust Behaviour Pattern for Obtaining Motion Parallax Information. *J Exp Biol* **76**, 237-241.

Cordula V. Mora, M. D., J. Martin Wild & Michael M. Walker. (2004). Magnetoreception and its trigeminal mediation in the homing pigeon. *Nature* **432**, 508-511.

Curtis, E. L. and Miller, R. C. (1938). The Sclerotic Ring in North American Birds. *The Auk* **55**, 225-243.

D'Eath, R. B. (1998). Can video images imitate real stimuli in animal behaviour experiments? *Biological Reviews* **73**, 267-292.

Daniel, E. and Willard, B. J. (1978). The interaction between some human obstacles and birds. *Environmental management* **2**, 331-340.

Davies, M. N. O. and Green, P. R. (1988). Head-Bobbing During Walking, Running and Flying: Relative Motion Perception in the Pigeon. *J Exp Biol* **138**, 71-91.

Davies, M. N. O. and Green, P. R. (1990). Optic flow-field variables trigger landing in hawk but not in pigeons. *Naturwissenschaften* **77**, 142-144.

Davies, M. N. O. and Green, P. R. (1991). The adaptability of visuomotor control in the pigeon during landing flight. . *Zoologische Jahrbucher* **95**, 331–338.

Dennis, E. B. (1997). Avian cataracts. *Seminars in Avian and Exotic Pet Medicine* **6**, 131-137.

Desholm, M. and Kahlert, J. (2005). Avian collision risk at an offshore wind farm. *Biology Letters* **1**, 296-298.

Dongen, M. W. M. and Boer, L. E. M. (1984). Chromosome studies of 8 species of parrots of the families Cacatuidae and Psittacidae (Aves: Psittaciformes). *Genetica* **65**, 109-117.

Dvorak, D., Srinivasan, M. V. and French, A. S. (1980). The contrast sensitivity of fly movement-detecting neurons. *Vision Research* **20**, 397-407.

Eckert, H. (1973). Optomotorische Untersuchungen am visuellen System der Stubenfliege <i>Musca domestica</i> L. *Biological Cybernetics* **14**, 1-23.

Eckmeier, D., Geurten, B. R. H., Kress, D., Mertes, M., Kern, R., Egelhaaf, M. and Bischof, H.-J. (2008). Gaze Strategy in the Free Flying Zebra Finch (*Taeniopygia guttata*). *Plos One* **3**, e3956.

Egelhaaf, M. and Borst, A. (1993). Movement detection in arthropods. In *Visual Motion and its Role in the Stabilization of Gaze.*, (ed. F. A. M. a. J. W. (eds)), pp. 53-77: Elsevier, Amsterdam.

Egelhaaf, M. and Kern, R. (2002). Vision in flying insects. *Current Opinion in Neurobiology* **12**, 699-706.

Emlen, S. T. (1967). Migratory Orientation in the Indigo Bunting, Passerina cyanea. Part II: Mechanism of Celestial Orientation. *The Auk* **84**, 463-489.

Erickson, W. P., Johnson, G. D., Stickland, M. D., Jr, D. P. Y., Sernka, K. J. and Good, R. E. (2001). Avian collisions with wind turbines: a summary of existing studies and comparisons to other sources of avian collision mortality in the United States. *National Wind Coordinating Committee, Washington, D.C., USA.*

Fermi, G. and Richardt, W. (1963). Optomotorische Reaktionen der Fliege Musca Domestica. *Biological Cybernetics* **2**, 15-28.

Fox, R., Lehmkuhle, S. W. and Bush, R. C. (1977). Stereopsis in the falcon. *Science* **197**, 79-81.

Fred, E. H. and Kenneth, R. O. (1984). Microvasculature of the avian eye: Studies on the eye of the duckling with microcorrosion casting, scanning electron microscopy, and stereology. *American Journal of Anatomy* **170**, 205-221.

Frost, B. J. (1978). The Optokinetic Basis of Head-bobbing in the Pigeon. *J Exp Biol* **74**, 187-195.

Gagliardo, A., Ioalè, P., Savini, M. and Wild, J. M. (2009). Olfactory Navigation in Homing Pigeons. *Annals of the New York Academy of Sciences* **1170**, 434-437.

Gibson, J. J. (1950). Perception of the visual world: Houghton-Mifflin. Boston

Ginsburg, N. and Nilsson, V. (1971). Measuring flicker thresholds in the budgerigar. *Jounal of Experimental Analysis of Behaviour* **15**, 189–192.

Goldsmith, T. and Butler, B. (2005). Color vision of the budgerigar (Melopsittacus undulatus): hue matches, tetrachromacy, and intensity discrimination. *Journal of Comparative Physiology A: Neuroethology, Sensory, Neural, and Behavioral Physiology* **191**, 933-951.

Goldsmith, T. H. and Butler, B. K. (2003). The roles of receptor noise and cone oil droplets in the photopic spectral sensitivity of the budgerigar, Melopsittacus undulatus. *Journal of Comparative Physiology A: Neuroethology, Sensory, Neural, and Behavioral Physiology* **189**, 135-142.

Götz, K. G. (1964). Optomotorische Untersuchung des visuellen systems einiger Augenmutanten der Fruchtfliege Drosophila. *Biological Cybernetics* **2**, 77-92.

Götz, K. G. (1965). Die optischen Übertragungseigenschaften der Komplexaugen von Drosophila. *Biological Cybernetics* **2**, 215-221.

Green, P. R., Davies, M. N. O. and Thorpe, P. H. (1992). Head orientation in pigeons during landing flight. *Vision Research* **32**, 2229-2234.

Green, P. R., Davies, M. N. O. and Thorpe, P. H. (1994). Head-bobbing and head orientation during landing flights of pigeons. *Journal of Comparative Physiology A: Neuroethology, Sensory, Neural, and Behavioral Physiology* **174**, 249-256.

Griffin, D. R. and Thompson, D. (1982). Echolocation by cave swiftlets. *Behavioral Ecology and Sociobiology* **10**, 119-123.

H Weimerskirch, J. M., Y Clerquin, P Alexandre, S Jiraskova (2001). Energy saving in flight formation. *Nature* **413** 697-698.

Harris, R. A., O'Carroll, D. C. and Laughlin, S. B. (2000). Contrast Gain Reduction in Fly Motion Adaptation. *Neuron* **28**, 595-606.

Hart, N. S. (2001). The Visual Ecology of Avian Photoreceptors. *Progress in Retinal and Eye Research* **20**, 675-703.

Hassenstein, B. and Reichardt, W. (1956). Systemtheoretische Analyse Der Zeit, Reihenfolgen Und Vorzeichenauswertung Bei Der Bewegungsperzeption Des Russelkafers Chlorophanus. *Zeitschrift Fur Naturforschung Part B-Chemie Biochemie Biophysik Biologie Und Verwandten Gebiete* **11**, 513 -524.

Hengstenberg, R. (1988). Mechanosensory control of compensatory head roll during flight in the blowflyCalliphora erythrocephala Meig. *Journal of Comparative Physiology A: Neuroethology, Sensory, Neural, and Behavioral Physiology* **163**, 151-165.

Higuchi, H., Nagendran, M. and Takekawa, J. (2003). Satellite telemetry and wildlife studies in India: Advantages, options and challenges. *Current Science* **85**, 1439-1443.

Hochberg, Y. and Tamhane, A. C. (1987). Multiple Comparison Procedures: Wiley.

Hogg, R. V. and Ledolter, J. (1987). Engineering Statistics. New York: MacMillan.

Ibbotson, M. R. (1991). A motion-sensitive visual descending neuron in Apis mellifera monitoring translatory flow-fields in the horizontal plane. . *Journal of Experimental Biology* **157**, 573–577.

Ibbotson, M. R. (2001). Evidence for velocity tuned motion-sensitive descending neurons in the honeybee. . *Proc R Soc Lond B* **268**, 2195–2201.

Ibbotson, M. R., Clifford, C. W. G. and Mark, R. F. (1998). Adaptation to Visual Motion in Directional Neurons of the Nucleus of the Optic Tract. *J Neurophysiol* **79**, 1481-1493.

Ingle, D. (1968). *Brain Behav. Evol.* **1**, 500-518.

Jeffery, G. and Williams, A. (1994). Is abnormal retinal development in albinism only a mammalian problem? Normality of a hypopigmented avian retina. *Experimental Brain Research* **100**, 47-57.

Jones, M. P., Pierce Jr, K. E. and Ward, D. (2007). Avian Vision: A Review of Form and Function with Special Consideration to Birds of Prey. *Journal of Exotic Pet Medicine* **16**, 69-87.

Kern, R., van Hateren, J. H. and Egelhaaf, M. (2006). Representation of behaviourally relevant information by blowfly motion-sensitive visual interneurons requires precise compensatory head movements. *J Exp Biol* **209**, 1251-1260.

Kirchner, W. and Srinivasan, M. (1989). Freely flying honeybees use image motion to estimate object distance. *Naturwissenschaften* **76**, 281-282.

Kram, Y. A., Mantey, S. and Corbo, J. C. Avian Cone Photoreceptors Tile the Retina as Five Independent, Self-Organizing Mosaics. *Plos One* **5**, e8992.

Krapp, H. G. and Hengstenberg, R. (1996). Estimation of self-motion by optic flow processing in single visual interneurons. *Nature* **384**, 463-466.

Kunze, P. (1961). Untersuchung des Bewegungssehens fixiert fliegender Bienen. *Journal of Comparative Physiology A: Neuroethology, Sensory, Neural, and Behavioral Physiology* **44**, 656-684.

Lau, K.-K., Roberts, S., Biro, D., Freeman, R., Meade, J. and Guilford, T. (2006). An edge-detection approach to investigating pigeon navigation. *Journal of Theoretical Biology* **239**, 71-78.

Lee, D. N., Davies, M. N. O., Green, P. R. and Van Der Weel, F. R. (1993). VISUAL CONTROL OF VELOCITY OF APPROACH BY PIGEONS WHEN LANDING. *J Exp Biol* **180**, 85-104.

Lee, D. N. and Reddish, P. E. (1981). Plummeting gannets: a paradigm of ecological optics. *Nature* **293**, 293-294.

Lehrer, M. (1987). To be or not to be a color-seeing bee. *Israel J Entomol* **21**, 51–76.

Lehrer, M., Srinivasan, M. V. and Zhang, S. W. (1990). Visual Edge Detection in the Honeybee and its Chromatic Properties. *Proceedings of the Royal Society of London. B. Biological Sciences* **238**, 321-330.

Leu, M. and Thompson, C. W. (2002). The potential importance of migratory stopover sites as ight feather molt staging areas: a review for neotropical migrants. *Biological Conservation* **106**, 45-56.

Lind, O. and Kelber, A. (2009). Avian colour vision: Effects of variation in receptor sensitivity and noise data on model predictions as compared to behavioural results. *Vision Research* **49**, 1939-1947.

Livingstone, M. S. and Hubel, D. H. (1987). Psychophysical evidence for separate channels for the perception of form, color, movement and depth. *Journal of neuroscience* 7, 3416–3468.

M.A.Farfan, J. M. V., J.Duarte and R.Real. (2009). What is the impact of wind farms on birds? A case study in southern Spain. *Biodiversity Conservation* **18** 3743–3758.

Mabee, T. J., Cooper, B. A., Plissner, J. H. and Young, D. P. (2009). Nocturnal Bird Migration Over an Appalachian Ridge at a Proposed Wind Power Project. *Wildlife Society Bulletin* **34**, 682-690.

Magat, M. and Brown, C. (2009). Laterality enhances cognition in Australian parrots. *Proceedings of the Royal Society B: Biological Sciences* **276**, 4155-4162.

Mandel, J. T., Ratcliffe, J. M., Cerasale, D. J. and Winkler, D. W. (2008). Laterality and Flight: Concurrent Tests of Side-Bias and Optimality in Flying Tree Swallows. *Plos One* **3**, e1748.

Martin, G. (2007). Visual fields and their functions in birds. *Journal of Ornithology* **148**, 547-562.

Mitkus, M., Lind, O. and Kelber, A. (2010). personal communication.

Moinard, C., Statham, P. and Green, P. R. (2004). Control of landing flight by laying hens: implications for the design of extensive housing systems. *British Poultry Science* **45**, 578 - 584.

Morton, E. S. (1977). On the Occurrence and Significance of Motivation-Structural Rules in Some Bird and Mammal Sounds. *The American Naturalist* **111**, 855.

Mouritsen, H. and Ritz, T. (2005). Magnetoreception and its use in bird navigation. *Current Opinion in Neurobiology* **15**, 406-414.

Nevitt, G. A., Losekoot, M. and Weimerskirch, H. (2008). Evidence for olfactory search in wandering albatross, Diomedea exulans. *Proceedings of the National Academy of Sciences* **105**, 4576-4581.

Nishimura, Y., Terada, S., Sekiguchi, M. and Shimai, K. (1980). Clasping Structure in the Double Cone of the Retina in Vertebrates. *J Electron Microsc (Tokyo)* **29**, 403-405.

Ohayon, S., van der Willigen, R., Wagner, H., Katsman, I. and Rivlin, E. (2006). On the barn owl's visual pre-attack behavior: I. Structure of head movements and motion patterns. *Journal of Comparative Physiology A: Neuroethology, Sensory, Neural, and Behavioral Physiology* **192**, 927-940.

Park, K. J., Rosen, M. and Hedenstrom, A. (2001). Flight kinematics of the barn swallow (Hirundo rustica) over a wide range of speeds in a wind tunnel. *J Exp Biol* **204**, 2741-2750.

Pearn, S. M., Bennett, A. T. D. and Cuthill, I. C. (2001). Ultraviolet vision, fluorescence and mate choice in a parrot, the budgerigar Melopsittacus undulatus. *Proceedings of the Royal Society of London. Series B: Biological Sciences* **268**, 2273-2279.

Pettigrew, J. D. and Konishi, M. (1976). Neurons selective for orientation and binocular disparity in the visual Wulst of the barn owl (Tyto alba). *Science* **193**, 675-678.

Plath, M. (1935). Über das Farbenunterscheidungsvermögen des Wellensittichs. *Journal of Comparative Physiology A: Neuroethology, Sensory, Neural, and Behavioral Physiology* **22**, 691-708.

Pyke, G. H. (1981). Why hummingbirds hover and honeyeaters perch. *Animal Behaviour* **29**, 861-867.

Railton, R. C. R., Mary Foster, T. and Temple, W. (2009). A comparison of two methods for assessing critical flicker fusion frequency in hens. *Behavioural Processes* **80**, 196-200.

Reichardt, W. (1969). Movement perception in insects. In: Processing of Optical Data by Organisms and by Machines. New York: Academic Press.

Ritchie, B. A. C. a. R. J. (1995). The altitude of bird migration in east-central Alaska: A radar and visual study. *Journal of Field Ornithology.* **66:**, 590–608.

Rogers, L. J. (1990). Light input and the reversal of functional lateralization in the chicken brain. *Behavioural Brain Research* **38**, 211-221.

Rogers, L. J. (2000). Evolution of Hemispheric Specialization: Advantages and Disadvantages. *Brain and Language* **73**, 236-253.

Ronacher, B., Gallizzi, K., Wohlgemuth, S. and Wehner, R. (2000). Lateral optic flow does not influence distance estimation in the desert ant Cataglyphis fortis. *J Exp Biol* **203**, 1113-1121.

Rothfels, K., Aspden, M. and Mollison, M. (1963). The W-chromosome of the budgerigar, Melopsittacus undulatus. *Chromosoma* **14**, 459-467.

Salewski, V. and Bruderer, B. (2007). The evolution of bird migration—a synthesis. *Review Literature And Arts Of The Americas*, 268-279.

Schefler, W. C. (1979). Statistics for the biological sciences: Addison Wesley, Reading, Mass.

Schilstra, C. and Hateren, J. H. (1999). Blowfly flight and optic flow. I. Thorax kinematics and flight dynamics. *J Exp Biol* **202**, 1481-1490.

Schmidt-Koenig, K. (1987). Bird Navigation: Has Olfactory Orientation Solved the Problem? . *The Quarterly Review of Biology* **62**, 31-47.

Schmidt-Koenig, K. (1990). The sun compass. *Cellular and Molecular Life Sciences* **46**, 336-342.

Scoble, J. and Clarke, M. F. (2006). Nectar availability and flower choice by eastern spinebills foraging on mountain correa. *Animal Behaviour* **72**, 1387-1394.

Scorer, R. S. (1954). The nature of convection as revealed by soaring birds and dragonflies. *Quarterly Journal of the Royal Meteorological Society* **80**, 464-467.

Sobel, E. C. (1990). The locust's use of motion parallax to measure distance. *Journal of Comparative Physiology A: Neuroethology, Sensory, Neural, and Behavioral Physiology* **167**, 579-588.

Srinivasan, M., Zhang, S. and Bidwell, N. (1997). Visually mediated odometry in honeybees. *J Exp Biol* **200**, 2513-2522.

Srinivasan, M., Zhang, S., Lehrer, M. and Collett, T. (1996). Honeybee navigation en route to the goal: visual flight control and odometry. *J Exp Biol* **199**, 237-244.

Srinivasan, M. V. (1993). How insects infer range from visual motion. *Reviews of oculomotor research* **5**, 139-156.

Srinivasan, M. V. and Davey, M. (1995). Strategies for Active Camouflage of Motion. *Proceedings of the Royal Society of London. Series B: Biological Sciences* **259**, 19-25.

Srinivasan, M. V., Lehrer, M., Kirchner, W. H. and Zhang, S. W. (1991). Range perception through apparent image speed in freely flying honeybees. *Visual Neuroscience* **6**, 519-535.

Srinivasan, M. V. and Zhang, S. (2004). VISUAL MOTOR COMPUTATIONS IN INSECTS. *Annual Review of Neuroscience* **27**, 679-696.

Srinivasan, M. V., Zhang, S., Altwein, M. and Tautz, J. r. (2000). Honeybee Navigation: Nature and Calibration of the "Odometer". *Science* **287**, 851-853.

Srinivasan, M. V. and Zhang, S. W. (2000). Visual navigation in flying insects. *International Review of Neurobiology* **44**, 67-92.

Srinivasan, M. V., Zhang, S. W. and Reinhard, J. (2006). Small brains, smart minds: vision, perception, navigation and 'cognition' in insects: In: Invertebrate Vision, Eds Eric Warrant and Dan-Eric Nilsson. Cambridge University Press.

Tobalske, B. and Dial, K. (1996). Flight kinematics of black-billed magpies and pigeons over a wide range of speeds. *J Exp Biol* **199**, 263-280.

Tobalske, B. W., Peacock, W. L. and Dial, K. P. (1999). Kinematics of flap-bounding flight in the zebra finch over a wide range of speeds. *J Exp Biol* **202**, 1725-1739.

Troje, N. F. (2001). Head-bobbing in pigeons: Evidence for differential motion parallax computation during landing flight. *Poster presented at the 6th International Congress of Neuroethology Bonn.*

Tucker, V. A. (1966). Oxygen Consumption of a Flying Bird. *Science* **154**, 150-151.

Tucker, V. A. (1968). Respiratory Exchange and Evaporative Water Loss in the Flying Budgerigar. *J Exp Biol* **48**, 67-87.

v. Campenhausen, M. and Kirschfeld, K. (1998). Spectral sensitivity of the accessory optic system of the pigeon. *Journal of Comparative Physiology A: Neuroethology, Sensory, Neural, and Behavioral Physiology* **183**, 1-6.

van der Willigen, R., Frost, B. and Wagner, H. (2002). Depth generalization from stereo to motion parallax in the owl. *Journal of Comparative Physiology A: Neuroethology, Sensory, Neural, and Behavioral Physiology* **187**, 997-1007.

van Hateren, J. H., Srinivasan, M. V. and Wait, P. B. (1990). Pattern recognition in bees: orientation discrimination. *J. Comp. Physiol. A* **167**, 649-654.

Videler, J. J. (2006). Avian Flight. Oxford: Oxford University Press.

Vorobyev, M. (2003). Coloured oil droplets enhance colour discrimination. *Proceedings of the Royal Society of London. Series B: Biological Sciences* **270**, 1255-1261.

Wagner, H. and Schaeffel, F. (1991). Barn owls (Tyto alba) use accommodation as a distance cue. *Journal of Comparative Physiology A: Neuroethology, Sensory, Neural, and Behavioral Physiology* **169**, 515-521.

Waldvogel, J. A. (1990). The Birds-Eye-View. *American Scientist* **78**, 342-353.

Wallace, G. K. (1959). Visual Scanning in the Desert Locust Schistocerca Gregaria Forskal. *J Exp Biol* **36**, 512-525.

Wang, Y. and Frost, B. J. (1992). Time to collision is signalled by neurons in the nucleus rotundus of pigeons. *Nature* **356**, 236-238.

Warrick, D. R., Bundle, M. W. and Dial, K. P. (2002). Bird Maneuvering Flight: Blurred Bodies, Clear Heads. *Integrative and Comparative Biology* **42**, 141-148.

Wehner, R. (2001). ECOLOGY: Bird Navigation--Computing Orthodromes. *Science* **291**, 264-265.

Wehrahn, C. (1986). Motion sensitive yaw torque responses of the housefly <i>Musca</i>: A quantitative study. *Biological Cybernetics* **55**, 275-280.

Willigen, R. F. v. d., Frost, B. J. and Wagner, H. (1998). Stereoscopic depth perception in the owl.: Neuroreport

Wiltschko, R. and Wiltschko, W. (2003). Avian navigation: from historical to modern concepts. *Animal Behaviour* **65**, 257-272.

Wolf-Oberhollenzer, F. and Kirschfeld, K. (1994). Motion sensitivity in the nucleus of the basal optic root of the pigeon. *J Neurophysiol* **71**, 1559-1573.

Woodcock, A. H. (1940). Observations on Herring Gull Soaring. *The Auk* **57**, 219-224.

Wyndham, E. (1981). Breeding and mortality of Budgerigars Melopsittacus undulatus *Emu* **81**, 240-243.

Wyndham, E. (1982). Movements and breeding seasons of the Budgerigar. *Emu* **82**, 276-282.

Yates, D., Moore, D. S. and McCabe, G. P. (1999). The Practice of Statistics.: WH New York: Freeman and Co.